



Faculty of Science and Technology

MASTER'S THESIS

Study program/ Specialization: Offshore Technology/ Marine and Subsea Technology	Spring semester, 2011 Open / Restricted access
Writer: Tonje Charlotte Stald (Writer's signature)
Faculty supervisor: Arnfinn Nergaard (UIS)	External supervisor(s): Bjørn Aalstad (Framo Engineering AS)
Title of thesis: Assessment of critical factors when running and retrieving Framo pump modules through moonpool	
Credits (ECTS): 30	
Key words: Moonpool, Lifting, Pump Modules	Pages: 79 + enclosure: 13 Stavanger, 14/06/2011 Date/year

This page is intentionally left blank

Abstract

The scope of this Master Thesis was to assess critical factors when running and retrieving Framo pump modules through the moonpool of a vessel.

The thesis has been presented in a twofold manner. The first part thoroughly describes Framo Engineering AS equipment. Internal procedures and discussions with Framo employees have been used to obtain needed information.

The second part has been dedicated to moonpool theory. Emphasize has been made on describing the behavior of the water inside the moonpool. The Bernoulli equation was used to prove that moonpool water motions have similar response characteristics as those of a mass-spring system. At the moonpool bottom opening the water motions are hard to describe.

Moonpool responses have been described based on formulas given in DNV-RP-H103. Possible natural periods has been presented for a standard moonpool, showing that resonance condition may arise during a North Sea operation. Large water oscillations are the main concern during a moonpool operation.

Hydrodynamic parameters have been discussed, including added mass and damping. Values for added mass and drag coefficients for Framo pump and running tool have been estimated according to DNV-RP-H103.

From this thesis it can be concluded that installation through the moonpool has both advantages and disadvantages compared to the overside crane operations. To be able to predict the forces in the moonpool adequate input data such as transfer functions and hydrodynamic parameters should be obtained from dedicated software. Due to the complex geometry of Framo equipment, estimates of hydrodynamic coefficients should come from models test or CFD-analysis.

Preface

This Master Thesis is written during the spring semester 2011 at the Faculty of Science and Technology at the University of Stavanger (UIS), in cooperation with Framo Engineering AS. The thesis is limited in time and work to one semester only.

It is emphasized that no software tools or results from model tests have been available during the work with this thesis.

The work has been carried out under supervision of Professor Arnfinn Nergaard at UIS. I owe him a great thank you for long-distance supervising. He has given me quick feedback and guidance whenever needed.

I would also like to thank my supervisor at Framo Engineering AS, Bjørn Aalstad. First, for giving me the opportunity of writing this thesis, and secondly for his every-day engagement regarding my work. A thank you also to all other employees at the Framo Subsea Department for their commitment and support.

Last, but not least, I would like to thank my dearest, Kim Andrè Haga. He has encouraged me throughout this period and tried his best to help me when I have faced the wall.

Table of Contents

Abstract	I
Preface	II
Table of Contents	III
Abbreviations	VI
Nomenclature	VII
1. Introduction	1
2. Framo Engineering AS Systems	3
2.1. Introduction	3
2.2. System Description.....	3
2.2.1. The Manifold Structure	4
2.2.2. Flowline Connectors	5
2.2.3. UTA (Umbilical Termination Assembly)	6
2.2.4. MPP (Multiphase Pump).....	8
2.2.5. Process Piping	10
2.2.6. Process Valves.....	11
2.2.7. Power Jumpers	13
2.2.8. Signal Jumpers	14
2.2.9. Hydraulic Jumpers.....	15
2.2.10. Hydraulic Tubing.....	16
2.2.11. Power and Control Module.....	16
2.2.12. Guide Posts	16
2.2.13. Dummy Pump.....	18
2.2.14. Pump Transport Skid	18
2.2.15. Pump Running Tool.....	19
2.2.16. Transport Skid for Pump Running Tool	21
2.2.17. Jumper Parking Panel	21
2.3. Installation Sequence	22
2.3.1. Installation of FDS	22
2.3.2. Installation of UTA	23

2.3.3.	Retrieval of Dummy Pump	23
2.3.4.	Installation of HV Power Jumper	26
2.3.5.	Installation of Signal and Barrier Oil Jumper	27
2.3.6.	Installation of MPP	27
2.4.	Tordis IOR	29
2.4.1.	Specifications and Requirements	30
3.	Moonpool Theory	31
3.1.	Introduction	31
3.1.1.	Challenges to Moonpool Operations	32
3.1.2.	Module Handling System	33
3.1.3.	Framo Pump Units through Moonpool	34
3.2.	Fluid Motion	35
3.2.1.	Fluid Motion in Moonpool Column	35
3.2.2.	Water Entering Moonpool	40
3.2.3.	Fluid Motion below Moonpool	42
3.2.4.	CFD-Analysis for Moonpool Water Motion	42
3.3.	Hydrodynamic Parameters	43
3.3.1.	Damping	43
3.3.2.	Drag	48
3.3.3.	Added Mass	53
3.3.4.	Mass and Drag Dominating System	59
3.4.	Wave Kinematics	61
3.5.	Transfer Functions	63
3.5.1.	Vessel	66
3.5.2.	The Water Plug	67
3.6.	Water Entry	69
3.6.1.	Moonpool vs. Overside Water Entry	71
3.7.	Moonpool Resonance Period	73
4.	Conclusion	75
5.	Recommendation for Further Work	77
6.	References	78
APPENDIX A - Comparison of Drag Coefficient and Forces for Square and Cylindrical Structure		80

APPENDIX B - Estimation of Drag Coefficient for Tordis Pump Unit	86
APPENDIX C - Estimation of Added Mass for Tordis Pump Unit and Running Tool.....	91

Abbreviations

BR	Barrier Return
BS	Barrier Supply
CFD	Computational Fluid Dynamics
COG	Center of Gravity
FDPSO	Floating, Drilling, Production, Storage and Offloading Vessel
FDS	Framo Dual Pump Station
HPU	Hydraulic Power Unit
HV	High Voltage
IOR	Improved Oil Recovery
LV	Low Voltage
MHS	Module Handling System
MHT	Module Handling Tower
MPP	Multiphase Pump
PCM	Power and Control Module
RAO	Response Amplitude Operator
ROV	Remotely Operated Vehicle
RT	Running Tool
SCM	Subsea Control Module
SHPU	Service Hydraulic Power Unit
SS	Signal Stab
SSBI	Subsea Separation Boosting and Injection System
UTA	Umbilical Termination Assembly
UTH	Umbilical Termination Head

Nomenclature

Greek Symbols

δV	Change in volume of displaced water from still water surface to wave crest or wave trough
ε_n	Phase angle component
ζ	Displacement of water plug [m]
$\dot{\zeta}$	Velocity of water plug [m/s]
$\ddot{\zeta}$	Acceleration of water plug [m/s ²]
ζ_s	Heave motion of vessel [m]
ζ_W	Sea surface elevation outside the vessel [m]
$\zeta(t)$	Wave elevation of an irregular sea [m]
η	Free surface elevation [m]
η_i	Displacement in one of the six degrees of freedom [m]
η^D	Relative damping ratio for moonpool
κ	Dimensionless parameter, 0,46 for rectangular moonpool
λ	Wave length [m]
ξ_0	Wave amplitude [m]
ρ	Fluid density, 1025 [kg/m ³] for sea water
ϕ	Velocity potential
\mathcal{V}	Velocity vector
ν	Fluid kinematic fluid viscosity [m ² /s]
ω	Frequency [rad/sec]
ω_0	Resonance frequency [rad/sec]

Latin Symbols

A	Cross-sectional area of moonpool [m ²]
A_b	Solid projected area of launched object [m ²]
A_b	Projected area on a horizontal plane that will be subject to slamming [m ²]
$A(0)$	Water plane area of moonpool [m ²]
$A(-h)$	Water plane area at moonpool bottom opening [m ²]
$A(z)$	Water plane area as function of local z [m ²]
A_{33}	Added mass of lifted object [kg]
A_{WP33}	Added mass of water plug [kg]
a_{ct}	Characteristic single amplitude vertical acceleration of crane tip [m/s ²]
a_w	Characteristic vertical water acceleration [m/s ²]
C	Integration constant

C_D	Drag coefficient
C_{D0}	Drag coefficient for unrestricted flow
C_{DS}	Drag coefficient for steady flow
C_b	Damping coefficient for relative motion between water plug and vessel [kg/m]
C_S	Damping coefficient for relative motion between water plug and lifted object [kg/m]
C_{Sl}	Slamming coefficient
C_{Sl}	Linearized damping [kg/s ²]
c	Damping
D	Characteristic body dimension [m]
F_D	Morrison drag force [N]
F_{hyd}	Resulting hydrodynamic force [N]
F_M	Morrison mass force [N]
F_{slam}	Slamming impact force [N]
F_{snap}	Snap load [N]
F_{wave}	Excitation force from waves [N]
F_{vessel}	Excitation force from vessel motion [N]
F_ρ	Buoyancy force [N]
$F(t)$	Hydrodynamic pressure force acting on the moonpool water plug [N]
G_s	Heave transfer function for vessel
G_w	Moonpool transfer function from the wave elevation
g	Gravity acceleration, 9,81 [m/s ²]
H_s	Significant wave height [m]
$H_{1/3}$	Significant wave height [m]
h	Vessel draft [m]
K	Stiffness of hoisting system [N/m]
K_w	Water plane stiffness = $\rho g A$ [N/m]
KC	Keulegan-Carpenter number
k	Wave number [rad/m]
k_{sm}	Stiffness of spring-mass system [N/m]
M	Mass of water plug [kg]
Re	Reynolds number
P_{FK}	Froude-Krylov dynamic pressure [Pa]
p	Pressure [Pa]
S	= A_b
$S(\omega)$	Wave spectrum
s	Vessel motion [m]
T	Wave period [s]
$T(h)$	Moonpool resonance period as a function of vessel draft [s]
T_n	Natural period of oscillating system [s]
T_p	Peak period [s]

t	Time [s]
v_m	Maximum particle velocity [m/s]
v_c	Hook lowering velocity [m/s]
v_{ct}	Characteristic single amplitude vertical velocity of the crane tip [m/s]
v_s	Slamming impact velocity [m/s]
v_w	Characteristic vertical water particle velocity [m/s]
v'	Fluid velocity [m/s]
x	Horizontal direction [m]
z	Vertical direction [m]

1. Introduction

“...It is the Government’s ambition that Norway shall remain a significant supplier of oil and gas to the world markets for a long time. One way to achieve this target, and perhaps the most important one, is to increase the recovery factor from existing fields. 1 per cent higher recovery from our shelf could be worth 30 billion USD, according to some estimates.”

The State Secretary, Per Rune Henriksen, at the Underwater Technology Conference in Bergen 2010, about the importance of improved recovery factor [23].

Subsea technology has grown to play an important part in today’s oil and gas industry. Fields are becoming more demanding, and the need to develop new and effective subsea solutions constantly increases. One of the main challenges is to keep the recovery factor as high as possible. Framo Engineering AS is one of the world’s leading suppliers of technology for subsea processing, multiphase boosting and wet gas compression. Framo product line consists of key equipment when it comes to keeping a high and stable production rate from the subsea wells.

It is important for the field operators to keep the operability of the subsea equipment as high as possible to reduce costly shut-downs. Therefore it is often a desire that the sea state in which the damaged equipment can be repaired or replaced is as high as possible. To date the sea state limit has been increased by use of monohull vessels with module handling systems that enables launch and recovery through a moonpool placed near the center of roll and pitch axis of the vessel. A moonpool can also be used to avoid exposure of equipment to very cold air and ice flows, which may become increasingly important in the future due to the increased activity in the Northern regions.

Installation of small subsea modules and tools through the moonpool is often the preferred method according to DNV [1]; this may reduce the dynamic forces, increase the limiting sea state and thus reduce the costs of installation and intervention operations. However, moonpool interventions are not straight forward and there are aspects that is important to be aware of when planning such operations. Some of these will be discussed in this thesis.

The Tordis field has become a pioneer in the Norwegian subsea technology history. With Tordis came the world’s first subsea separation system. Framo delivered two pumps for the system; one water-injection pump and one multiphase boosting pump. Statoil, as today’s operator of the field, has expressed a desire to replace the Framo pumps through the moonpool to ensure an all-year around operability. This request is the primary motivation for this thesis.

The given text

The scope of this thesis can be summarized to the following points:

- Review Framo Engineering AS present practices based on the Azurite and Tordis IOR projects
- Discuss applied methods and potential alternatives with focus on moonpool operations
- Review critical issues related to moonpool operations
- Perform preliminary simplified calculations based on the DNV-RP-H103 guideline
- Propose further work

Literature

In general, papers written on marine lifting operations, and particular those related to moonpool operations, has been very useful. Papers on standard lifting operations have been applied as the theory is comparable to launching through the moonpool. There also exist some reports on model testing of moonpool launching and these results have been used as references. Apart from this, O.M Faltinsens *Sea Loads on Ships and Offshore Structure* [7] and the DNV-RP-H103 guideline [1] has been used extensively throughout the writing.

Outline of thesis

Chapter 2 gives a thorough description of Framo equipment related to the subsea multiphase boosting, as well as the installation of the equipment.

Chapter 3 is dedicated to the moonpool theory. Included in this chapter is description of the hydrodynamic parameters damping, drag and added mass. Emphasize has also been made on trying to explain moonpool water motions.

Conclusion and recommendations for further work are given in *chapter 4 and 5*.

2. Framo Engineering AS Systems

2.1. Introduction

The primary objective of this chapter is to give a description of a standard type of pump arrangement in the Framo assortment. It will only describe one solution as the intention is to give the reader an understanding of how a pump station can be assembled, rather than to point out differences between the varieties of solutions.

The description will take basis in the Azurite subsea multiphase pumping system. The system is a dual-pump configuration delivered to the oil and gas company Murphy West Africa Ltd for the oil field Azurite, offshore Congo. The Azurite field development consist of a spread moored FDPSO tied to a subsea drill centre. The reason why Azurite has been chosen for system description is simply the fact that this system comprises many of the essential system components desirable to outline in this thesis. Also, it constitutes a fine basis when further explanation shall be given for the pump arrangement for the Tordis field.

The following descriptions are entirely based on Framo Engineering AS internal documents [23] and discussions with Framo employees.

2.2. System Description

The Azurite pumping system is a subsea multiphase pumping system, consisting of the following main components: a Framo Dual Pump Station (FDS), an Umbilical Termination Assembly (UTA) interconnecting jumpers for electrical power, signals and fluids, an umbilical between the UTA and the FDPSO and a topside Power and Control Module (PCM).

The FDS comprises three main packages, the structural framework, the piping arrangement and the retrievable items. The retrievable items include two multiphase pumps (MPP), the choke insert, the control modules and the electrical and hydraulic jumpers. Azurite does not include a subsea control module.

The Azurite FDS is located downstream a combined production and water injection manifold. It has two individual flow lines connected to it, and each pump is pumping each of these independently. The pump station is a self-standing, single lifted structured, installed onto a single pile on the seabed.

Figure 2.1 shows the installed Azurite FDS, with UTA and jumpers. The station is viewed from aft end where multiphase pump number one is located. The umbilical is not shown. The following text passages will separately outline the different parts of the pumping system on the figure. It will be a logical connection between different parts and for that matter a description of one part may take reference in another part. Thus should the descriptions be read in context to each other.

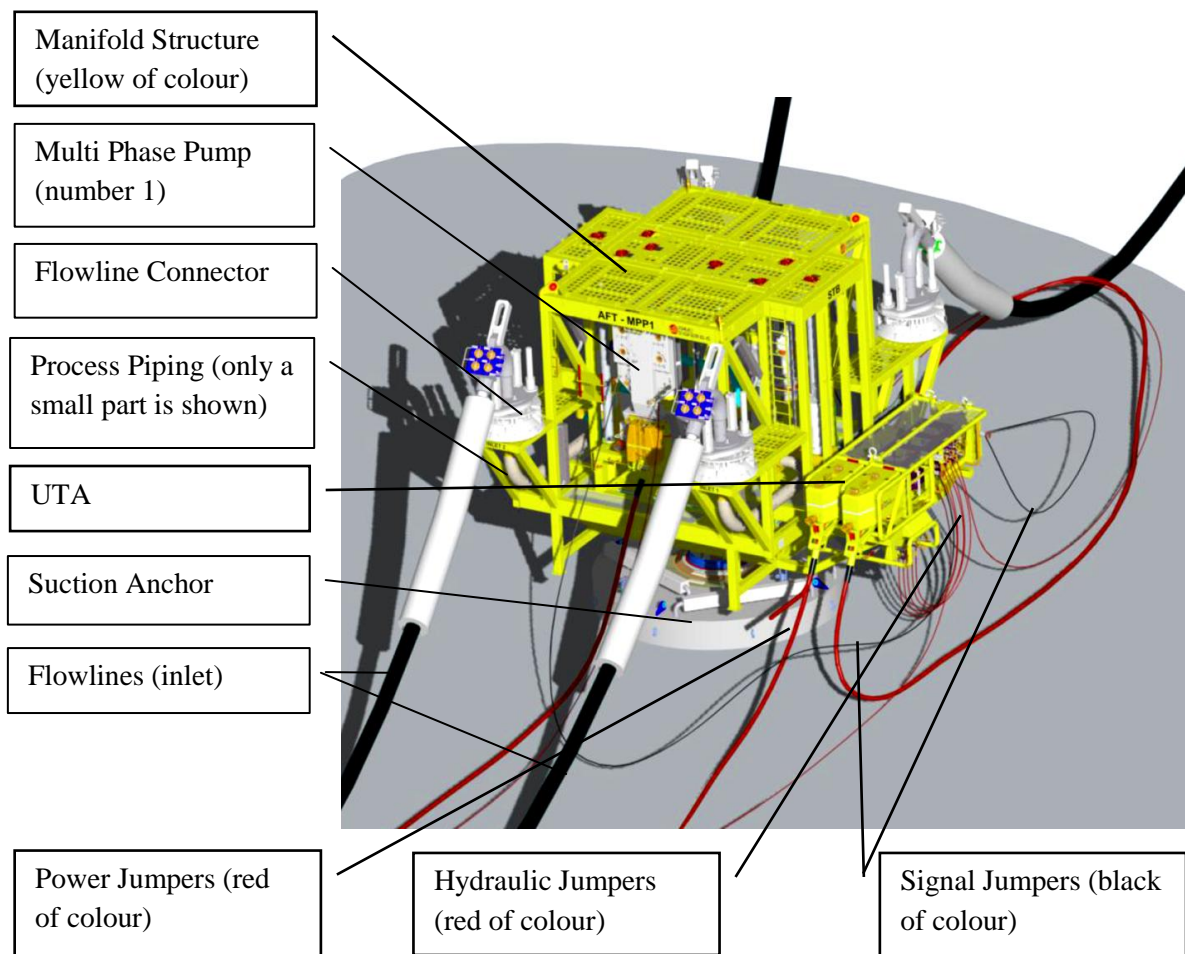


Figure 2.1: Overview of installed Azurite multiphase pump system

2.2.1. The Manifold Structure

The manifold structure is mainly rectangular carbon steel beams which are welded together. Beams are perforated to prevent from collapsing due to external pressure in water column.

Pump stations may be anchored to the seabed in a variety of ways, depending on bottom characteristics. The Azurite pump station uses a single suction anchor. On top of the anchor sits a single pile which is the connection point to the foundation of the pump station. Both anchor and pile are shown in grey colour in figure 2.2. A funnel is welded onto the foundation structure, and it interfaces the single pile. Inside the funnel are alignment keys to assure structure is landed in right position when installed.

The structure includes a porch where the UTA will be landed. Beneath the porch is a ROV-panel. Hydraulic jumpers will be installed to interface UTA and ROV-panel.

The top hatch is a hinged hatch. It has handles to lift and pull/push over the hatch. These handles are equipped with monkey fists for ROV access. The top hatch provides protection

against dropped objects. The manifold structure has four anchorage points on top for installation rigging.

Figure 2.2 shows the manifold structure at first-time installation. Included in structure are process piping, process valves, flow line connectors, guide posts, jumper parking panel and anchor.

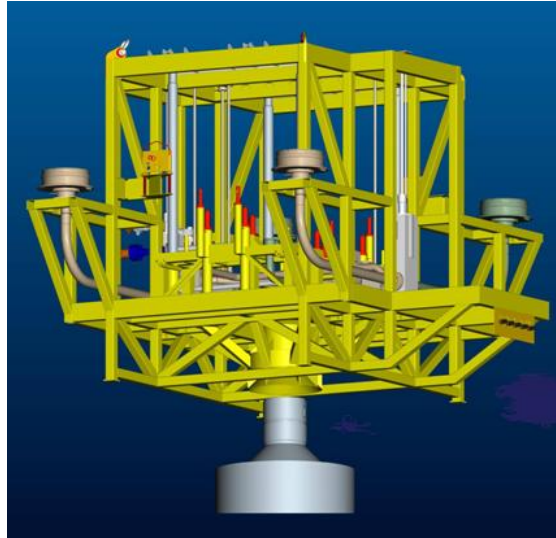


Figure 2.2: The manifold structure at first-time installation

2.2.2. Flowline Connectors

The flow lines are connected to main headers, both for inlet and outlet. The main headers have integrated vertical hubs as the connection point, and the hubs are bolted to the FDS structure and welded to the piping. Figure 2.3 shows the Azurite flowline connector.

Hubs may come from external contractors, mainly due to the high costs related to fabrication. It is for that reason not given that hubs automatically can be welded onto piping in FDS-structure. In those cases a pup piece is used as an extension of piping that can be welded both to hub and to piping.

Flow line connectors are included in manifold structure during fabrication.

Figure 2.3: Flowline connector



2.2.3. UTA (Umbilical Termination Assembly)

The UTA is an assembly for terminating the subsea end of the umbilical. The umbilical is a combined power and control umbilical and it provides the necessary mechanical, electrical and hydraulic conduits to the subsea installation. Jumpers interconnect the umbilical's individual conduits with the remainder of the subsea equipment.

The umbilical itself comprises of high voltage electric cables for power supply to the pump (or compressor in other projects), low voltage electric cable for power supply to the subsea communication and hydraulic lines for control fluid, chemical injection and barrier oil supply. If a subsea control system is included in the system there will also be fiber optic lines for communication with the control system (which is not the case on Azurite).

Inside the UTA sits the Umbilical Termination Head (UTH), which is the subsea end of the umbilical. Figure 2.5 shows a picture of UTH only, and one can see that umbilical is brought in as a single unit and that conduits in the umbilical are organized and distributed in the UTH. The UTH includes termination of high voltage power jumpers and a ROV-panel for hydraulic stabs and signal stabs. The ROV-panel is faced outwards on the starboard side of the FDS. The hook up of the UTH inside the UTA is done offshore on appropriate installation vessel, where the UTH is bolted into the UTA on a hang off flange.

During hook up, low voltage pigtails are connected to UTA junction box, and low voltage jumpers from junction box to ROV-panel. Further, the high voltage connectors are mounted to connector plates and pigtails are secured onto cable trays. The high voltage protection head is mated to high voltage receptacles on UTA. The hydraulic lines are connected to respective spots on ROV-panel. The hydraulic and signal receptacles on the ROV-panel are secured with protection stabs (dummy connectors). Figure 2.4 shows UTH installed in UTA, with high voltage protection heads.

The UTA is located on the porch on the FDS structure. UTA is equipped with a guide post that interfaces with guide funnel on FDS porch. It is installed in a single, individual operation after the FDS structure has been installed. The UTA is designed to lift its own weight plus the submerged weight of the umbilical, and can thus be lowered into sea hanging from umbilical.

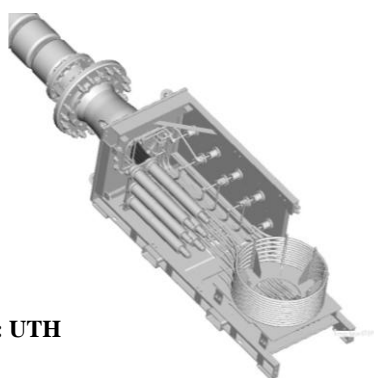


Figure 2.5: UTH



Figure 2.4: UTH installed in UTA

There are certain limits to the inclination of the three degrees of freedom of the UTA during landing on the FDS: plus minus maximum 5 degrees in lateral, longitudinal and horizontal orientation. Figure 2.6 shows the UTA at first-time installation. At this stage the UTA will be fitted with the following items:

- 2 high voltage connector protection heads (to be removed by ROV prior to jumper installation)
- 8 hydraulic female dummy connectors (to be removed by ROV prior to jumper installation)
- 2 low voltage dummy receptacle connector shorted (to be removed by ROV prior to jumper installation)

The UTH is protected against dropped object through a lattice structure which is shown on figure 2.6

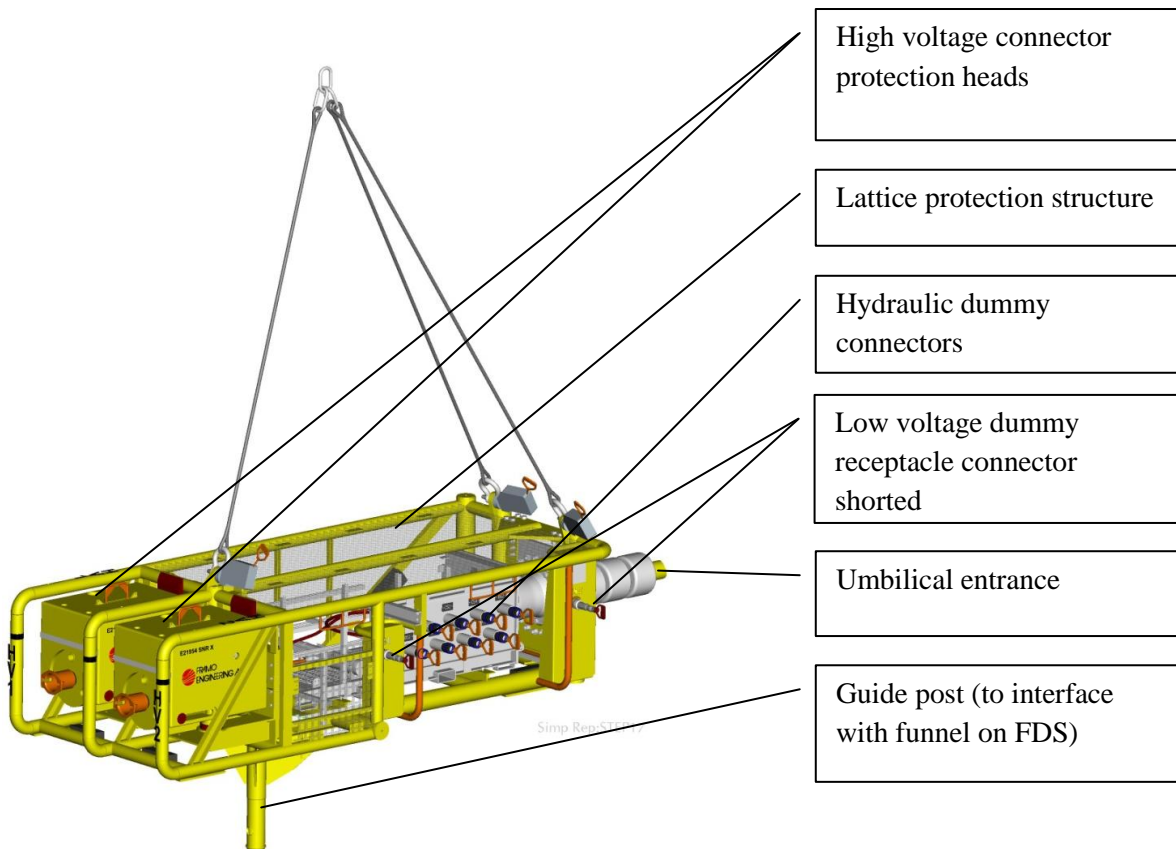


Figure 2.6: UTA at first time installation

2.2.4. MPP (Multiphase Pump)

A MPP can accommodate the complete production from a well, for example oil, gas, water and sand, without having to separate or process the production stream near the wellhead.

Framo MPP uses helicon-axial technology based on the rotodynamic pumping principle. Figure 2.7 is a typical Framo pump design, showing the Azurite multiphase pump. Framo pump units are designed with identical interfaces to ensure the ability of replacement independent of project. It also enables the possibility of re-using running tools.

Electrical pumps must be isolated from surrounding fluids to keep the pump from short circuit. The Framo MPP uses an oil filled electrical motor. The oil works as a barrier system, and it is at all times kept at an overpressure compared to external water pressure to keep water from penetrating protected areas. It is of great importance that the pressure is monitored and maintained both during installation and operation. The fluid used is hydraulic oil with de-electric properties.

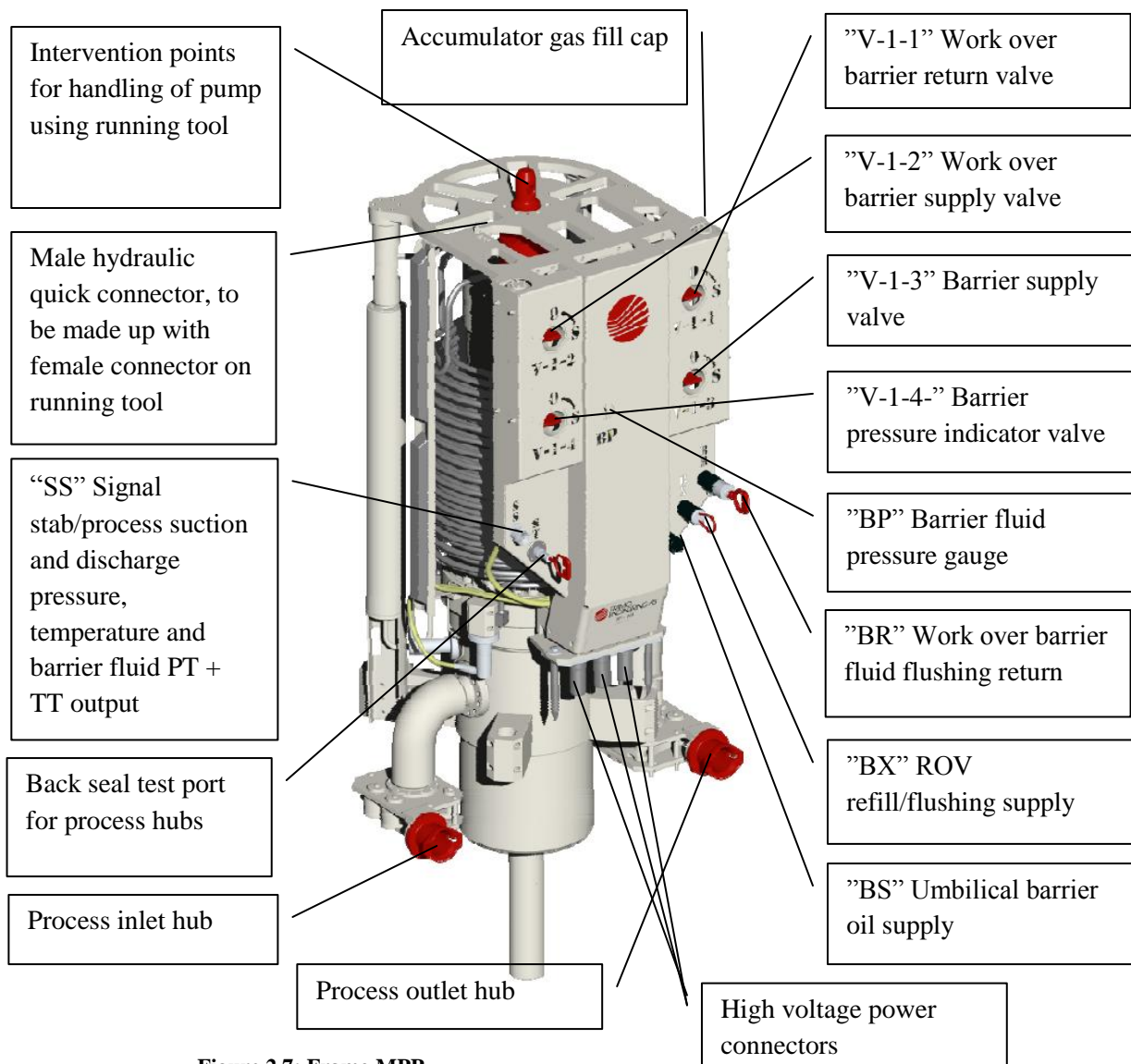


Figure 2.7: Framo MPP

During normal conditions when pump has been installed, the barrier fluid is supplied to pump through the umbilical. From ROV-panel on FDS, the barrier oil runs through a hydraulic jumper to the pump, through the BS-inlet. Barrier supply valve must then be open.

During installation or interventions, the pump is supplied with barrier fluid from accumulators on the running tool. Barrier fluid is supplied to pump through an inlet on top of pump (accumulator gas fill cap). The work over barrier supply valve must be kept open in order for this to happen.

When the pump has been landed on seabed, the barrier supply jumper from the umbilical is connected to the BS-inlet on the pump. A wet connector like this one may cause unwanted components to infiltrate system and connection points must be flushed before barrier fluid can run from umbilical to pump. A barrier return jumper is installed between BR on pump and the running tool. The pink line on the flow diagram on figure 2.8 shows how system is flushed. When system has been flushed in approximately five minutes, the valve position of V-2-3 will be changed to *Sample* (green line and accumulator). The sample will be brought to surface with disconnected running tool for inspection. In the time from running tool is disconnected until sample has been checked and approved, the barrier oil is supplied from accumulators in the pump, which can be seen in the flow diagram. If acceptable sample values are obtained, barrier supply valve will be opened and pump will receive barrier fluid from umbilical.

The ROV-operated valves on the MPP ROV-panel, V-1-1, V-1-2-, V-1-3, V-1-4 and V-2-1, V-2-2, V-2-3, are 90 degrees actuated valves; they can either be in open modus or in shut/closed modus, marked with *O* and *S* respectively.

The pressure gauge on the ROV-panel of the pump shows the pressure of the barrier fluid. When not employing submerged ROV there is no need for gauge to display pressure. To avoid potential leakages the barrier pressure indicator valve is therefore normally closed. However, during installation this valve will remain open. ROVs will record pressure gauge at a regular basis during all installation activities. During descent of the Azurite pump, the crane operations will stop at four different water depths and ROV will monitor pressure gauge. Water depth will influence the number of stops.

As mentioned, the motor section and seals are during installation and operation filled up with barrier oil. During transportation the pump may not be filled up completely due to temperature changes and consequent changes in volume of the oil.

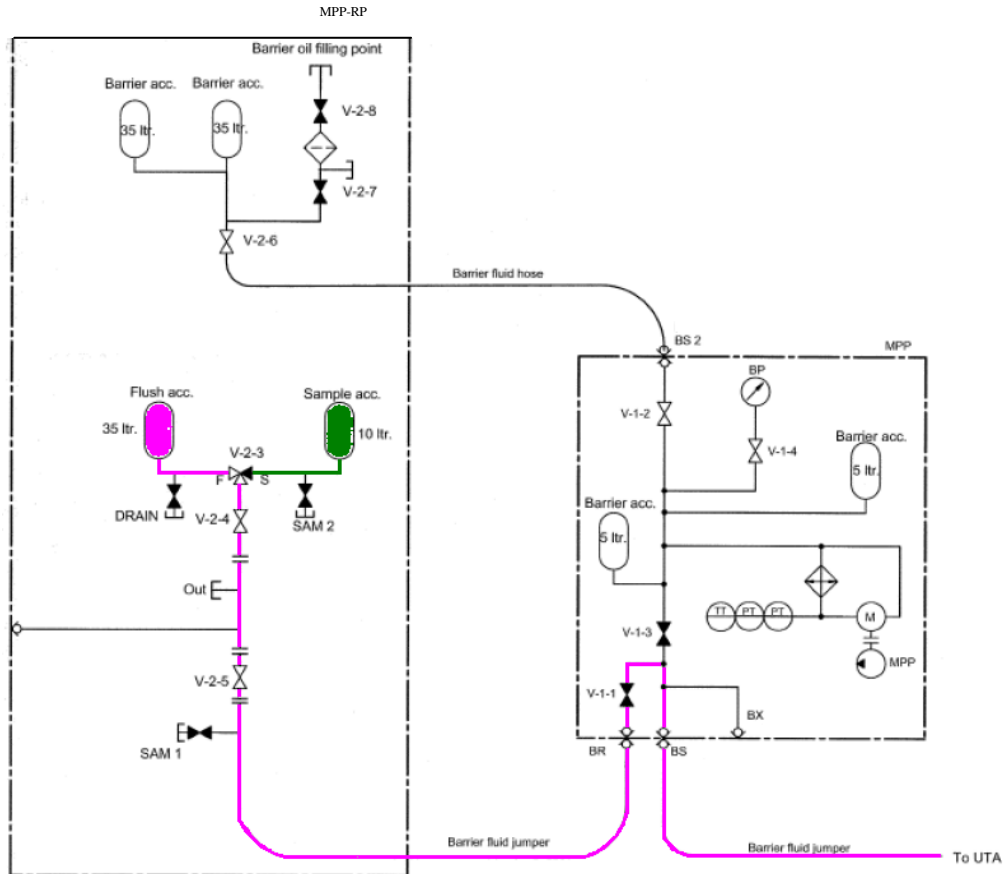


Figure 2.8: Flow diagram between MPP running tool and MPP

2.2.5. Process Piping

The process piping within a FDS can be configured to allow for a variety of pump operations. The Azurite development consists of two individual pumping systems in bypass to the main headers, but other system may use the pumping systems in parallel or in serial, depending on need from client. The two systems on Azurite are identical and located downstream the manifold. There is also full flexibility to route all wells into any header. Figure 2.9 shows the process flow diagram.

The process piping is installed during fabrication. The piping is arranged in a way that allows for re-circulation of fluid; discharged flow from MPP may enter the re-circulation line to assure stable suction. The re-circulation line is controlled by one ROV operated gate valve (V6) and also a choke to control flow rate (V4). Re-circulation lines can be seen in pink colour in figure 2.9.

A methanol injection line is connected to the re-circulation line. A valve controls the injection of methanol. The valve (V5) is normally closed but can be opened by ROV if needed.

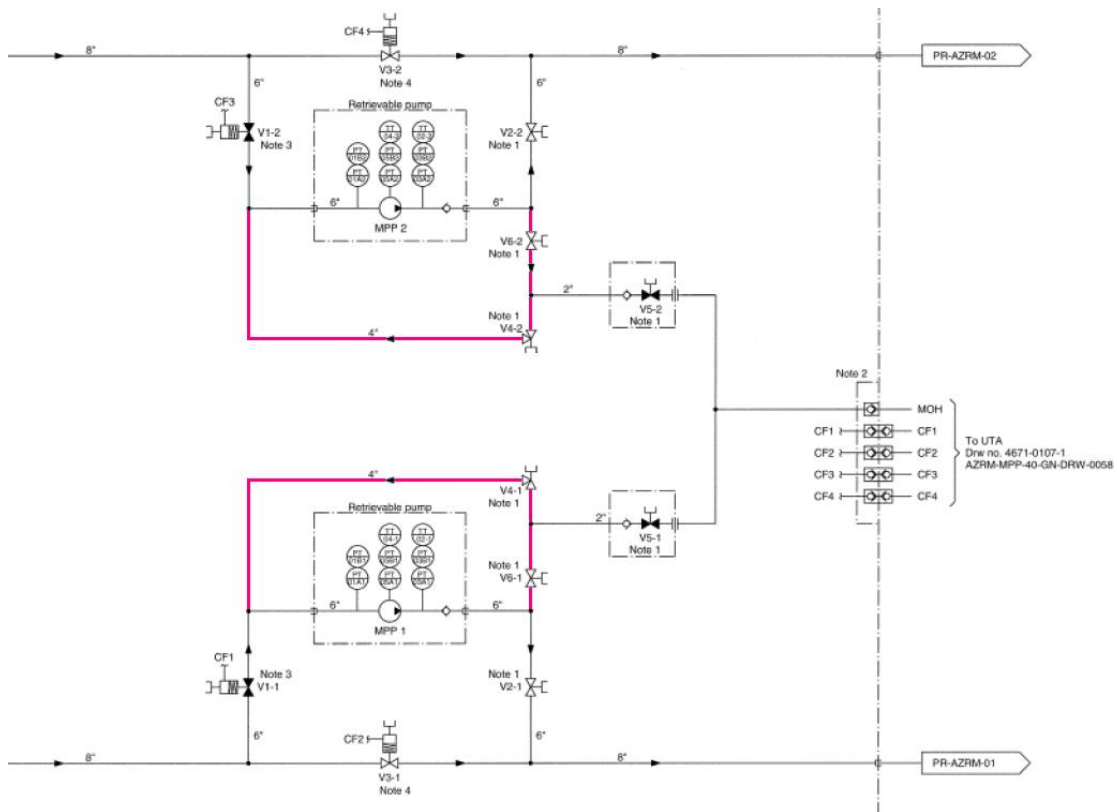


Figure 2.9: Flow diagram for process piping

2.2.6. Process Valves

The process valves are devices that direct the process flow through the FDS. In the Azurite pump station there are six process valves. The valves can be seen in figure 2.9. The process valves are as follows:

- ***V1 – Actuated gate valve***
The V1-valve controls if process fluid can enter the multi phase pump or not. This valve needs to be a fail-safe-close valve, and will shut if unwanted events occur and pump must be isolated from process flow. The gate valve is operated through hydraulic lines and is controlled from topside. The valve can also be closed/opened manually by ROV.
- ***V2 – Manual gate valve***
The V2-valve is the discharge valve from the multiphase pump. The gate valve is normally open, but can be closed if one wants to isolate discharge from the flow line. The valve is manually operated by ROV.
- ***V3 – Actuated gate valve***
The V3-valve controls if fluid is directed pass or through the multi-phase pump, and is a fail-safe-open valve. The gate valve is operated through hydraulic jumper and is controlled from topside. The valve can also be closed/opened manually by ROV.
- ***V4 – Manual choke***

The V4-choke is located on the re-circulation line. The choke does not close flow line completely, but it chokes the flow to desirable flow rate. The choke is manually operated by ROV.

- **V5 – Manual gate valve**

The V5- valve is a methanol injection valve. This valve is normally closed, but can be opened if methanol is needed in the system. Methanol is supplied to pump through umbilical, and the flow can only go from UTA to pump. The valve is manually operated by ROV.

- **V6 – Manual gate valve**

The V6-valve is a gate valve located on the re-circulation line. When closed the valve keeps fluid from entering re-circulation line after it has been through the multi-phase pump. The valve is manually operated by ROV.

The valves V1-V4 are manually operated by ROV on top of FDS-structure. Flexible extension shafts are included between top of valve and the ROV-buckets. The valves V5 and V6 are accessed horizontally via a ROV-panel. See figure 2.10 for location of these interfaces.

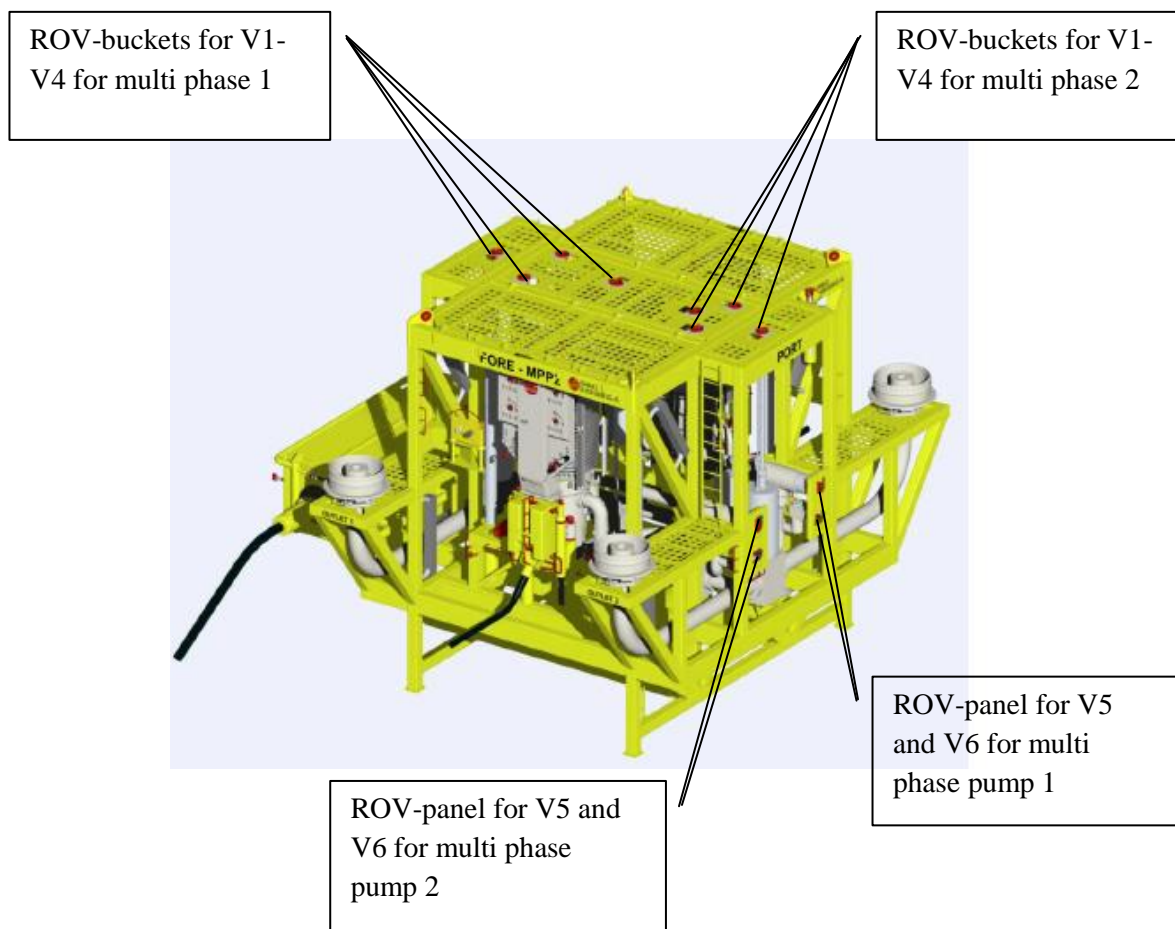


Figure 2.10: ROV-interfaces on FDS

2.2.7. Power Jumpers

High voltage cables are used for power supply to pumps. A multiphase pump demands for three-phase electric power, and it is supplied to the FDS through an umbilical. The HV jumper transports high voltage power from UTA to multiphase pump and it is a long cable (45 meters for the Azurite FDS) with two different heads: one for mounting of the UTA and one for mounting on the multiphase pump. Each HV jumper (one for each pump) includes three separate lines with three different phases. Figure 2.11 shows how HV jumpers are organized on Azurite FDS.

The HV jumpers are installed close up to installation of multiphase pump. The dummy pump must be removed before HV jumper head are installed, and the HV jumper head on pump side must be installed before pump is installed. The FDS has dedicated guide posts where HV jumper head is locked onto.

The HV connectors on the UTA side are installed with protection heads, as was shown in figure 2.6. These protection heads are installed to protect the connections from the environment in the time period from UTA is landed on FDS and until pumps are installed. The protection head must be removed before installing the HV jumper head on the UTA side.

There are certain limits to the bending radius of the HV jumper. Consequently must cable be of certain length to have the ability to be routed to ensure bending radius is of satisfactory value.

The power jumpers inside the UTA are shown in red colour in the flow diagram in figure 2.12.

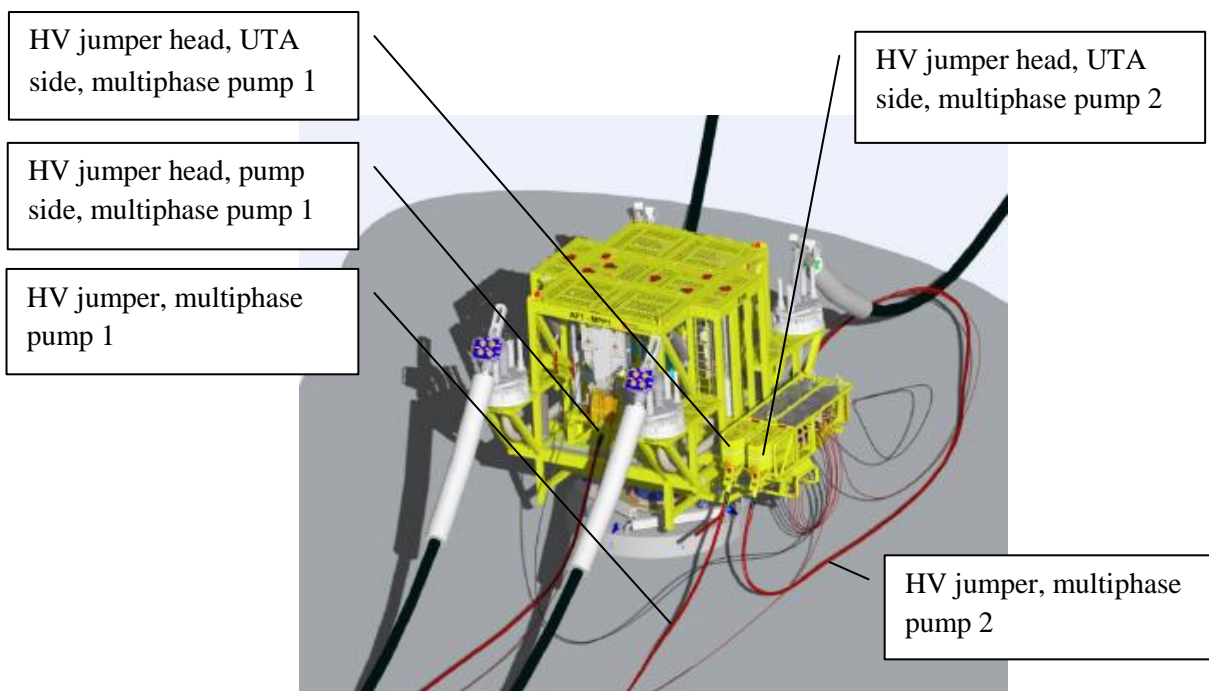


Figure 2.11: Power jumpers and jumper heads on UTA and MPP

2.2.8. Signal Jumpers

Low voltage (LV) cables are used for power supply to the communication system between subsea installation and topside. LV power is supplied to FDS through the umbilical. The LV cables include five quad lines which are distributed through a junction box in the UTA. From junction box the LV power goes on in two separate lines, one to each connection point on the ROV-panel on the UTA. Signal jumpers are the connection between UTA and pumps. The two jumpers are connected to the SS-inlet on each pump.

During interventions the signal cable can be temporary parked in the jumper parking panel if needed.

The LV jumpers, or signal jumpers, convey information about process temperature and pressure and barrier fluid temperature and pressure from seabed to topside.

The low voltage cables inside the UTH are shown in green colour in the flow diagram in figure 2.12.

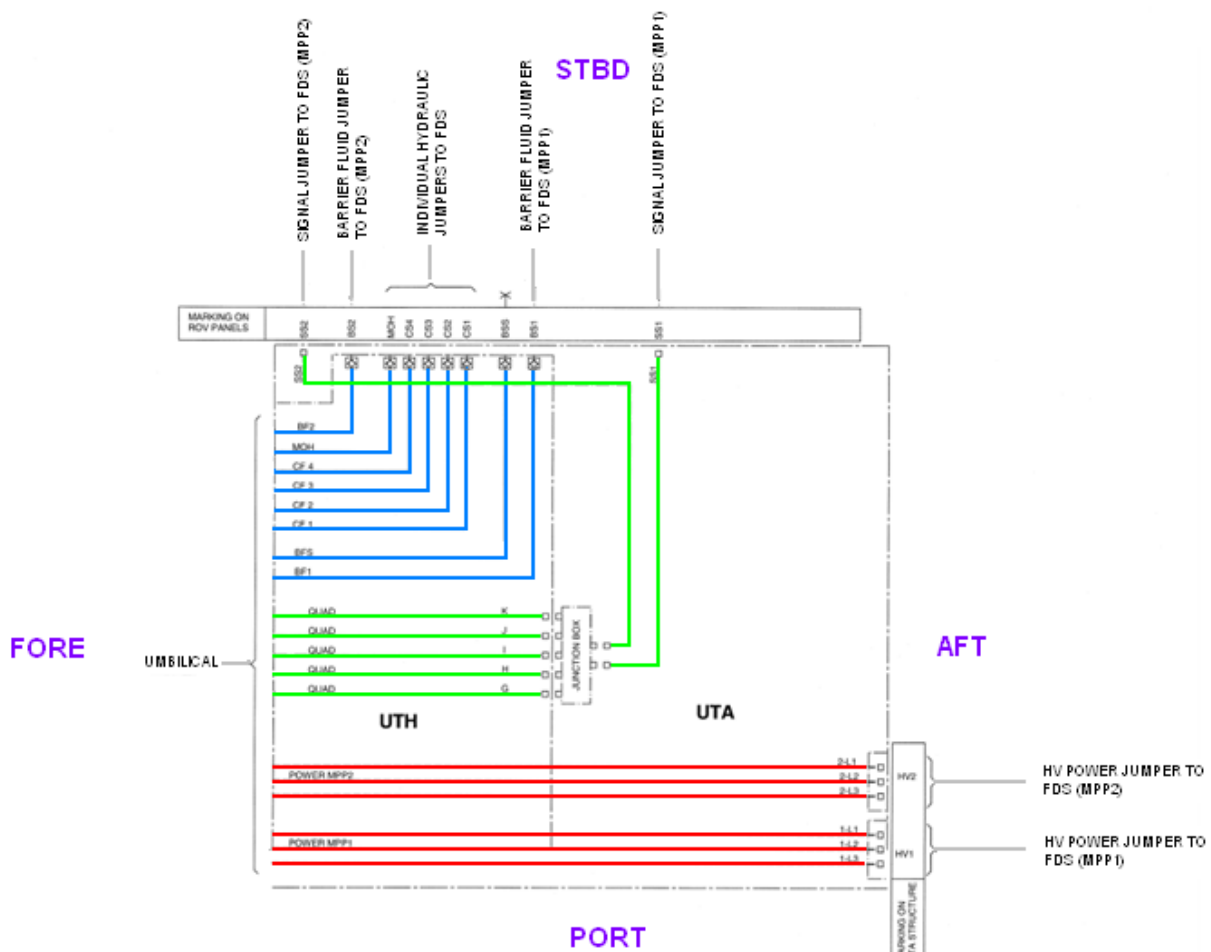


Figure 2.12: Flow diagram showing HV power jumper, LV power jumper and hydraulic jumpers

2.2.9. Hydraulic Jumpers

Hydraulics is provided to the subsea installation through lines in the umbilical. Hydraulic lines deliver chemicals, control fluid and barrier oil to the FDS. The hydraulic lines terminate in the UTA and from there hydraulics flow in hydraulic jumpers. Figure 2.13 shows how hydraulics is transported in jumpers from UTA to FDS.

There are seven hydraulic jumpers in the Azurite FDS system. There are two barrier fluid supply jumpers, one to each pump. They run from the UTA to corresponding multi phase pump. There are four jumpers with control fluid supply. These lines run from the UTA to the ROV-panel on the FDS-structure. The distribution channels from ROV-panel to dedicated end targets are the hydraulic tubing. There is also one methanol supply line that runs from UTA to ROV-panel on the FDS-structure. The methanol line is connected to flow lines and a methanol injection valve governs the inlet.

The umbilical also houses one barrier fluid spare line. It is connected to UTA ROV-panel like the other lines, but under normal conditions no jumper runs from its outlet on the UTA. Both two other barrier supply jumpers can be connected to the spare line in case of unexpected events.

The hydraulic lines in the UTH are shown in blue colour in the flow diagram on figure 2.12. The diagram shows how all eight hydraulic lines terminate on the inner side of the ROV-panel of the UTA. Further, seven of the eight are connected to jumpers while one is the spare line, marked with a cross.

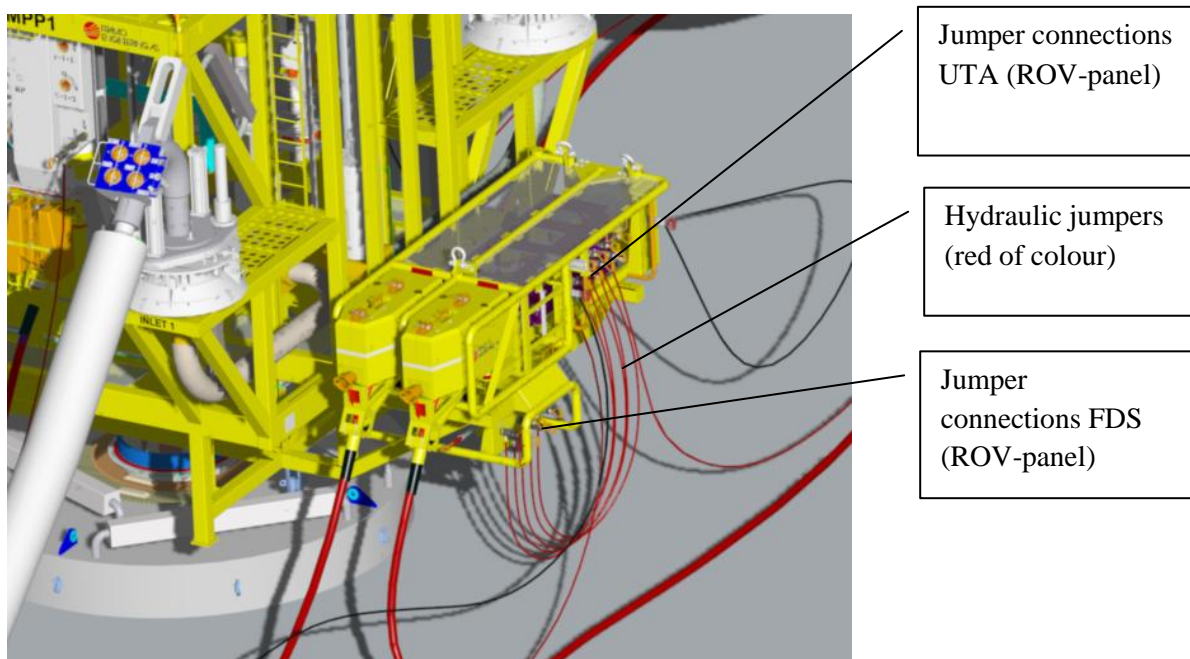


Figure 2.13: Hydraulic jumpers running from UTA to FDS ROV-panel

2.2.10. Hydraulic Tubing

Hydraulic tubing is the distributions channels for the hydraulics in the FDS. The tubing is routed in protected areas to avoid damage from dropped objects and other damaging occurrences.

Hydraulic tubing is installed in FDS during fabrication.

2.2.11. Power and Control Module

Power and control modules can either be installed as a part of the subsea installation, or it can be included in topside facilities. It is an important part of the total system as it monitors and controls installed equipment, as well as supplying the necessary power. For Azurite the power and control module is located topside.

2.2.12. Guide Posts

Guide posts are used as steering units during interconnection of two items. Figure 2.14 shows an example of a guidepost and a guidepost receptacle. The interconnection on the figure is between the UTA and the FDS. A guide post is mounted onto the UTA, while a funnel is welded onto the FDS. During installation, the guide post will slide down the funnel walls leaving the UTA in the correct position. Alignment keys are often included in funnel to make sure the retrievable item has the right alignment.

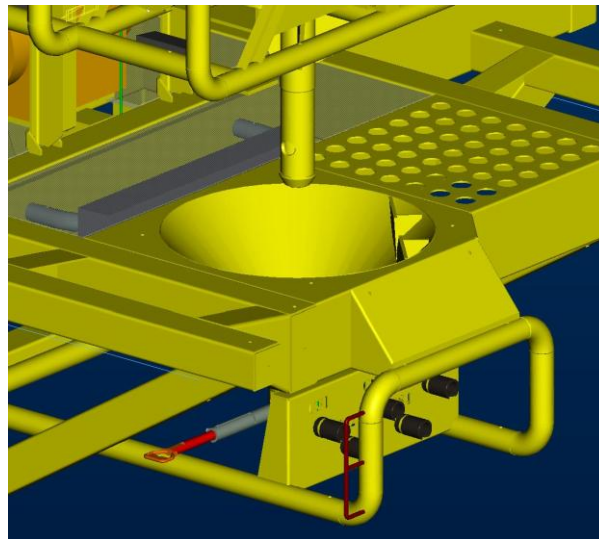


Figure 2.14: UTA guidepost interfaces FDS funnel

The FDS includes guide posts that interface with guide funnels on running tool during pump interventions. The guideposts are extracted to top hatch. Guideposts extensions are used to make the entry of the running tool easier. Two different-length extensions are attached to posts before intervention. Running tool will land on highest post first as it is difficult to land on two posts simultaneously, and will thereafter find its way to the second post, either by

ROV-assistance, guide wires or vessel movement. The configuration also ensures correct mating of running tool so that pump is landed in the correct direction relative to FDS; long guide post shall meet left side of pump and short shall meet right side of pump. If water depth is sufficiently small, guide wires can be connected to the guide posts on the FDS and to the running tool funnel. Running tool will then slide straight onto guide posts. The water depth on Azurite field does not allow for this.

The guide posts on the transport skid interface with the same guide funnel on running tool as FDS-structure does. Figure 2.15 shows the configuration with the transport skid. The FDS-structure also has three mini guide posts that pump is landed on, two on the front side of the pump and one on the back side. The transport skid is equipped with similar mini posts with same interface point on pump.

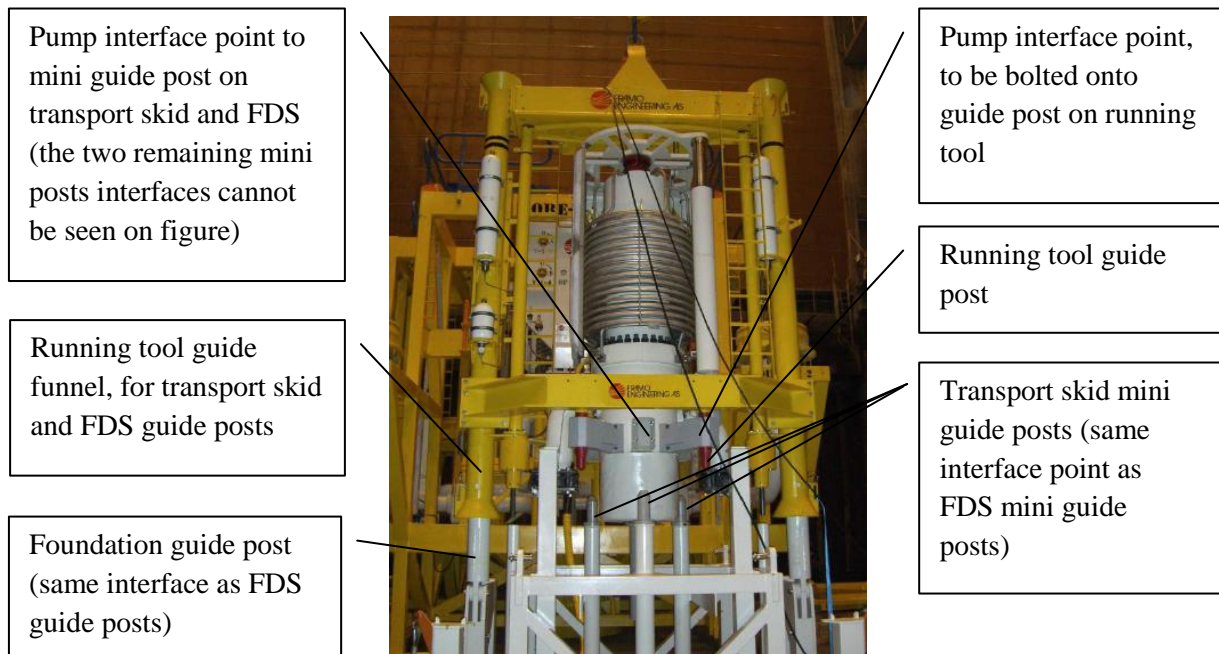


Figure 2.15: Interface points between pump, running tool and transport skids, seen from pump rear side

2.2.13. Dummy Pump

A dummy pump is installed in FDS during first time installation. The dummy pump is connected to process pipes and provides with that a protection of the process hubs. The process inlet and outlet, which can be seen on figure 2.16, are blind hubs. The process fluid will consequently flow straight through the FDS without interference. A back seal test port and electrical HV connectors are also included on dummy pump. The HV connectors provide protection of the HV jumpers.

The dummy pump is designed to be maneuvered with same running tool as the MPP. It is also to be installed in MPP transport skid during offshore lifting and transportation. The dummy pump does with that not require any special adjusted equipment.

The dummy pump will replace the MPP if it is retrieved for a longer period without redundant MPP being installed.



HV connector protection stabs

Figure 2.16: Dummy Pump

2.2.14. Pump Transport Skid

The pump transport skid is meant to work as a physical protection case for the pump during different activities. Such activities are road transport in the horizontal condition, horizontal yard lift and lifting from horizontal to vertical and vice versa, vertical sea transport and vertical offshore lift in air. Figure 2.17 shows the transport skid with and without the pump inside. The transport skid has three guide posts that interface with pump. These guide posts are similar to the mini guide posts on the FDS-structure and both utilize same interface points on pump.

The transport skid is a two-piece structure in the vertical direction, bolted together with a single bolt in each corner. This configuration makes it possible to tilt the top part of the skid using the bolted connection as a hinged mechanism. When the top part is tilted, it allows for access to the top part of the pump.

The four corners on top of the transport skid have lifting arrangements welded on.



Figure 2.17: Pump transport skid, with and without pump

2.2.15. Pump Running Tool

The pump running tool accommodates the pump during transfer from topside to subsea installation. It is designed to intervene on both the pump and the dummy pump.

Figure 2.18 shows the running tool without any pump attached to it.

The running tool consists of a structural main frame. On each side of the frame, there is a funnel. The bottom part of the funnels is landed on dedicated guide posts on the FDS-structure during installation of the pump. The side wall funnels also interface with guide posts on the running tool transport skid. A guide wire lock sits on each funnel and provides the ability to interface an installation tower cursor system. The running tool can be used with or without guide wire assistance.

Next to the bottom funnels, there are two vertical shock absorbers whose task is to damp vertical movement when the running tool interfaces with other objects. When the pump is suspended inside the running tool, the tool will thus function as a bumper protection for the pump, due to both shock absorbers and structural frame.

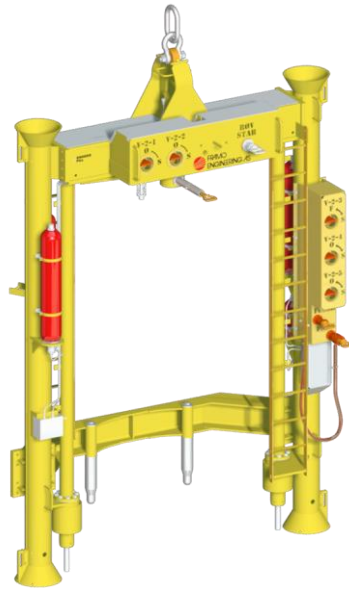


Figure 2.18: Pump Running Tool

Transverse on running tool is a beam with two guide posts. These mates with funnels on the pump rear side, keeping the pump in place inside the running tool during interventions. The dummy pump has two holes in the main plate serving the same purpose.

When the running tool has landed on the FDS guide posts, the final installation is done with a hydraulic cylinder. The FDS has got dedicated guide pins to ensure final alignment. When the pump has reached its final landing position, the running tool will lift off on the guide posts using the hydraulic cylinder.

The right guide funnel includes a ROV-panel for flushing and verification of barrier fluid supply. The three ROV-operated valves, V-2-3, V-2-4 and V-2-5 are found here. These are flush/sample valves for the work over system. In addition there is a flush stab and a connector with a barrier return jumper. This is the jumper connected to the BR on the MPP when flushing and it is shown on figure 2.8. The jumper comes down connected to the flushing return accumulator in one end, and parked on a parking panel in the other end.

The barrier oil supply valve, V-2-6, the barrier oil filling of accumulators valves, V-2-7 and V-2-8, and the sampling and draining point valves of the running tool can only be operated in air. During installation these valves are left in *Open* position.

On the transverse interconnection on the top of the running tool there is a secondary ROV-panel. On this panel sits two hydraulic supply valves. These valves, V-2-1 and V-2-2, control operation of running tool hydraulic cylinder. On ROV-panel there is also a running tool stab where control fluid is supplied from ROV through a jumper.

An interface connector mechanism is also located on the transverse interconnection on top of running tool. It connects and locks MPP to running tool. The mechanism has an ROV-handle.

2.2.16. Transport Skid for Pump Running Tool

The transport skid for the pump running tool provides protection and support for the running tool during lifting operations and transportation. It is designed to handle horizontal transportation of the running tool, and horizontal lifting of the skid with the running tool installed in it.

The transport skid for the running tool is designed so that it interfaces with the pump running tool, which can be seen in figure 2.19. This enables running tool to connect to pump without either of them having to be removed from respective transport skids.

The guide posts on the running tool are hinged posts, allowing for running tool to be tilted while still parked in skid. Consequently can running tool be lifted directly from the skid in lying position.

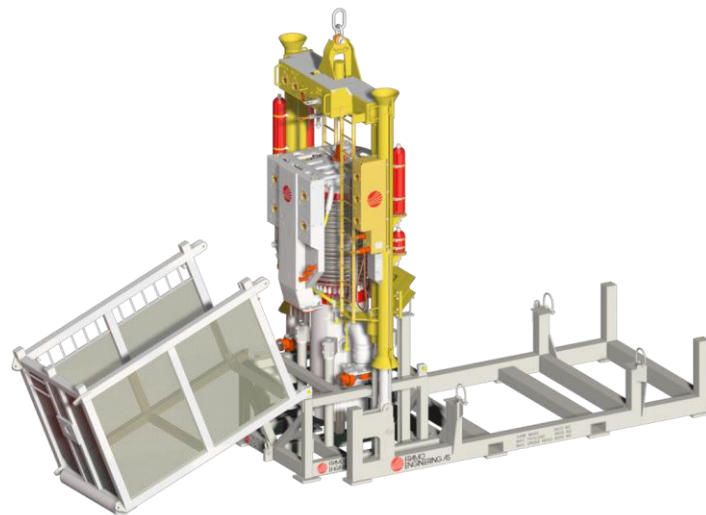


Figure 2.19: MPP, MPP RT, MPP transport skid and MPP RT transport skid mounted together

2.2.17. Jumper Parking Panel

In the case where a unit needs to be retrieved, a dedicated parking panel provides temporary parking of jumpers. The parking panel is installed onto the FDS in such cases, and does not form a part of the permanent subsea system. The panel is an expensive piece of equipment, and thus is parking panel often not stationed at one particular vessel, but moved around to where it is needed. Figure 2.20 shows a jumper parking panel used on Azurite, where one can park the barrier fluid jumper and the signal jumper.



Figure 2.20: Jumper Parking Panel

2.3. Installation Sequence

This chapter will give an overview of the activities related to installation of the different parts of the Azurite subsea multi phase pumping system. FDS, process risers and jumpers, UTA and umbilical are installed prior to FDPSO arrival on site. It requires temporary wet park of topside ends.

It is assumed that suction anchor has been installed on seabed prior to installation of all components of the MPP.

2.3.1. Installation of FDS

The FDS is the first component to be installed. During initial installation the FDS will consist of the following main items:

- 1 off manifold structure including process piping, process valves, flow line connectors (hubs), guidepost, ROV-panel and UTA landing platform
- 2 off dummy pumps (individual retrievable with dedicated running tool)
- 4 off retrievable pressure caps for the process hubs
- Installation rigging (see figure 2.21)

A survey of the installation area on seabed shall be accomplished prior to installation of FDS.

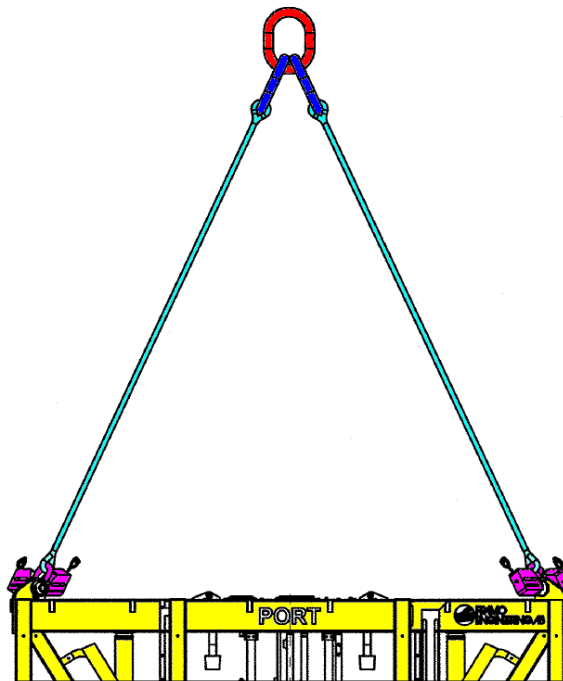


Figure 2.21: Installation rigging during first time installation of FDS

The FDS will be stored and transported on sea on a typical supply vessel. The structure will be launched by a crane from a lifting vessel. The crane's lifting equipment is attached to the FDS through four anchorage points in each corner of FDS. The interfaces are equipped with ROV-shackles, allowing for ROV to open and close the shackle using a manipulator arm.

Before the lifting operation starts the vessel is offset from installation position. This assures no potential dropped objects hit any installations on seabed during launching.

Tugger winches are attached to FDS for stabilization during the topside lift. The winches are removed after FDS has been lowered through splash zone. Lowering the FDS through the splash zone shall be done in a continuous movement to prevent FDS from residing in the zone.

A mid-water transfer of FDS is performed during the lift. The load is transferred from the crane to a pennant winch on the lifting vessel. The hang-off frame allows for finer control during the last part of the lift. The crane hook is brought back to the surface in order to bring the FDS load through pennant winch onto the crane hook again.

When the FDS has been lowered to about 10 meters above the seabed, the vessel is shifted to bring FDS above the suction anchor with the landing pile. Tugger winches or clump weights are attached at this point if applicable. The FDS is slowly lowered to engage its guide funnel onto the pile. The structure is adjusted with alignment keys to assure correct orientation between pile and FDS. The FDS is then landed carefully onto the pile and it is verified that the structure is rotated correctly into position. The ROV shackles will be disconnected and the lifting equipment retrieved to surface. A FDS valve check and reconfiguration is performed with ROV.

2.3.2. Installation of UTA

Some deck preparations must be done prior to the installation of the UTA. The umbilical shall be leak tested and be kept at an overpressure to ensure no ingress of water throughout the wet park period until topside pull in and establishing supply from the barrier system. The UTH is assembled into UTA.

The UTA is lifted through the splash zone and water column in the same manner as for the FDS. It is landed into the guide funnel on the FDS shown in figure 2.14, aligned and locked to the structure. After landing ROV shackles are opened and lifting sling is removed.

2.3.3. Retrieval of Dummy Pump

Prior to retrieval of dummy pump it is important that FDS valves are configured in correct positions. V1 and V2, which are the in and out gate valves of the pump must both be closed. Consequently must the gate valve V3 be open to allow process fluid to flow through FDS without interfering with pump. V4 choke valve must be more or equal to 5. The methanol

injection valve V5 must be closed, while re-circulation line gate valve can remain open. The dummy stab in the ROV stab manifold on running tool is removed to allow supply of hydraulics from ROV and the manifold is checked for damages. Accumulators on running tool are flushed and sampled to assure clean barrier fluid.

The area on the landing deck on the installation vessel must be prepared for the retrieval of the dummy pump. The MPP transport skid for the dummy pump must be empty, and it is mated into the running tool transport skid. The two are locked together with bolts which allows for the running tool and the dummy pump to be landed and installed into respective transport skid on the same location on deck. The transports skids and the running tool shall be visually inspected for damages prior to the retrieval operation.

Before running tool is put to use one must verify that the lifting cylinder is in retracted position, ready to handle the dummy pump. It is also important that the dampers are in extended position. The connector on the running tool that interfaces with pump top end must be unlocked before retrieval, and handle pulled out.

The running tool is connected to crane hook through its top anchorage point. Running tool can be raised to vertical without disconnecting from transport skid due to the flexibility of the transport skid guide posts. When preparing for operation, running tool is raised to vertical and guide posts are locked to keep their vertical position. The bolts locking running tool funnels to guide posts are released and running tool is lowered until crane gets slack. Running tool is now resting on guide posts, and it is free to be lifted off transport skid at any time.



Figure 2.22: Testing of FDS hatches in dry dock

Before the lifting operation starts, a ROV opens both hatches on the FDS above pump to be retrieved. Figure 2.22 shows a picture of a ROV opening one of the hatches above MPP 1. The picture is taken during onshore testing. After hatches have been opened, the guide posts extensions are installed. A ROV also opens inlet and outlet clamps on dummy pump before lifting starts, so that pump is free to be retrieved.

The installation vessel is moved offset from any subsea installations before lifting of running tool starts. The running tool is lifted off transport skid and launched overboard. To ensure safe handling one rope runs through each funnel to control running tool manually from deck. Running tool is lowered until 20 meters above seabed. At this location the installation vessel repositions so that running tool sits straight above MPP. The running tool is lowered onto the longest guide funnel first, and then lowered further down to meet the smallest guide post. A ROV verifies that running tool guide funnel match the correct guide post; the running tool ROV-panel shall face out of FDS. The running tool is lowered until the lifting line goes slack. A ROV is used to observe. ROV also observes and verifies that the running tool is in correct landing position. When accomplished, lifting line may be disconnected and installation vessel moved off location, if requested by Contractor.

While installation vessel possibly is off location, the running tool is prepared for lifting the pump. The handle on the locking mechanism is pulled out and jumper from HPU is connected to ROV STAB on the running tool. The valves V-2-1 and V-2-2 which control operation of running tool hydraulic cylinder must be verified open. The running tool is now ready for mating with pump. The hydraulic cylinders are extended until the running tool starts to lift off from structure. The interface connector between pump and running tool will be locked by pushing in handle and folding over a locking mechanism. The cylinder is thereafter fully retracted. The valves, V-2-1- and V-2-2 are shut.

If lifting line has been disconnected the vessel will now be moved onto location again and lifting line reconnected. Same procedure will follow as when lowering running tool: lift running tool with dummy pump to a height of 20 meters above seabed and stop. Thereafter move installation vessel offset from any subsea installations and continue the operation.

A ROV will carry out an inspection of FDS piping, process hubs, HV connector head, the guide post system and the pump landing area after dummy pump has been retrieved. It will move any debris and wash if needed to remove any fouling. A ROV will in addition visually inspect the dummy pump and the running tool.

The running tool is retrieved with dummy pump to surface. It is landed in its prepared arrangement and secured before any work on equipment is started. The dummy pump is then released from the running tool by extending hydraulic cylinders. Hydraulic is supplied from SHPU. When the running tool starts to lift off, the handling head locking bolt is released. Lifting cylinder is subsequently fully retracted. Running tool is lifted completely off dummy pump and gently landed in running tool transport skid, which is not longer mated with pump transport skid. Running tool is secured with locking bolts and locking pins. The dummy ROV hot stab is mounted back on.

The jumpers and MPP are to be installed immediately after retrieval of dummy pump in order to protect interfaces on FDS. Installation shall proceed within hours, not days.

2.3.4. Installation of HV Power Jumper

Prior to any HV related operation, the installation vessel must receive information from the FDSPO that the MPP power system is isolated and ready for subsea work. Before lifting operations begin the vessel is offset to avoid potential dropped objects from damaging subsea installations.

The HV jumper is mounted on a deployment frame when launched. The frame is designed with cylindrical bars to coil up the HV jumper during installation. The jumper heads interface with frame through funnels and the connection can be locked by use of the ROV D-handles, see figure 2.23. The deployment frame provides lifting points during installation and shall also serve as a protector for jumper and jumper heads when launched and lowered to seabed. The frame has two or more anchorage points for steady lifting and weight distribution. Tugger lines are attached to the deployment frame for stabilization during topside lift. The tugger lines are released when frame has been shifted over the vessel side. Lowering the deployment frame through the splash zone shall be in a continuous movement to keep the assembly from residing in the zone.

When deployment frame is lowered to about 20 meters above seabed, the vessel is repositioned to bring frame straight above landing position. The frame is then lowered and landed as a single item on seabed. After deployment frame is landed ROVs will release jumper heads from frame and land them on the dedicated guide posts on FDS. There must be at least one ROV to do the transfer and one to monitor the jumper departure from the frame. The jumper head on pump side is the first to be installed. Second operation is to remove the HV protection head from UTA and thereafter connect the HV jumper head to its dedicated position on the UTA. Figure 2.24 shows a simplified illustration of the HV power jumper extracted from UTA to MPP.

The deployment frame will be retrieved to surface after accomplished installation, following same procedure as when immersing: retrieve to about 20 meters above seabed and stop. Installation vessel will be moved offset any subsea installation and thereafter retrieval to surface will continue.

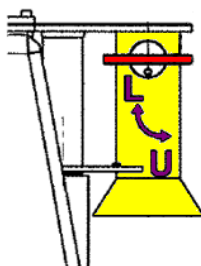


Figure 2.24: ROV D-handle

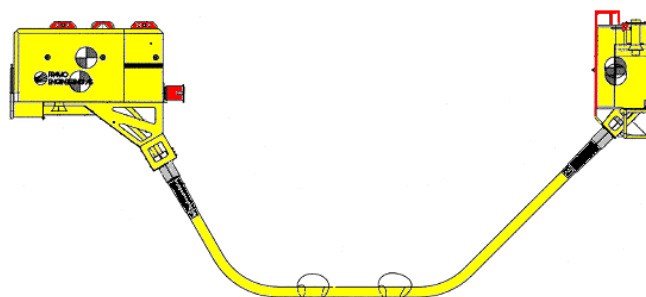


Figure 2.23: HV Power Jumper extracted from UTA to MPP

2.3.5. Installation of Signal and Barrier Oil Jumper

Before the jumpers are launched, the jumper parking panel must be installed.

Signal and barrier jumpers can be launched in different ways. It is desirable to coil jumpers up on a frame to protect them as best as possible when lower through the water column. However, jumpers may be installed using other tools, as for example a bucket. For the Azurite project the signal and barrier jumpers were coiled up on the same deployment frame as the HV jumper. The frame was a two-layer frame allowing for HV jumper to be coiled up on one side, and signal and barrier jumpers on the other side.

Before jumpers can be installed a ROV must remove the dummy connectors from the signal and barrier receptacles on the UTA ROV-panel. When they have been removed and retrieved, the ROV connects the jumpers, first end to the UTA and second end to the jumper parking panel. Jumpers are forced to intersect with flow line path, and must thus be routed in a sensible manner.

All jumper ends have ROV D-handle connectors. Figure 2.25 shows the signal jumper connectors for parking panel side and UTA side, respectively.

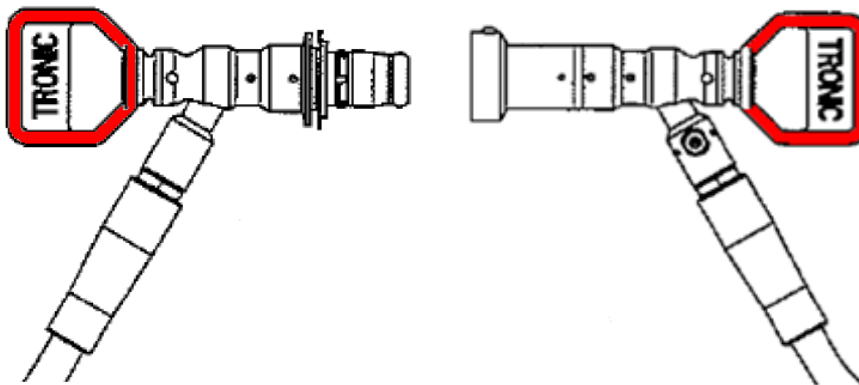


Figure 2.25: Signal jumper connectors with ROV D-handles

2.3.6. Installation of MPP

There are certain activities that must be carried out prior to the installation of the MPP. Protection stabs from hydraulic couplers in the MPP ROV-panel are replaced with dummy connectors. Couplers shall be inspected and checked for fluid leakages during the replacement. The MPP ROV-panel is thereafter flushed and an oil sample is taken to assure no unwelcome ingredients have intruded. The MPP is then filled with correct barrier fluid and pressure tested.

Running tool and transport skids shall be inspected and prepared as described in 2.3.3.

The running tool is mated with MPP while both still mounted in transport skids. Running tool with pump is raised to vertical by the crane. Transport skid locking bolts are removed. Running tool is lowered until the crane gets slack and running tool funnels rest on MPP guide posts. The hydraulic cylinders on running tool are thereafter extended until the running tool starts to lift off and running tool is locked to MPP. Dummy stab from ROV STAB on running tool is disconnected and a barrier supply line is connected between MPP and running tool. The protection stab on the MPP ROV-panel with D-handle must be removed before installation; otherwise the handle will interfere with beam in FDS when the pump is lowered into it.

Before the lifting operation start the vessel must be moved offset any subsea installation. One rope will be mounted in each funnel prior to lifting to be able to manually control running tool from deck. Running tool with pump is lifted free from transport skid and launched overboard.

Pressure should be monitored four times during descent of Azurite MPP by help of ROV.

Running tool with pump is lowered until 20 m above seabed where vessel is repositioned above correct location of MPP. Running tool is lowered down on guide post as during retrieval of dummy pump. BR, BS and SS jumpers are connected to dedicated locations on MPP ROV-panel. Running tool flush and sample accumulators are filled before running tool is disconnected and retrieved to surface, following the same procedure as during retrieval of dummy pump. The oil sample is retrieved to the surface and immediately evaluates. If sample is not accepted the running tool must be prepared for new oil sample. If the sample is accepted the barrier supply valve can be opened, allowing umbilical to supply barrier oil to MPP.

The running tool should be hosed down with fresh water on deck. The extended guide posts on FDS on the seabed may be moved to second pump position if only the first pump is installed. If not they shall be retrieved to the surface. A ROV will close respective hatches above installed pumps.

2.4. Tordis IOR

The Tordis field is an oil field located in the Tampen area in the North Sea where production was started in 1994. Tordis is developed with subsea installations only, and the well stream is tied back to the Gullfaks C platform. The water depth is approximately 200 meters.

After some years of production the Tordis field experienced a marked decline in the production rate, and also a rise in the water cut. This resulted in Tordis Improved Oil Recovery (Tordis IOR) project, and in 2007 the world's first full-scale commercial subsea separation boosting and injection system (SSBI) was installed. Included in the system was a separator that removes water from the well stream, a multiphase pump for boosting the production rate, and a water injection pump to discharge separated water into a disposal well. Framo delivered both pumps for the project, in addition to a power umbilical, an umbilical termination assembly, jumpers, a topside hydraulic power unit and a topside pump control system. Figure 2.26 shows the two Framo pumps as a part of the complete SSBI.

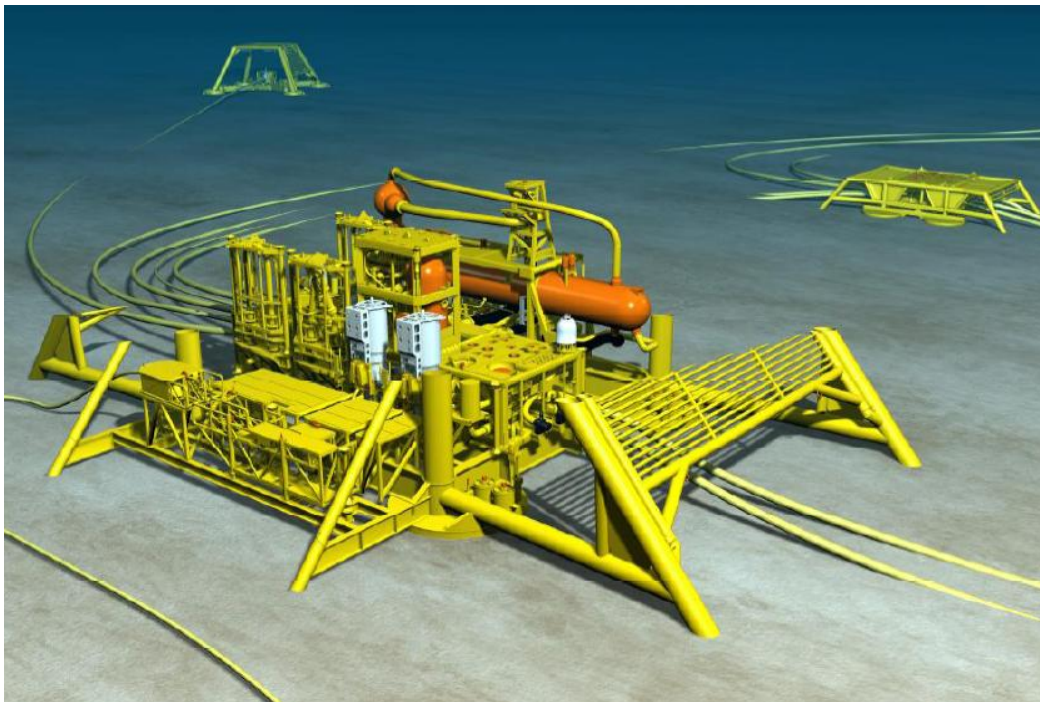


Figure 2.26: Tordis SSBI [20]

In operation from late 2007, the separator removed water and sand from the well stream for injection into a sand stone deposit 1000 meters beneath the seabed [6]. In 2008 an oil leak was discovered, and the water injection well was proven to be the source of it. The subsea separation system was closed down immediately and it is still out of function. The MPP now boosts the complete well stream back to the platform.

As shown in figure 2.26, both the MPP and the water injection pump are installed as an integral part of the total SSBI system. Both pumps are individually retrievable.

2.4.1. Specifications and Requirements

Statoil is the operator of Tordis from January 2003. The MPP is an important contributor to the production rate of the field, and it is thus desirable to Statoil to have as little downtime as possible on the pump. Consequently should the ability to replace the MPP immediately if it fails be present. This may result in interventions during winter time and in harsh weather conditions. For that reason Statoil has requested the ability to launch and retrieve MPP through moonpool, where it is protected from external loads such as strong waves and winds.

The main characteristics of the pumps are given in table 2.1 (MPP and water injection pump are identical in size).

Size (L x W x H)	1841 x 2335 x 5207 mm
Dry Weight	21 000 kg

Table 2.1: Main characteristics of Tordis pumps

The main characteristics of the pump running tool are given in table 2.2.

Size (L x W x H)	1000 x 3600 x 5400 mm
Dry Weight	4500 kg

Table 2.2: Main characteristic of Tordis pump running tool

The MPP and its dedicated running tool are shown in figure 2.27.

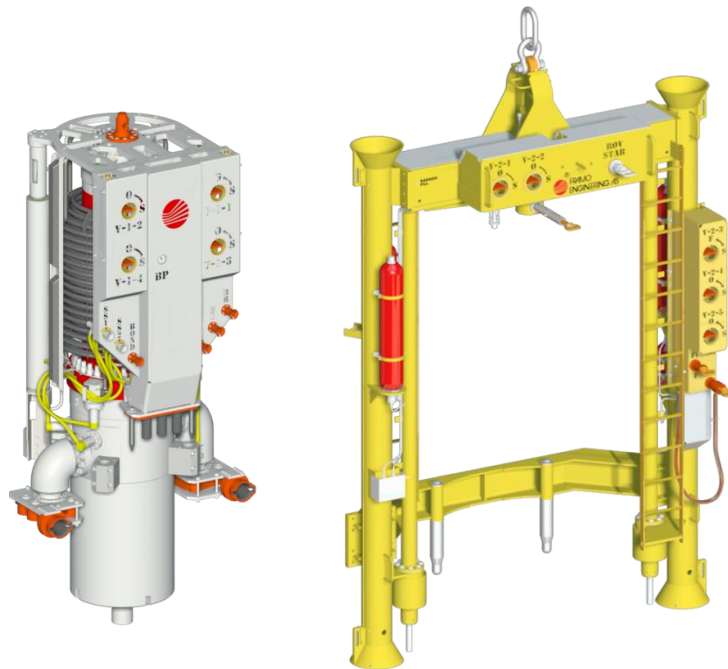


Figure 2.27: Tordis MPP and dedicated running tool

3. Moonpool Theory

3.1. Introduction

A moonpool is a vertical wall-sided passage through the ship hull as illustrated in figure 3.1. The moonpool allows for subsea modules and tools to be launched from vessel deck or recovered from seabed through the protective shelter provided by moonpool walls. Some subsea construction vessels also have a dedicated moonpool used for launch and recovery of ROVs. This chapter will focus on moonpool operations related to subsea modules; however the theory presented in the following sections will be directly transferrable to the ROV moonpools. The moonpool is in most cases located close to vessel roll and pitch axis to minimize the effect from vessel angular motions.

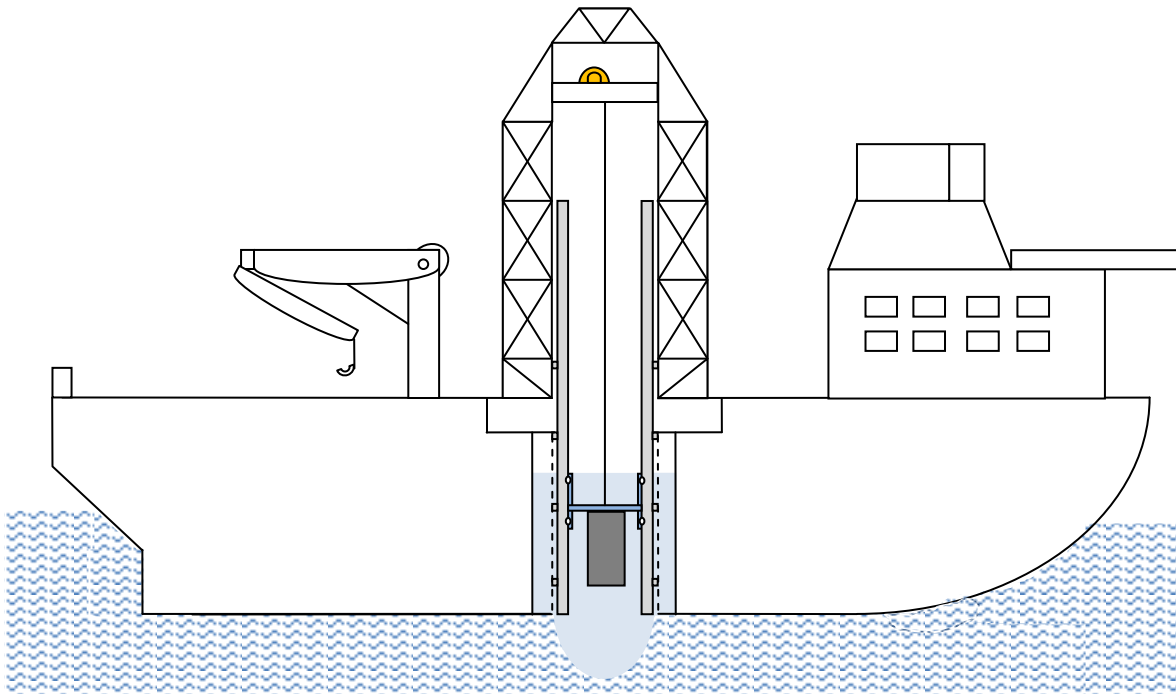


Figure 3.1: Illustration of a vessel with lifting arrangement through the moonpool

The basic idea of launching an object through a moonpool is simple, move object from deck through a protective area and down to the seabed. However, theory related to moonpool operations can get very complex. This chapter will outline different aspects related to moonpool theory. It is assumed a constant cross-sectional area of moonpool, if not mentioned otherwise.

3.1.1. Challenges to Moonpool Operations

There are both advantages and disadvantages with launch and recovery through the vessel moonpool compared with conventional overside crane operations. Some of these are listed in table 3.1

Advantages	Disadvantages
Subsea unit is protected from horizontal components of environmental forces, such as waves, winds, currents and ice flows	Large amplitude oscillations of the water column inside the moonpool may occur which can result in flooding of equipment handling areas or unacceptable loadings on equipment in moonpool
By positioning moonpool close to centre of roll and pitch axis, the adverse effects of vessel angular motions can be minimized	Lack of reliable data related to moonpool operations
Avoid lifting on deck by use of skidding system	Internal sloshing may occur, resulting in transverse breaking waves
Damping features can be installed to reduce dynamic amplification of water oscillations	Difficult to predict the moonpool dynamics
Milder water entry during normal conditions	Limitations with regards to size when installing through moonpool

Table 3.1: Advantages and disadvantages with installations through moonpool

The advantages with moonpools are well known: it provides a protective shelter under normal circumstances. However, the water motions that takes place in the moonpool under wave-induced pressures and vessel motion may cause unpredicted high loadings. This water motion is most likely to occur at the natural modes of the moonpool [18]. There are two particular motions; one is the sloshing mode where the water moves back and forth in between the vertical moonpool walls. The second one is the piston mode where the water heaves up and down more or less like a rigid body. In moonpool operations piston mode is dominating, and therefore this thesis is devoted to the vertical water oscillation problem alone. The sloshing mode is outside scope of this study. Nevertheless, when planning a moonpool operation sloshing may be included in analysis work. Attention must also be drawn to the fact that vertical forces may be enlarged when coupled with horizontal forces.

If exited at resonance, oscillations inside the moonpool may give larger water elevation than outside the vessel. Therefore it is important to know the resonance period of the moonpool. Often the resonance period lies within expected wave periods in the wave spectrums, hence the water in the moonpool may get large motions and should be reduced. Knowing that damping will significantly reduce the fluid motions when close to resonance, it is therefore desired to increase the damping in the moonpool. This is commonly done by introducing perforated walls or fittings.

3.1.2. Module Handling System

A typical Module Handling System (MHS) consists of a lifting structure or tower, a lifting arrangement, a guiding arrangement and a skidding system on the vessel deck. The MHS is located above the moonpool opening. This section will emphasize only on the type of moonpool configurations likely to be used during installation of the Tordis pump unit. Such a moonpool is a standard 7,2 x 7,2 m with corresponding MHS.

There exist different types of lifting arrangements. Figure 3.2 shows a Grenland Group tower, which is a cube shaped frame work steel construction. The structure is commonly called a module handling tower (MHT). The tower dimensions depend on the objects to be handled. It is vital that lifting height of the tower is sufficiently large to handle the height of lifted object. Integrated in tower structure is a lifting frame which deploys the lifting arrangement. The lifting arrangement typically includes one main winch, 2-4 guide wire winches and a cursor system. Moonpool guide wires are used when lifted object leaves cursor system and shall prevent it from rotating during deployment. The cursor system comprises of rails which are mounted along the internal structure of tower, and down into the moonpool. A cursor framework runs on the rail guides. Lifted object is fixed to the cursor. According to [15] rail guides provide the most effective horizontal control due to the strength that can be achieved. Thus are rails ideal to use within areas that require tightly constrained horizontal motion, which exceedingly is the case for moonpool operations.

It is also possible to design the MHT such that the vessel crane can be used as the lifting device. If the crane is to be used it is important to ensure that hatches and guide structures are designed and dimensioned for it.

During transit conditions the moonpool is enclosed from environment using hatches. The bottom opening hatch must be strong enough to withstand external forces from waves and currents. The top hatch has integrated skidding rails. The skidding rail enables movement of equipment from moonpool and to its dedicated storage locations on deck. The common procedure is to sea fasten the object to pallets that can move on the skidding rails. With this arrangement crane lifts on deck is avoided, reducing risk of asset damage and personnel accidents.

The module handling winches are preferably heave compensated to better control the lifted structure through the water column. The system allows for retrieval or launching at a constant velocity or to keep the load at a fixed position relative to the seabed. It is desirable that both main winch and guide wire winches are heave compensated.



Figure 3.2: Illustration of a module handling tower and skidding system [10]

3.1.3. Framo Pump Units through Moonpool

Normally, Framo pump units are deployed with the vessel crane. However, there have been some projects where the vessel moonpool has been used, latest at the Troll field year 2000.

The main challenge during moonpool installation of the Framo pump unit is the height. MHTs are normally too small to handle this height and the tower therefore requires modifications to be able to launch the pump unit through moonpool. Such modifications may be to disassemble some parts in top of MHT. However, removing part of the lifting tower will influence the function of the tower. Remaining parts will experience higher loadings. This may reduce the capability of the crane and consequently maximum sea state for lifting will be decreased. Fatigue issues may also arise sooner.

When a pump unit is individually installed it is often combined with installation of other equipments to reduce costs. The removed parts of MHT may thus be parts which are essential during launching of other equipment. We may lose the ability to combine installations, or, if MHT is remounted, the lifting operation will be of a longer duration.

The transport skids which are skidded to moonpool hatches may also be reconfigured to decrease height of pump unit. It is possible to move pump unit from its dedicated transport skid into a skid designed for moonpool installations. Such a skid is of smaller dimensions to reduce the overall height.

3.2. Fluid Motion

3.2.1. Fluid Motion in Moonpool Column

The Bernoulli equation can be used to explain motions of the water plug in the moonpool. The following assumptions are made to justify the use of Bernoulli:

- The fluid is incompressible
- The fluid motion is unsteady
- Viscous forces are neglected

For simplification matters it is also assumed that the fluid motion does not vary across the moonpool. In addition one will assume a still water line outside the vessel, hence h is constant from figure 3.3.

The derivation of the formulas takes reference in Faltinsen [7].

The Bernoulli equation yields:

$$p + \rho gz + \rho \frac{\partial \varphi}{\partial t} + \frac{\rho}{2} \mathbf{v}|\mathbf{v}| = C \quad (3.1)$$

where p is the pressure, φ is the velocity potential, and where \mathbf{v} is the velocity vector:

$$\mathbf{v} = \nabla \varphi = \mathbf{i} \frac{\partial \varphi}{\partial x} + \mathbf{j} \frac{\partial \varphi}{\partial y} + \mathbf{k} \frac{\partial \varphi}{\partial z} \quad (3.2)$$

It is common procedure to exclude horizontal motions and focus on vertical motions and forces only in the moonpool [16]. It can also be mentioned that when an object is lifted through the moonpool it will be fixed to a cursor that prevents horizontal motions relative to the vessel. Based on this assumption we may simplify the moonpool problem to 2D pure heave motion, see figure 3.3.

From this the velocity vector will be reduced to:

$$\mathbf{V} = \nabla \varphi = \mathbf{k} \frac{\partial \varphi}{\partial z} \quad (3.3)$$

Hence, the Bernoulli equation will reduce to:

$$p + \rho gz + \rho \frac{\partial \varphi}{\partial t} + \frac{\rho}{2} \left(\frac{\partial \varphi}{\partial z} \right)^2 = C \quad (3.4)$$

Differentiation of 3.4 with respect to z gives:

$$\frac{\partial p}{\partial z} + \rho g + \rho \frac{\partial}{\partial t} \frac{\partial \varphi}{\partial z} + \frac{\rho}{2} \frac{\partial}{\partial z} \left(\frac{\partial \varphi}{\partial z} \right)^2 = 0 \quad (3.5)$$

$$\frac{\partial p}{\partial z} = -\rho g - \rho \frac{\partial}{\partial t} \frac{\partial \varphi}{\partial z} - \frac{\rho}{2} \frac{\partial \varphi}{\partial z} \frac{\partial^2 \varphi}{\partial z^2} \quad (3.6)$$

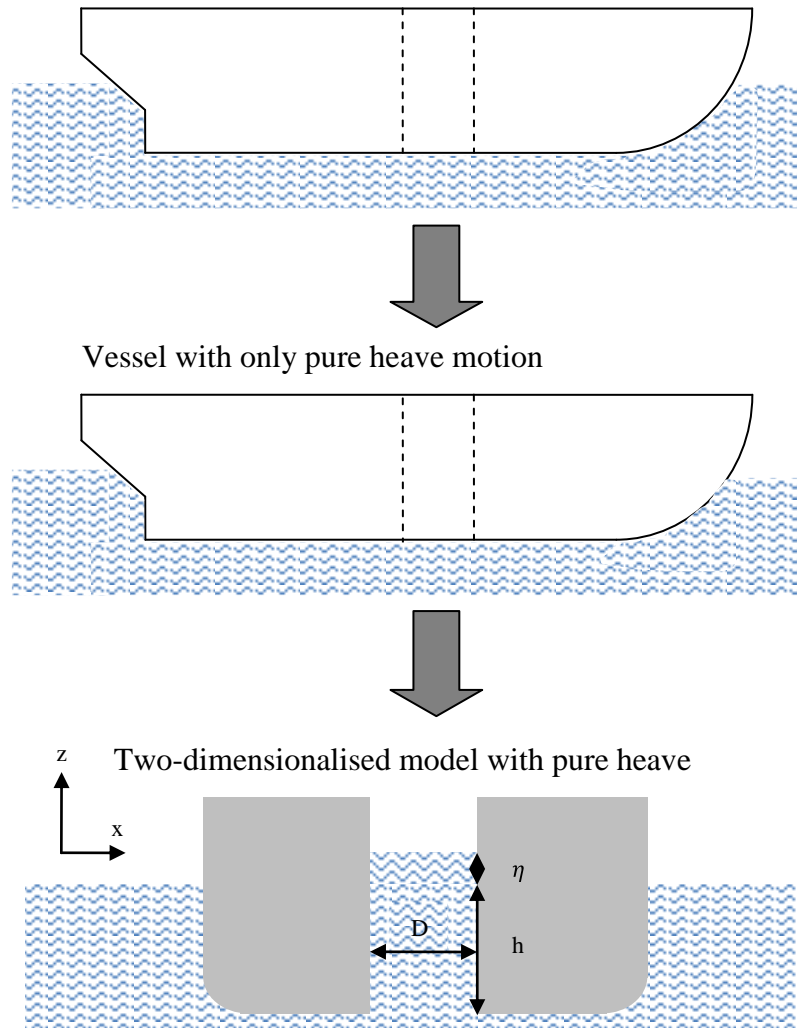


Figure 3.3: Simplification of vessel geometry for water motions in moonpool

When assuming water is incompressible, the velocity potential must satisfy the Laplace equation:

$$\frac{\partial^2 \varphi}{\partial x^2} + \frac{\partial^2 \varphi}{\partial y^2} + \frac{\partial^2 \varphi}{\partial z^2} = 0 \quad (3.7)$$

Assuming heave motion only, 3.7 reduces to:

$$\frac{\partial^2 \varphi}{\partial z^2} = 0 \quad (3.8)$$

Substituting 3.8 into the Bernoulli equation gives us:

$$\frac{\partial p}{\partial z} = -\rho g - \rho \frac{\partial}{\partial t} \frac{\partial \varphi}{\partial z} = -\rho \left(g + \frac{\partial}{\partial t} \frac{\partial \varphi}{\partial z} \right) \quad (3.9)$$

Idealistically, the fluid motion will be constant across the moonpool area, and thus can the velocity be expressed as $\frac{\partial \varphi}{\partial z}$ at every point. Consequently, we have $\frac{\partial \varphi}{\partial z} = \frac{d\eta}{dt}$. Equation 3.9 can thus be written as:

$$\frac{\partial p}{\partial z} = -\rho \left(g + \frac{\partial}{\partial t} \frac{d\eta}{dt} \right) \quad (3.10)$$

$$\frac{\partial p}{\partial z} = -\rho \left(g + \frac{d^2\eta}{dt^2} \right) \quad (3.11)$$

or

$$\frac{d^2\eta}{dt^2} = -\frac{1}{\rho} \frac{\partial p}{\partial z} - g \quad (3.12)$$

Equation 3.12 relates the pressure gradient in the moonpool to the vertical fluid acceleration.

Integration of 3.12 over the moonpool area gives:

$$\int_{-h}^{\eta} \frac{d^2\eta}{dt^2} dz = \int_{-h}^{\eta} \left(-\frac{1}{\rho} \frac{\partial p}{\partial z} - g \right) dz \quad (3.13)$$

$$\left[\frac{d^2\eta}{dt^2} z \right]_{-h}^{\eta} = \left[-\frac{1}{\rho} p(z) - gz \right]_{-h}^{\eta} \quad (3.14)$$

$$\frac{d^2\eta}{dt^2} (\eta + h) = -\frac{1}{\rho} (p(\eta) - p(-h)) - g(\eta + h) \quad (3.15)$$

$$(p(\eta) - p(-h)) = \rho \left(\frac{d^2\eta}{dt^2} (\eta + h) + g(\eta + h) \right) \quad (3.16)$$

Using the Bernoulli equation on the form $(p(\eta) - p(-h))$ gives us:

$$\begin{aligned}
 p(\eta) - p(-h) &= \rho g \eta - \rho \frac{\partial \varphi}{\partial t} \Big|_{z=\eta} - \frac{\rho}{2} \left(\frac{\partial \varphi}{\partial z} \right)^2 \Big|_{z=\eta} \\
 &\quad - \rho g h - \rho \frac{\partial \varphi}{\partial t} \Big|_{z=\eta} - \frac{\rho}{2} \left(\frac{\partial \varphi}{\partial z} \right)^2 \Big|_{z=\eta}
 \end{aligned} \tag{3.17}$$

which, due to the Laplace equation, reduces to:

$$p(\eta) - p(-h) = \rho g \eta - \rho \frac{\partial \varphi}{\partial t} \Big|_{z=\eta} - \rho g h - \rho \frac{\partial \varphi}{\partial t} \Big|_{z=-h} \tag{3.18}$$

By substitution of equation 3.18 into 3.16 we obtain the following expression:

$$\frac{d^2 \eta}{dt^2} (\eta + h) = -\frac{1}{\rho} \left(-\rho g \eta - \rho \frac{\partial \varphi}{\partial t} \Big|_{z=\eta} - \rho g h - \rho \frac{\partial \varphi}{\partial t} \Big|_{z=-h} \right) - g (\eta + h) \tag{3.19}$$

$$\frac{d^2 \eta}{dt^2} (\eta + h) = g \eta + \frac{\partial \varphi}{\partial t} \Big|_{z=\eta} + g h - \frac{\partial \varphi}{\partial t} \Big|_{z=-h} - g \eta - g h \tag{3.20}$$

The equation for the moonpool wave elevation can then be written as:

$$\frac{d^2 \eta}{dt^2} (\eta + h) = \frac{\partial \varphi}{\partial t} \Big|_{z=\eta} - \frac{\partial \varphi}{\partial t} \Big|_{z=-h} \tag{3.21}$$

To give a better picture of the water motion inside the moonpool, equation 3.21 can be linearized. The linear dynamic free surface condition is assumed, and this condition is simply that the water pressure is equal to the constant atmospheric pressure p_0 on the free surface [7]. The free surface in the moonpool will be at $z = \eta$ from figure 3.3. The dynamic free surface condition yields:

$$\eta g + \frac{\partial \varphi}{\partial t} = 0 \quad \text{at } z = \eta \tag{3.22}$$

Inserted in 3.21 gives:

$$\frac{d^2 \eta}{dt^2} (\eta + h) = -\eta g - \frac{\partial \varphi}{\partial t} \Big|_{z=-h} \tag{3.23}$$

$$\frac{d^2\eta}{dt^2} = \frac{-\eta g}{(\eta + h)} - \frac{1}{(\eta + h)} \frac{\partial \varphi}{\partial t} \Big|_{z=-h} \quad (3.24)$$

Assuming wave amplitude is small relative to a characteristic wavelength and body dimension, we can use that $\eta \ll h$, which again simplifies 3.24 to:

$$\frac{d^2\eta}{dt^2} = \frac{-\eta g}{h} - \frac{1}{h} \frac{\partial \varphi}{\partial t} \Big|_{z=-h} \quad (3.25)$$

$$\frac{d^2\eta}{dt^2} + \frac{g}{h} \eta = -\frac{1}{h} \frac{\partial \varphi}{\partial t} \Big|_{z=-h} \quad (3.26)$$

Equation 3.26 is like the equation for a mass-spring system without damping, where the right hand side of the equation is the exciting force. In terms, this means that the fluid motion inside the moonpool can be treated as a mass-spring system with one degree of freedom. The equation is valid for small amplitudes.

. Figure 3.4 shows a linearly damped forced spring-mass system.

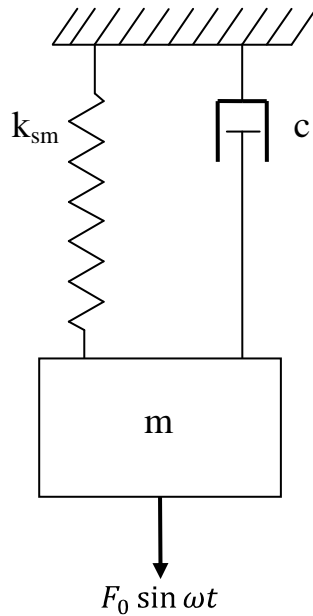


Figure 3.4: A mass-spring system with linear damping

The equation of motion for the mass-spring system is given as [3]:

$$m\ddot{x} + c\dot{x} + k_{sm}x = F_0 \sin \omega t \quad (3.27)$$

where m is the mass of the system, which in hydrodynamics also will include added mass, c is the damping and k_{sm} is the stiffness of the system.

Faltinsen [7] regards the moonpools water motions as a mass-spring system without damping, and presents the natural period of the system:

$$T_n = 2\pi \sqrt{\frac{h}{g}} \quad (3.28)$$

DNV [1] introduces a modification of the same formula where added mass and increased draught has been accounted for:

$$T_n = \frac{2\pi}{\sqrt{g}} \sqrt{h + \kappa\sqrt{A}} \quad (3.29)$$

assuming a constant cross-sectional area, A , of moonpool. κ is a dimensionless parameter found to be 0,46 for all realistic rectangular moonpools. (3.29) has been derived by energy conservation. If the moonpool has a varying cross-sectional area, then the natural frequency is defined as [1]:

$$\omega_0^2 = \left\{ \int_{-h}^0 \frac{A(0)}{A(z)} dz + \frac{A(0)}{A(-h)} \kappa \sqrt{A(-h)} \right\} - g = \quad (3.30)$$

As for all mechanical oscillating systems, dynamic amplification occurs at a certain frequency. Day [4] states that the RAO of the oscillations exhibits a large response at the natural frequency, falling toward zero at high frequencies, and unity at low frequencies. If the peak of the RAO occurs at a frequency at which there is a significant amount of wave energy, then the response in that sea state will be large, and the moonpool may not be operable.

3.2.2. Water Entering Moonpool

Water will flow into the moonpool as soon as the bottom hatch is opened. The water aims to find its equilibrium position, and thus will water level inside moonpool rise until it reaches the still water level.

When a vessel is situated in a sea state with the moonpool hatch open, water will enter and exit the moonpool in every wave period. Considering this vertical fluid motion only, initiated by the vessel heave motion, an idealization of the flow at the bottom opening of the moonpool can be seen in figure 3.5.

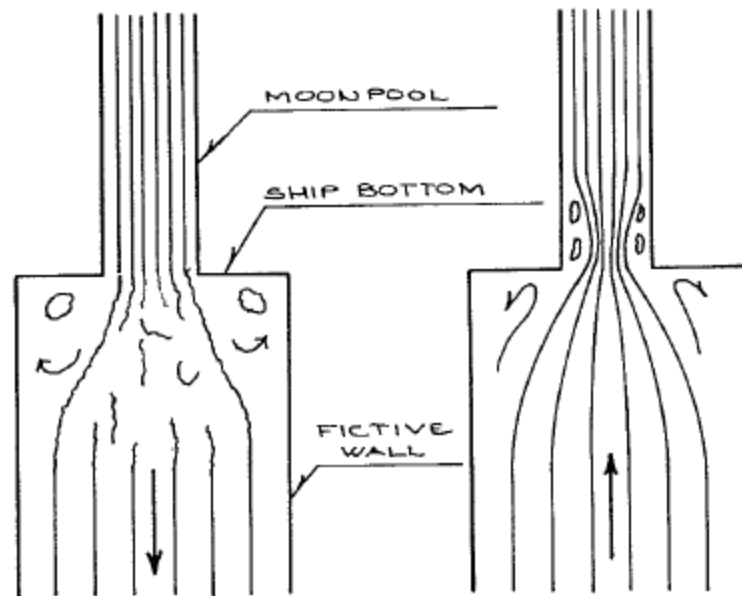


Figure 3.5: Idealization of the flow at the bottom opening of the moonpool (Madsen, 1980)

The pressure at the bottom opening for the ideal moonpool flow in figure 3.5 is equal to the dynamic pressure excited by the wave force, following the Froude-Krylov hypotheses. The excitation force from the waves then becomes [17]:

$$F_{wave} = P_{FK}A \quad (3.32)$$

where P_{FK} is the Froude-Krylov dynamic pressure and A is the cross-sectional area of the moonpool bottom opening. The Froude-Krylov pressure is mathematically introduced in 3.4. In reality, however, the excitation force is also affected by the vessel motion. Wave diffraction may also influence the exciting force.

According to Madsen [17] a damping force will also arise at due to energy loss at the bottom opening. From figure 3.5 we see that the flow forms a contraction just above the bottom opening when it flows into the moonpool. After which, the stream widens again and fills the moonpool. A damping force is thus created due to loss in turbulent eddies between the contraction and the wall of the moonpool. When the flow runs out of the moonpool the velocity is approximately uniform over the cross-section of the moonpool. At the abrupt enlargement, the flow forms turbulent eddies in the corner which result in an energy loss. Sufficiently far away downstream from the enlargement, the velocity will again be uniform. The damping values depend upon the geometry of the bottom opening.

3.2.3. Fluid Motion below Moonpool

The real flow field below the moonpool will be of higher complexity than figure 3.5 indicates. Waves and currents will form transverse force components. The vessel itself will disturb the dynamic pressure field arising from these components, and thus will surrounding fluid accelerations and velocities be affected. In addition, tons of water will enter and exit the moonpool every wave period as already explained. Due to the many factors influencing the flow field below the moonpool, it is very difficult to predict the water motions in this area. DNV [1] states that a conservative approach to this problem is to analyze the dynamics, using hydrodynamic forces based on the wave kinematics of undisturbed waves and hydrodynamic coefficients for unrestricted flow condition. Linear wave theory may be applied to estimate transverse forces.

Konopka [13] tried to calculate forces acting on a diving bell in the area below the moonpool and compared it to test results. The calculations deviated greatly from the test results, and thus he concluded with an unsuccessful attempt of modeling the diving bell below the moonpool entrance. He considered the forces from the undisturbed linear wave theory to be the strongest contribution to the error.

3.2.4. CFD-Analysis for Moonpool Water Motion

Computational Fluid Dynamics (CFD) is a numerical approach for predicting physical fluid flows and heat transfer. For subsea lifts it may be used to analyze wave loads.

DNV [1] recommends not using CFD-analysis for moonpool dynamics. It states that even though CFD can analyze the fluid dynamic interaction between the lifted object and the water plug inside the moonpool, it is difficult to couple with the dynamic characteristics of vessel in waves and the response of the lifting system. Force predictions may hence be uncertain.

However, Alsgaard [2] has numerically investigated the piston mode resonance in a moonpool using CFD. He found that added mass and resonance period was fairly well predicted. He obtained conservative results, and recommended it as a supplement to experiments. He met greater trouble when trying to capture the damping phenomenon, with a 10 – 20 % error. He concludes that there exists little full-automatic tools for prediction of loadings where damping is important, but potential is seen if further development of the CFD-tool takes place.

3.3. Hydrodynamic Parameters

Estimating hydrodynamic coefficients is an important part to any lifting analysis. The estimation needs to be as accurate as possible to predict realistic hydrodynamic loads. This can however be challenging due to the complex geometrical shape of most subsea structures. DNV [1] presents two different types of hydrodynamic coefficients; one for when the structure is lifted through the splash zone and the other for a fully submerged structure. This thesis assumes a fully submerged pump unit if not stated otherwise.

3.3.1. Damping

3.3.1.1. Damping in General

As already mentioned, moonpool oscillations are a typical resonance phenomenon. The moonpool is a system with large dynamic effects, and the amplification of the water motion therefore depends upon the level of damping.

Damping is normally expressed by the relative damping coefficient, which represents the relationship between the actual damping and the critical damping [11]. The damping coefficient determines how quickly the oscillations are damped. In an underdamped system the oscillations decrease exponentially. The water moonpool is a typically underdamped system, with a relative damping coefficient below 1.

In addition to inviscid damping due to wave generation, damping is provided by viscous drag damping caused by various structures in the moonpool. Every obstacle on the smooth moonpool wall will hence contribute to an increased damping factor. DNV [1] presents an empirical relative damping ratio as the damping coefficient of the water plug. The ratio is presented for different types of fittings inside the moonpool:

Naked moonpool:	$\eta^D = 8 - 9 \%$
Minor fittings:	$\eta^D = 13 - 14 \%$
Guidance structure:	$\eta^D = 18 - 19 \%$
Guidance structure + 50% bottom plate:	$\eta^D = 40 - 45 \%$
Cofferdam:	$\eta^D \approx 45 \%$

Testing has been done to measure the relative motion between the moonpool water plug and the ship at the moonpool centre axis. An amplitude RAO for this relative motion has been defined as [1]:

$$RAO = \left| \frac{\zeta - \zeta_s}{\zeta_w} \right| \quad (3.33)$$

where

- ζ = motion of the water plug [m]
 ζ_s = heave motion of the ship [m]
 ζ_w = sea surface elevation outside the ship [m]

3.3.1.2. Damping Approaches in Moonpool

Horizontal Cofferdam

A horizontal cofferdam illustrated in figure 3.6, increases the surface area in the moonpool. A greater surface area will reduce surface pressure and hence the surface elevation, following the basic pressure equation $p = F/A$. Here, F is the exciting force, A is the area of the moonpool and p is the pressure. If A increases with constant F , it is easy to see that the pressure will decrease. Thus will the cofferdam increase the difference between the surface pressure in the moonpool and the exciting fluid pressure from below [13], resulting in a reduced water elevation.

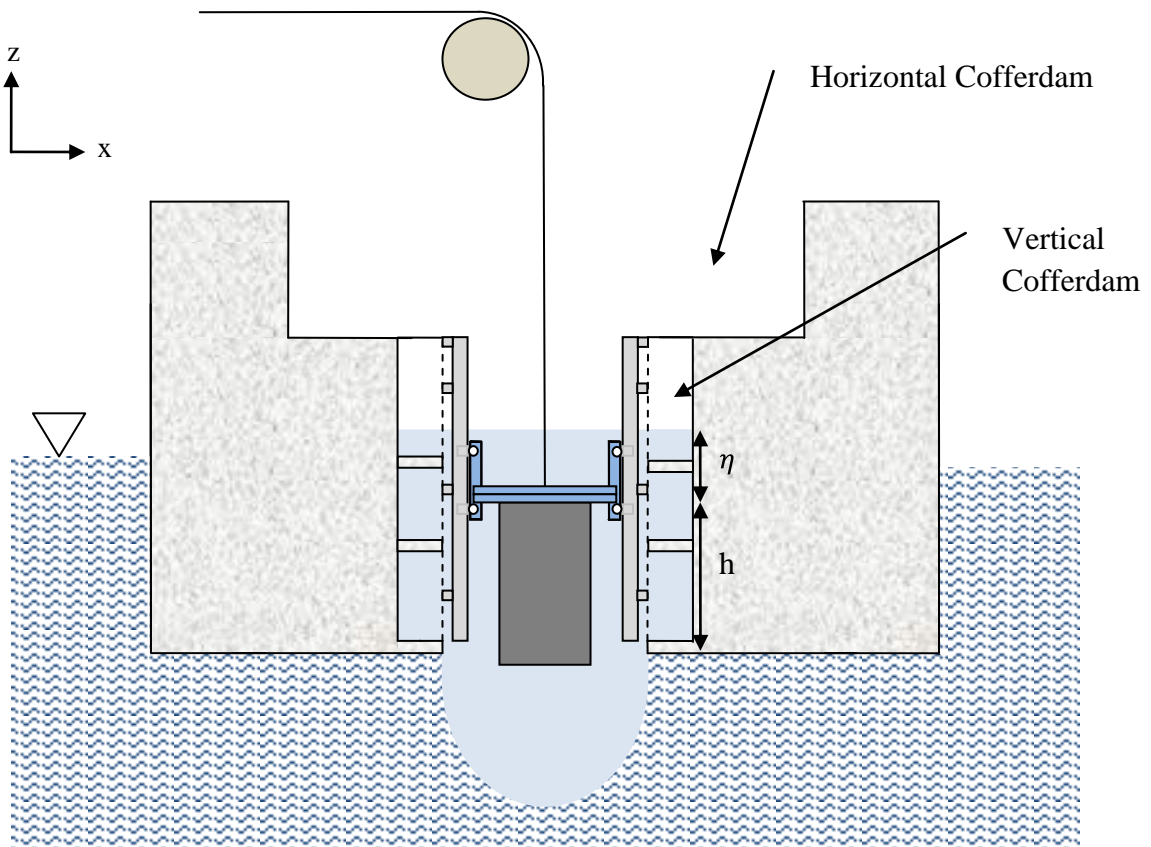


Figure 3.6: An illustration of the moonpool, including damping devices

Vertical Cofferdam

Another effective damping is a vertical cofferdam which is a baffling structure with damping chambers, shown in figure 3.6. [8] refers to an investigation done by Spangenberg and Jacobsen about the effect of damping chambers. Results showed that vertical wave motions are converted into horizontal wave motions and the wave energy, to a large extent, dissipated as heat energy by reflecting and conflicting currents from the holes of the perforated bulkheads. Figure 3.7 gives an example of the mentioned damping device: when water level rises, the water will run through perforated longitudinal bulkheads into damping chambers. When the water level decreases, the water will run from the damping chambers back into the moonpool.

Øritsland [22] have carried out measurements of surface elevation in moonpool, aiming to find the damping effect of the damping chambers arrangement. For perforated bulkheads with horizontal decks, as shown in figure 3.7 he states that moonpool RAO_{max} is reduced with approximately 70 % compared to a test without structure in the moonpool. It shall thus be noted that this was a model test with moonpool dimensions of 0.157 x 0.157 m, and that result may differ somewhat in a bigger moonpool.

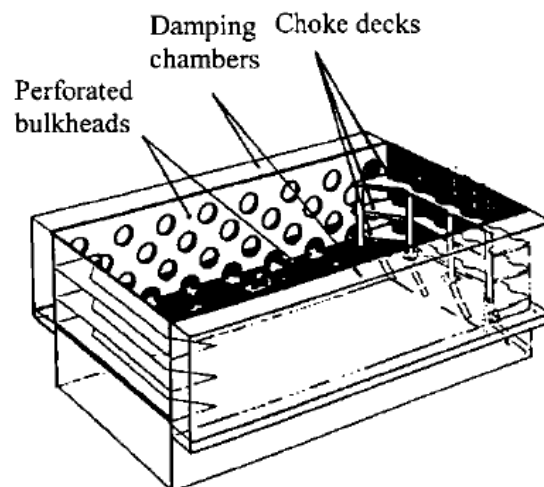


Figure 3.7: Illustration of damping chambers [8]

The vertical cofferdam effect is also introduced in DNV [1] and can be read from figure 3.8; Marintek has measured the relative water elevation in a moonpool per unit incoming wave amplitude for different fittings in the moonpool. One can see that the cofferdam highly reduces the RAO for the relative motion, and in resonance the RAO is only about 0.5 in the cofferdam, compared to 3 for a naked moonpool.

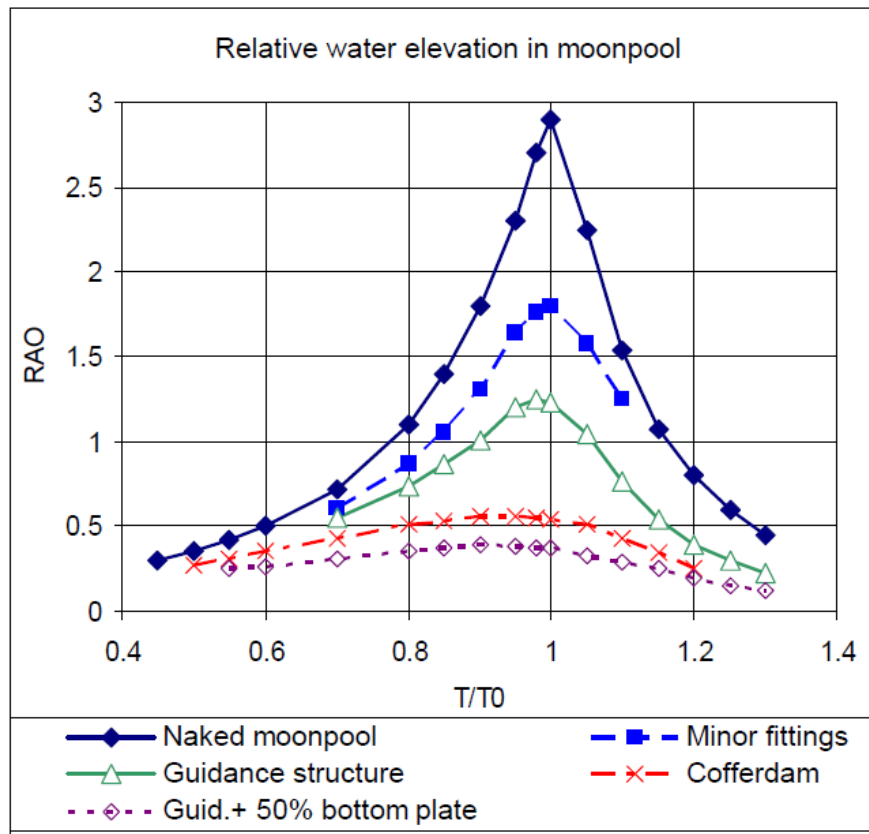


Figure 3.8: Measured relative water elevation in a moonpool per unit incoming wave amplitude (DNV [1] Courtesy of Marintek)

Bottom plates

Installing bottom plates in the moonpool will work as a flow constriction and thus avoid some of the excitation force to be transmitted to the water inside the moonpool. Øritsland [22] has tested a circular bottom plate, which reduced the opening by 48.8 %. He found this to be a very favorable damping feature of the relative motion; RAO_{max} had an 80 % reduction and significant values had a reduction of 65 % in 2,3 m waves. Figure 3.9 also shows the same indicating results, guidance structure and a 50 % bottom plate significantly reduces maximum RAO values.

Attention must however be drawn with regards to the decrease of the cross-sectional area of the opening. Reduced moonpool opening means only smaller structures can be launched through it. However, the Framo pump unit constitutes a small part of the moonpool cross-sectional area and thus could a bottom plate have been implemented.

Air injection

A number of moonpool construction vessels have applied an air bubble system that aerates the water in the moonpool. It is done by adding air to the water and this will decrease the impact load on the equipment passing through the moonpool but not reduce the oscillations [8].

Øritsland [22] states that combined with the damping chambers, the injection of air has little effect upon the relative motion.

Other damping devices

We can read from figure 3.8 that any fittings inside the moonpool will be subject to increased damping. Cursor system rests in the moonpool opening and will thus act as a damping device even though it is not the main purpose of the system.

An airtight casing above the moonpool will also reduce oscillations by increasing the damping. Assuming air is incompressible the air above the water surface will create damping of the water inside the moonpool. Kuo [14] speaks about design considerations related to this solution: One can build a housing over the top opening of the moonpool at the weather deck level. This would enclose all the lifting mechanism as well as the entry to decompression chambers, which may be installed within the housing or outside the housing with the mating flange inside. The solution requires airtight housing and that double doors are introduced for entry and exit of personnel and equipment.

3.3.2. Drag

3.3.2.1. Drag in General

When an object moves in fluid, or fluid flows past an object, the object will experience forces exerted by the fluid. Theoretically, there are two main contributions to the drag force; friction force between the object and the fluid, and the pressure difference between the upstream and downstream side of the object.

The friction force between the object and the fluid, the skin friction, is caused by the viscous behavior of the fluid and the roughness of the objects surface. Skin friction is a velocity dependent force and will always work in opposite direction of the movement.

When a water flow separates and flows past an object, vortices are created around the corners of the object. The fluid is accelerated, resulting in a higher velocity of the water particles of the vortices compared to the water particles of the upstream flow. Thus, according to Bernoulli, a pressure difference arises between upstream and downstream side of the object, creating a force opposite of the direction of the movement.

Faltinsen [7] states that for steady incident flow past a circular cylinder the major contribution to the drag force comes from the pressure difference between downstream and upstream. Normally this also yields for lifting operations.

3.3.2.2. Drag Coefficients

Drag coefficients for lifting analysis may be fairly difficult to estimate and the most accurate method is to carry out model tests. The coefficient will depend upon several different parameters like the Reynolds number, Keulegan-Carpenter number, geometrical shape of the lifted object as well as the roughness of it, and also the nature of the flow. These parameters will be described in brief in this section, except from the Keulegan-Carpenter number which is described in 3.3.4. Some difficulties around the drag coefficient will also be shown attention in this section.

The Reynolds number is defined as:

$$Re = \frac{v'D}{\nu} \quad (3.34)$$

where v' is the velocity of the fluid, D is the characteristic body dimension, and ν is the kinematic viscosity of the fluid. The Reynolds number is a dimensionless number and can be thought of as a comparative measure of inertial effects to viscous effects in the flow.

Understood from equation 3.34 is that the Reynolds number will vary with depth as the water velocity profile is depth dependent, hence different drag coefficient should be used for different depths. Figure 3.9 shows different drag coefficients as a function of the Reynolds number.

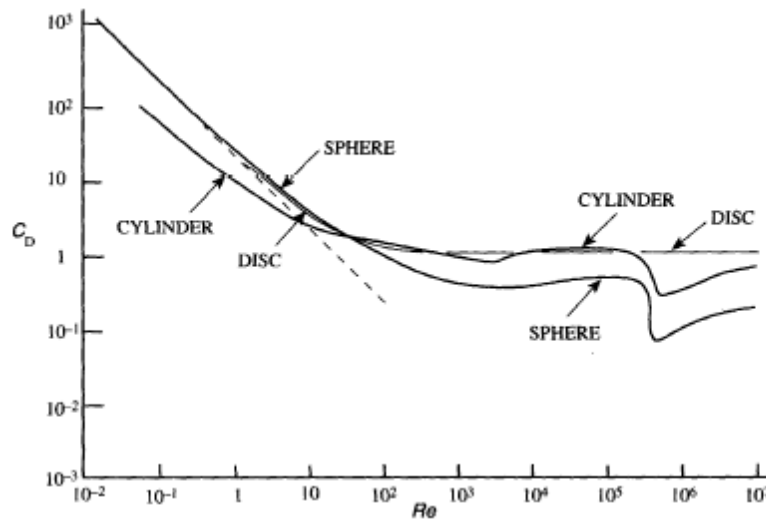


Figure 3.9: Log-log plot of drag coefficient C_D as a function of Reynolds number Re for spheres, transverse cylinders, and face-on disc [11]

The drag coefficients dependence on the Reynolds number can be divided into different flow regimes. Faltinsen [7] refers to the four different flow regimes: subcritical flow, critical flow, supercritical flow and transcritical flow. For a flow around a smooth cylinder this refers to $Re < \approx 2 \cdot 10^5$ for subcritical flow, $\approx 2 \cdot 10^5 < Re > \approx 5 \cdot 10^5$ for critical flow, $\approx 5 \cdot 10^5 < Re > \approx 3 \cdot 10^6$ for supercritical flow, and $Re > 3 \cdot 10^6$ for transcritical flow.

Based on values in the range of 10^0 for both the moonpool particle velocities and the characteristic dimensions, and the kinematic viscosity in the range of 10^{-6} for water, approximate values of the Reynolds number for the pump unit will be in the range of 10^6 .

The geometrical shape of the launched object plays an important role when estimating the drag coefficient. Different shaped objects may have very different drag coefficients, even though the same Reynolds number and identical frontal areas, ref. figure 3.10. The drag coefficient's dependence on geometrical shape also appears from figure 3.9.

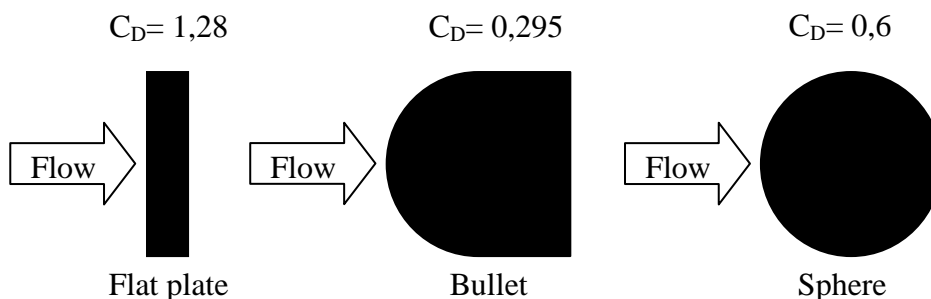


Figure 3.10: Drag coefficients of standard shapes [9]

In subsea lifting operations roughness is often referred to as marine growth and it may have great influence on the drag coefficient. However, the Framo pump unit is preferably stored

dry, and associated with all other uncertainties with the drag coefficient, the roughness may be disregarded. The pump unit is installed at 200 meters water depth, and marine growth is not a major problem at these depths. Consequently the pump can be assumed smooth also during retrieval.

DNV [1] states that test results of typical subsea modules show that the drag coefficient increases significantly when lifted object undergoes oscillatory motion. Using a steady-flow drag coefficient instead of an increased drag coefficient for oscillatory flow may underestimate the damping force and overestimate resonant motions of the object. However, Sarkar & Gudmestad [21] points out that for large structures whose hydrodynamic is inertia dominated, higher drag coefficients should be used with caution since it may induce unrealistic damping in the simulation of the motion. Numerically, this may reduce resulting maximum wire tension when analyzing. Thus, a conservative approach may be to assume non-oscillatory flow. Konopka [13] states that long periods and relatively large amplitudes of the moonpool oscillations also leads to the assumption of treating the flow as non-oscillatory.

A commonly adopted procedure for finding drag coefficients is to consider the 2D surface of the lifted object perpendicular to the flow direction, and to modify it due to the body extension in flow direction. DNV [1] provides a simplified calculation method for this. Table 3.2 shows this method for some well-known geometrical shapes.

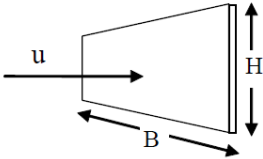
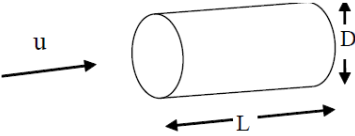
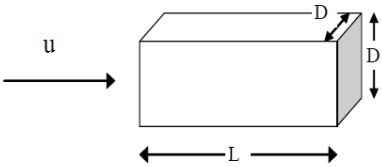
Table B-2 Drag coefficient on three-dimensional objects for steady flow C_{DS} . Drag force is defined as $F_D = \frac{1}{2}\rho C_{DS} S u^2$. S = projected area normal to flow direction [m ²]. Re = uD/ν = Reynolds number where D = characteristic dimension.		
Geometry	Dimensions	C_{DS}
Rectangular plate normal to flow direction 	B/H 1 5 10 ∞	1.16 1.20 1.50 1.90 $Re > 10^3$
Circular cylinder. Axis parallel to flow. 	L/D 0 1 2 4 7	1.12 0.91 0.85 0.87 0.99 $Re > 10^3$
Square rod parallel to flow 	L/D 1.0 1.5 2.0 2.5 3.0 4.0 5.0	1.15 0.97 0.87 0.90 0.93 0.95 0.95 $Re = 1.7 \cdot 10^5$

Table 3.2: Drag coefficients for some well-know geometrical shapes, recommended by DNV [1]

3.3.2.3. Drag Forces in Moonpool

Even though non-oscillatory flow is assumed, the drag coefficient will increase when adapted to moonpool operations, due to the restricted flow conditions provided by moonpool walls. DNV [1] suggests the following way of calculating the increased drag coefficient:

$$\frac{C_D}{C_{D0}} = \frac{1 - 0,5 \frac{A_b}{A}}{\left(1 - \frac{A_b}{A}\right)^2} \quad \text{for } \frac{A_b}{A} < 0,8 \quad (3.35)$$

where

- C_D = drag coefficient for moonpool [-]
- C_{D0} = drag coefficient for unrestricted flow [-]
- A_b = solid projected area of the object [m²]
- A = cross-sectional area of the moonpool (at the vertical level of the object) [m²]

C_{D0} in 3.35 is identical to the C_{DS} presented in table 3.2. From 3.35 we read that the drag coefficient for moonpool will increase as the blockage ratio defined as $\frac{A_b}{A}$ increases. Figure 3.11 graphically shows the relation between the drag coefficient and the blockage ratio. The blockage ratio influences the drag coefficient significantly more than the added mass coefficient, see section 3.3.3.3. When the object to be launched has a cross-section half of moonpool cross-section, the drag coefficient will increase by a factor of 3. The Framo pump unit though, is small compared to a standardized moonpool area and its blockage ratio will be in the range of 0,1 – 0,2.

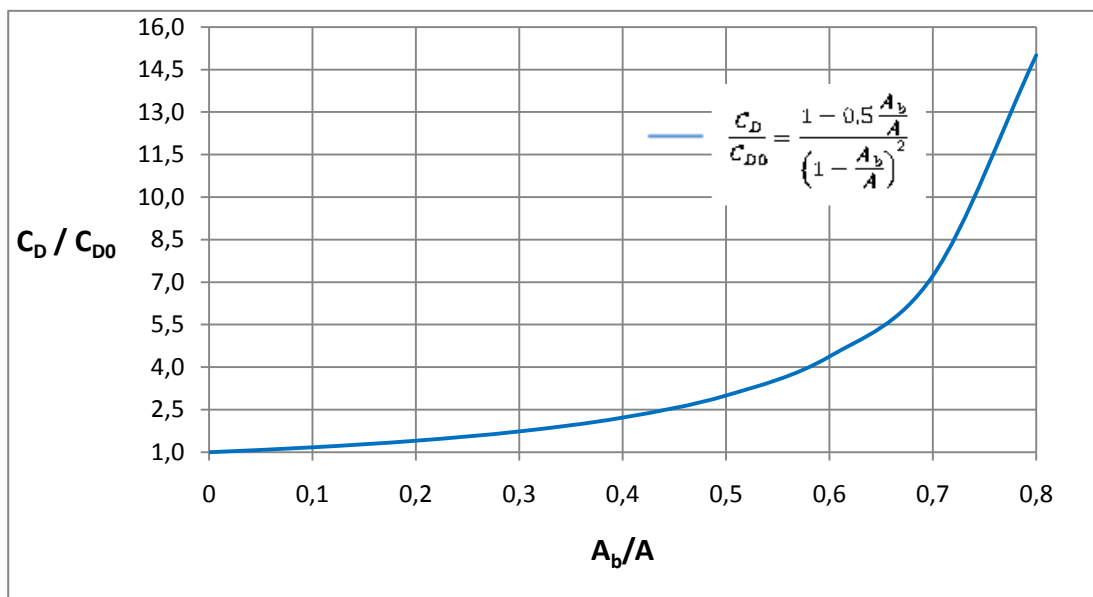


Figure 3.11: Drag coefficient as a function of moonpool blockage ratio

From table 3.2 one can see that DNV-RP-H103 defines the drag force as:

$$F_D = \frac{1}{2} \rho C_{DS} S u^2 \quad (3.36)$$

For moonpool calculations, C_{DS} is replaced by C_D which is the moonpool drag coefficient.

To estimate the drag coefficient for a structure as complex as the Framo pump unit with running tool is more complicated than to estimate the added mass coefficient. Konopka [13] states that for a diving bell with protection structure and gas-bottles outside, it is almost impossible to estimate correct drag coefficient without model testing. A very simplified approach is to treat the pump as either a cylindrical or a square structure. Appendix A compares the drag coefficient and corresponding drag forces for cylindrical and square structure, based on the DNV [1] approach. Results show that the square structure will have a somewhat higher drag coefficient than the cylindrical structure.

The approach in Appendix A does not account for any sharp edges of the pump surface which may underestimate drag forces, and the approach seems far too simplified to be used in practice. The Framo pump unit has a varying cross-section and some surfaces may be in the wake of others. Using all elements that are moving normal to the wave force may be an overestimation due to this. On the other side, using only the projected area may be an underestimation due to the distance between the elements. Hence, it may be reasonable to divide the pump unit into a number of separate parts and calculate the drag coefficient for each of them and then find a middle value. The different coefficients must in that case be weighted by the projected area of that particular part.

Appendix B shows how the pump unit with the running tool and cursor is divided into separate parts and their individually calculated drag coefficients. Some elements are neglected, and in some cases where the parts consist of different elements, a middle value of the projected area is found. Table 3.3 presents the estimated coefficients for the fully submerged pump unit, and modified coefficient applicable for moonpool operations.

C_{DS} [-] Estimated	C_{DS} [-] Applied	C_D [-] Applied in MP	Projected Area [m ²]
1,451	1,5	2,0	8,73

Table 3.3: Calculated drag coefficients for fully submerged pump unit

3.3.3. Added Mass

3.3.3.1. Added Mass in General

A forced motion of an object in water generates waves because it must move some of the surrounding fluid as it moves through it. The fluid adjacent to the object will thus be accelerated with the body to varying degrees, depending on what position they have relative to the object. The added mass is a weighted integration of this entire mass.

Added mass values for lifted objects are important when evaluating dynamic forces during a lifting operation. Ideally added mass should be accurately found from free decay or forced oscillation model tests. From decay tests we find the natural frequency of the system in both air and water. By neglecting added mass in air, the added mass in water can be determined by the following relation:

$$A_{33} = \left[\left(\frac{\omega_{a0}}{\omega_0} \right)^2 - 1 \right] M_{tot} \quad (3.37)$$

where ω_{a0} is the natural frequency in air and ω_0 is the natural frequency in water.

A well adapted conservative approximation for calculating the added mass of simple objects is by adding the volume of two water-hemispheres on top and bottom of the object, as shown in figure 3.12. The extra volume will be the object's added mass.

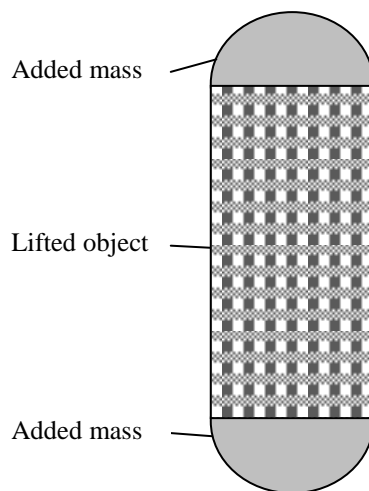


Figure 3.12: A simplified approach when estimating added mass

3.3.3.2. Mass Coefficients

It is far from a trivial operation to determine added mass coefficients. The proximity of the lifted object to the free surface or fixed boundaries, shape of object, frequency, perforation and motion mode all have influence on the mass coefficient. The following will in brief outline these parameters and their affect on the mass coefficient.

Added mass values tend to show strong frequency dependence. Faltinsen [7] reads that the added mass in heave for a surface-piercing two-dimensional body in deep water goes logarithmically to infinity when $\omega \rightarrow 0$. If choosing to estimate added mass values as functions of frequency, we may define 6x6 added mass matrices for different frequencies. However, this is not a straight forward operation and dedicated software tool is needed. DNV [1] does not account for this frequency dependence in their added mass formulas.

Perforation of objects will also reduce the added mass. The added mass of a perforated object is normally calculated from the added mass of the same but non-perforated object by multiplying with a reduction factor [21].

The proximity of an object to another one, to the free surface or a wall, will influence the added mass. Figure 3.13 is taken from DNV [1] and it shows how the added mass for a cylinder varies when lifted object is in the vicinity of the free surface. The frequency of the motion goes to infinity in this specific case. Fully developed added mass should be applied when the top surface of the structure is at a depth greater than the radius of the cylinder, i.e., $h/r \geq 2$ [21].

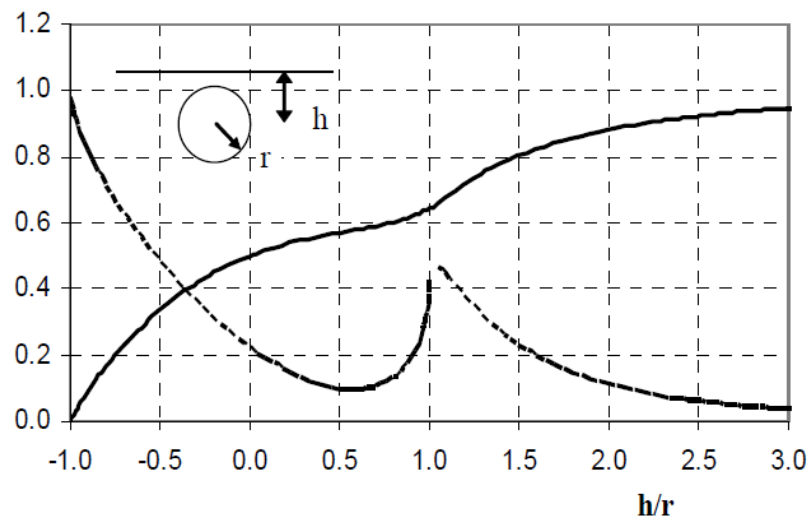


Figure 3.13: High frequency limit of vertical added mass coefficient and its derivative close to a free surface as a function of water depth. Solid line: $a_{33}/\rho\pi r^2$. Dotted line: $(da_{33}/dh)/\rho\pi r$ (DNV [1])

As mentioned in section 3.3.3.1 added mass values may be estimated as equivalent to two hemispheres of water of top and bottom surface. The approach may also be an approximation for objects close to the free surface; the added mass is taken as the available volume of the water-hemisphere depending on the depth of submergence [21]. Figure 3.14 shows an illustration of such a procedure.

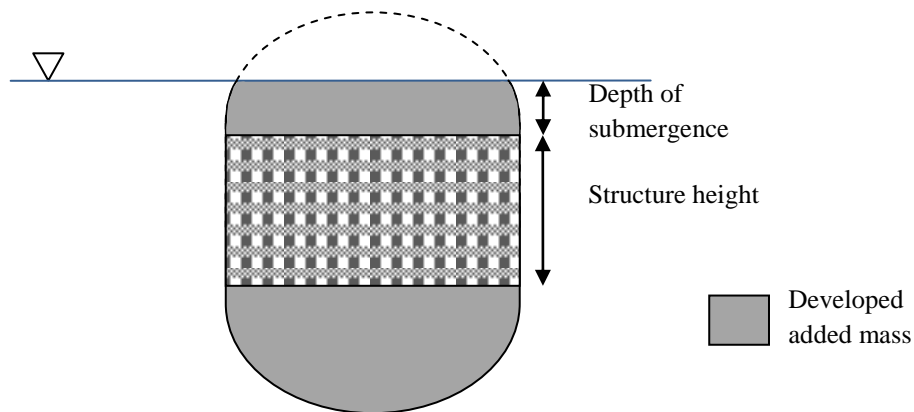


Figure 3.14: Approximation of added mass values of a rectangular plate close to the free surface.

Added mass coefficients depend on the motion mode [7]. This means that added mass in heave for a body is not necessarily the same as added mass in sway, as opposed to Newton's equation $F = ma$ where the mass m is independent of the direction of the acceleration a . However, it is convenient to ignore coupled motions and consider heave motion only for moonpool operations.

The shape of the object has a significant influence on the added mass coefficient. Considering a rectangular shaped object, the added mass will differ drastically with direction. DNV [1] has introduced an analytic approach for calculating the added mass coefficient for simple geometrical structures, see table 3.4.

Most subsea structures are complex geometries and hence it is difficult to determine hydrodynamic coefficients. Added mass values can be obtained by dividing the structure into different well-known geometries, and add resulting values together. Appendix C shows how total added mass is calculated for pump with running tool by simply combining different geometries introduced in DNV [1], assuming a fully submerged structure. Interactions between the different geometries which may increase the added mass is disregarded in the calculations, neither has perforation been accounted for; it is very difficult to determine which reduction factor to use due to structure complexity. Added mass values calculated should be considered to be rough estimates, and more realistic values should be obtained from model tests or CFD-analysis.

Table A-2 Analytical added mass coefficient for three-dimensional bodies in infinite fluid (far from boundaries). Added mass is $A_{ij} = \rho C_A V_R$ [kg] where V_R [m³] is reference volume

Body shape		Direction of motion	C_A				V_R
Flat plates	Circular disc 	Vertical	$2/\pi$				$\frac{4}{3} \pi a^3$
	Elliptical disc 	Vertical	b/a	C_A	b/a	C_A	$\frac{\pi}{6} a^2 b$
	∞		1.000	5.0	0.952		
	14.3		0.991	4.0	0.933		
	12.8		0.989	3.0	0.900		
10.0	0.984		2.0	0.826			
7.0	0.972	1.5	0.758				
6.0	0.964	1.0	0.637				
Rectangular plates 	Vertical	b/a	C_A	b/a	C_A	$\frac{\pi}{4} a^2 b$	
1.00		0.579	3.17	0.840			
1.25		0.642	4.00	0.872			
1.50		0.690	5.00	0.897			
1.59		0.704	6.25	0.917			
2.00		0.757	8.00	0.934			
2.50		0.801	10.00	0.947			
3.00	0.830	∞	1.000				
Triangular plates 	Vertical	$\frac{1}{\pi} (\tan \theta)^{3/2}$				$\frac{a^3}{3}$	

Table 3.4: Added mass coefficients for some well-know geometrical shapes, recommended by DNV [1]

3.3.3.3. Mass Forces in Moonpool

As for the drag coefficient, the added mass coefficient is also increased when exposed to restricted flow conditions in moonpool. DNV [1] suggests the following way of calculating the increased added mass coefficient:

$$\frac{C_A}{C_{A0}} = 1 + 1,9 \left(\frac{A_b}{A} \right)^{\frac{9}{4}} \quad (3.38)$$

where

- C_A = added mass coefficient for moonpool [-]
- C_{A0} = added mass coefficient for unrestricted flow [-]
- A_b = solid projected area of the object [m²]
- A = cross-sectional area of the moonpool (at the vertical level of the object) [m²]

From 3.38 we read that the added mass coefficient for moonpool will increase as the blockage ratio defined as $\frac{A_b}{A}$ increases. Figure 3.16 graphically shows this relation. We see that the added mass coefficient is not significantly affected by the moonpool flow conditions; when the lifted object has a cross-section half of moonpool cross-section, the moonpool added mass coefficient is approximately 1,4 times greater than the coefficient for unrestricted flow. For a

Framo pump the cross-section is much smaller than the moonpool and the added mass coefficient will only increase slightly.

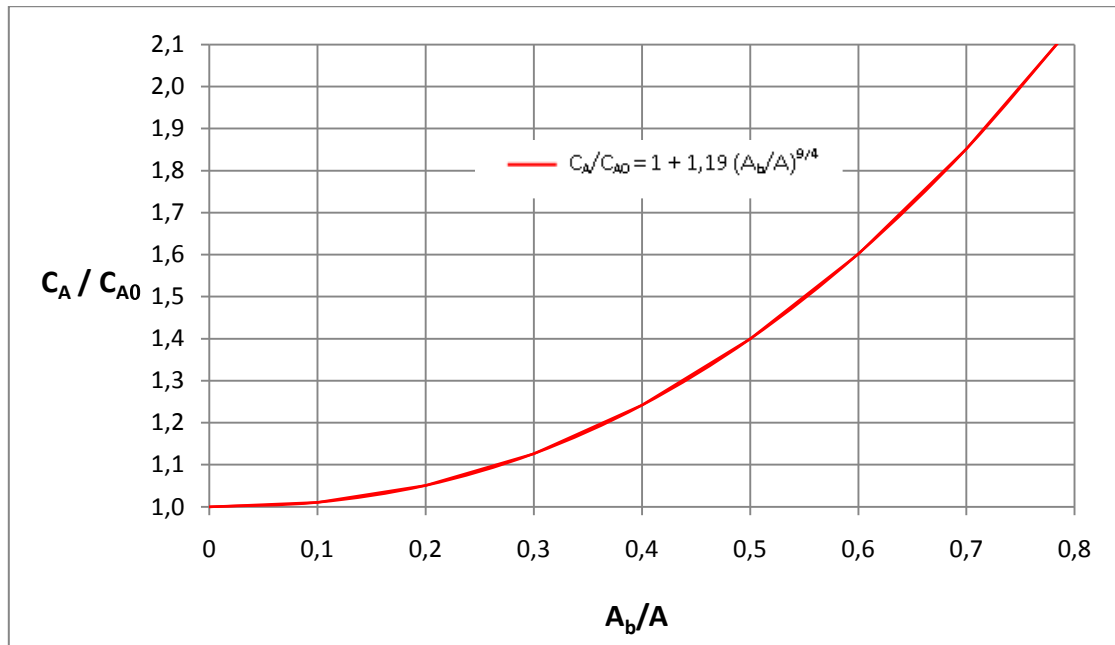


Figure 3.15: Added mass coefficient as a function of moonpool blockage ratio

From table 3.4 we see that added mass can be calculated as:

$$A_{33} = \rho C_A V_r \quad (3.39)$$

For moonpool operations C_A is here taken to be the modified added mass coefficient as given in 3.38. Table 3.5 shows results for added mass values in moonpool for a fully submerged pump with running tool, cursor system is disregarded. The modified added mass coefficient accounts for restricted flow conditions in the moonpool. However, as we see from table 3.5, added mass values do not increase when shifted to moonpool. This is a consequence of dividing the structure into smaller elements. Added mass values are calculated for each individual element and projected area therefore becomes a very small part of the total moonpool area. From equation 3.38 we then get the same values for C_A and for C_{A0} . This must be considered an error to the simplified approach and a somewhat higher added mass should be expected.

It should also be noted that 3.38 accounts for the size of launched object, but not for where in moonpool the object will be launched. Some cursor systems only sit on one of the moonpool walls and in that case the object should be considered to be in the vicinity of a fixed wall. Hence, added mass coefficient will increase further as figure 3.13 indicates.

The added mass has been calculated using two different approaches, the first one entirely based on known geometries presented in DNV [1]. The second approach is based on both the DNV [1] and the approximation of adding the volume of two water-hemispheres on top and bottom of the object. Further explanations and illustrations can be found in Appendix C.

	A_{33} [kg] Estimated	A_{33} [kg] in MP	A_{33} [kg] Applied in MP	Projected Area [m ²]
Total Added Mass, Approach 1	5093,3	5093,3	5110	7,19
Total Added Mass, Approach 2	4339,8	4339,8	4355	6,71

Table 3.5: Calculated added mass for fully submerged pump unit

3.3.4. Mass and Drag Dominating System

When added mass and drag coefficients has been presented, we should discuss their use and importance. One way of studying mass and drag dominance is by use of the Morrison equation. Konopka [13] has investigated Morrison forces when launching a diving bell and cursor through a moonpool. He found that the diving bell was clearly added mass dominated, while the cursor was drag dominated. Based on the geometry of the Framo pump unit with running tool it is not obvious from the above results if the structure is mass or drag dominated.

Many engineers avoid using the Morrison equation as it includes a quadratic drag term. Instead the Keulegan-Carpenter number is used to prove drag or mass dominance. The Keulegan-Carpenter number is defined as:

$$KC = \frac{v_m T}{D} \quad (3.40)$$

where v_m is the maximum particle velocity of the flow and T is the wave period. The Keulegan-Carpenter number is a dimensionless parameter describing the relative importance of drag forces over inertia forces. Gudmestad [11] presents a rule of thumb on deciding if a system is mass or drag dominated. H is here the wave height, i.e. double amplitude and D is the characteristic dimension of object:

- The drag term will dominate for $\frac{D}{H} < 0,1 \rightarrow \frac{H}{D} > 10 \rightarrow \pi \frac{H}{D} = KC > 30$
- The mass term will dominate for $0,5 < \frac{D}{H} < 1,0 \rightarrow 2\pi > \pi \frac{H}{D} = KC > \pi$
- In between, both drag and added mass terms must be taken into account

Figure 3.16 graphically shows the approach from above ([3], in DNV [1]). Here H is the wave height, λ is the wave length and D is the characteristic dimension. To be able to give an approximately prediction of what forces we may expect, we can use some reasonable values for the wave height and the wave length. As an upper limit, Statoil has set $H_s = 5\text{m}$ for installation activities of pump through moonpool. To estimate an appropriate wave length we investigate two realistic cases; $H_s = 5\text{m}$, $T_p = 10$ seconds and $H_s = 3\text{m}$, $T_p = 7$ seconds. Pump with running tool have the approximate dimension of 3,6 meter. However, this is not solid area and perforation should to some extent be accounted for. Characteristic dimension is therefore set to 3 meters. Table 3.6 shows expected values for H/D and $\pi D/\lambda$ and respective force regime. We see that according to the force regime presented in figure 3.17 the pump unit is expected to be mass dominated. Note that these results are based on statistical information and should not be used without further analysis.

H_s [m]	T_p [s]	λ [m]	D [m]	H/D	$\pi D/\lambda$	Force Regime
5	19	156	3	1.67	0,06	V
3	7	77	3	1	0,12	III

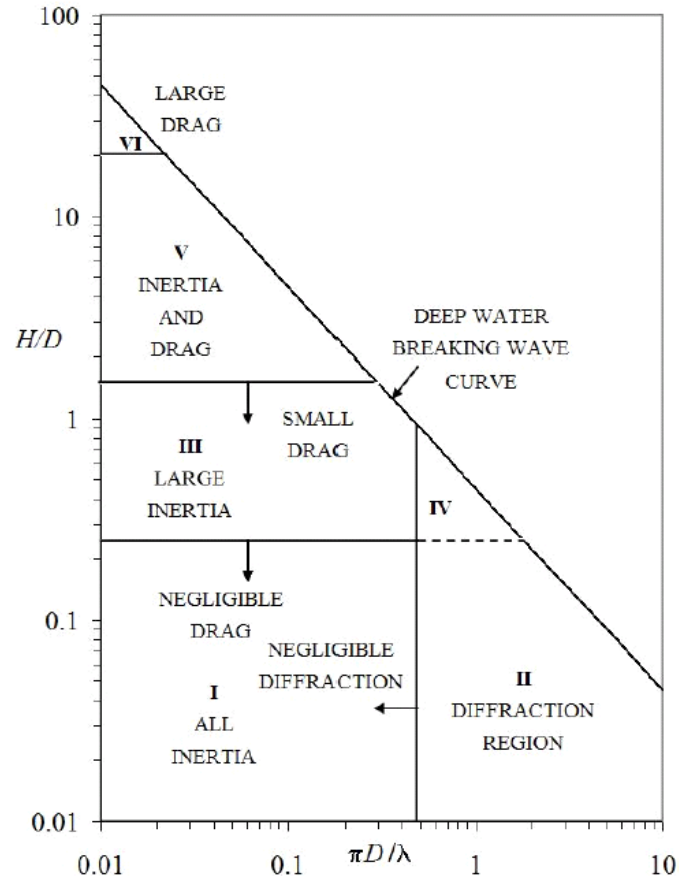
 Table 3.6: Estimated values for H/D and $\pi D/\lambda$


Figure 3.16: Different wave force regimes [3], figure taken from DNV [1]

3.4. Wave Kinematics

Information about water particle motions is on the main input requirements when studying marine lifting operations. The velocity of the fluid particles around lifted object must be expected to give a significant contribution to the forces acting on the object, especially when it is hoisted or lowered close to surface. This chapter will in brief outline some of the derived formulas related to linear wave theory.

Faltinsen [7] presents results from derivation of linear wave theory for propagating waves in finite water depth, some of who shown in table 3.7. Linear wave theory can, to a large extent, describe the wave induced motions and loads on large-volume structures, like a construction vessel. The theory put to use the assumptions of incompressible, inviscid and irrotational fluid.

Velocity potential	$\phi = \frac{g\xi_0}{\omega} \frac{\cosh k(z+h)}{\cosh kh} \cos(\omega t - kx) \quad (3.41)$
Dynamic pressure	$P_D = \rho g \xi_0 \frac{\cosh k(z+h)}{\cosh kh} \sin(\omega t - kx) \quad (3.42)$
x-component of velocity	$u = \omega \xi_0 \frac{\cosh k(z+h)}{\sinh kh} \sin(\omega t - kx) \quad (3.43)$
y-component of velocity	$w = \omega \xi_0 \frac{\sinh k(z+h)}{\sinh kh} \cos(\omega t - kx) \quad (3.44)$
x-component of acceleration	$a_1 = \omega^2 \xi_a \frac{\sinh k(z+h)}{\sinh kh} \cos(\omega t - kx) \quad (3.45)$
z-component of acceleration	$a_3 = -\omega^2 \xi_a \frac{\sinh k(z+h)}{\sinh kh} \sin(\omega t - kx) \quad (3.46)$

Table 3.7: Velocity potential, pressure, velocity and acceleration for regular sinusoidal propagating waves on finite water depth according to linear theory [7]

A real sea state (irregular waves) can be considered a combination of regular waves with different amplitudes and frequencies. To be able to apply formulas in table 3.7 to an irregular sea state we must allow the linear theory to superposition plane wave solutions. Superposition simply summarizes the regular waves in an irregular sea state accounting for the phase lags. We assume that waves have the same propagating direction, which also is a simplification of a real sea state where waves may propagate in different directions. For a realistic record of uni-directional waves, a superposition of at least 15-20 components is required in practice if one is only interested in the mean value of an output [12]. Superposition of two sinusoidal waves is shown in figure 3.17. A real sea state will consist of a number of surface profiles.

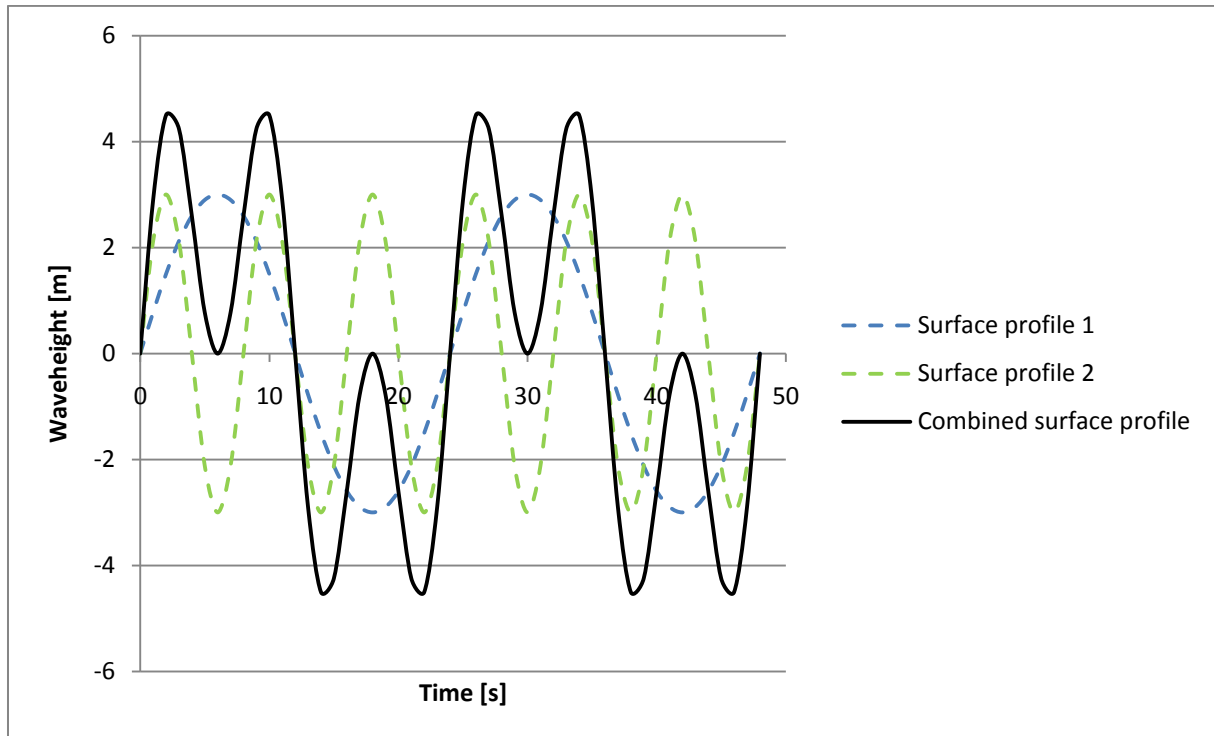


Figure 3.17: Superposition of two sinusoidal waves

It is only logical to study the frequency dependency of an irregular wave train. Thus, the wave elevation (in the time domain) of a long-crested irregular sea, propagating along the positive x -axis, can be written as the sum of a large number of regular wave components (in the frequency domain) [12]:

$$\zeta(t) = \sum_{n=1}^N \zeta_{a_n} \cos(kx - \omega_n t + \varepsilon_n) \quad (3.47)$$

where ε_n is the phase angle component. Phase angle is included to obtain a random irregular sea state.

The applicability of linear wave theory is an important issue to address. According to DNV [5] three wave parameters determine which wave theory to apply in a specific problem. These are the wave height, the wave period and the water depth. Konopka [13] has computed different wave series for moonpool operations and found that his conditions are well outside the limits recommended for linear wave theory, and that 2nd or 3rd order Stokes theory may be better choices. Further, he states that since the conditions are within (or on the limit of) the definition of deep water, the wave potential derived by 2nd order Stokes theory would be equal to the first order velocity potential derived by linear theory for regular waves. Stokes theory is also not applicable due to the irregular waves, and it is therefore reasonable to use linear theory. However, using this model may give some predictive errors.

3.5. Transfer Functions

To be able to predict water motions in the moonpool, we must know how the moonpool response to wave excitation pressure combined with the vessel motion, as well as the sea keeping capabilities of the vessel. Such responses are commonly described by transfer functions.

DNV [1] introduce the following assumptions in their simplified prediction of moonpool water motions:

- The moonpool dimensions are small compared to the breadth of the ship.
- Only motion of water and object in vertical direction is considered.
- The blocking effect of the lifted object on the water in the moonpool is moderate.
- Cursors prevent impact into the moonpool walls. Only vertical forces parallel to the moonpool axis are considered.

A discussion of these assumptions is appropriate in this context. The proposed moonpool for our use is a standard moonpool of 7,2 x 7,2 m. The breadth of typically construction vessel is in the range of approximately 20 m. Assuming small moonpool dimensions compared to the breadth of the ship is hence questionable and should be subject to further discussions before applying the simplified approach recommended by DNV [1].

To only consider vertical water motions seems reasonable, especially when the object to be lifted is fixed to cursor. The moonpool is also preferably located close to centre of roll and pitch axis where translatory motions are minimized.

The blocking effect of a Framo pump unit lifted through the moonpool will be rather small, as already mentioned. The cross-sectional area of a pump unit will be about 4 m², compared to about 52 m² for the moonpool cross-sectional area, which justifies the assumption of a moderate blocking effect.

To assume that cursor prevents impact into the moonpool walls is a reasonable assumption.

The DNV simplified approach [1] is based on the model in figure 3.18.

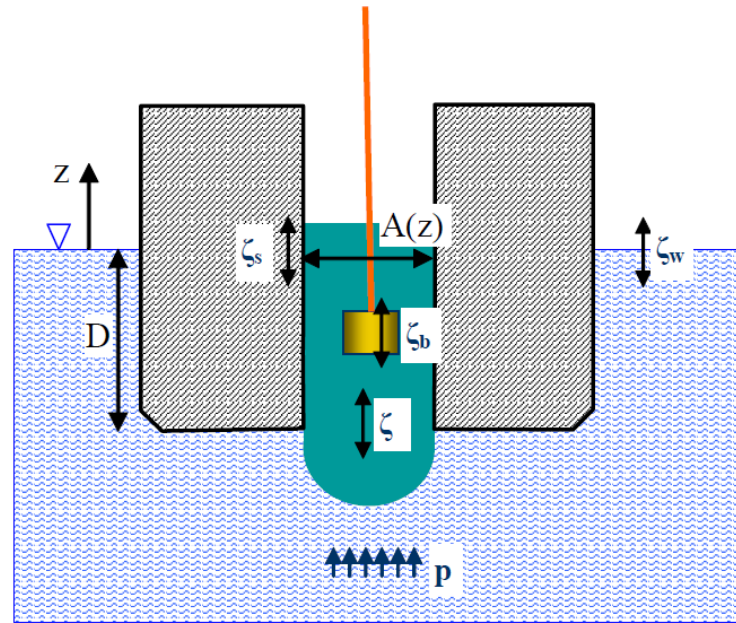


Figure 3.18: Moonpool definitions for DNV-RP-H103 simplified approach [1]

The starting point for the simplified approach is the equation of motion of the water plug. The equation is similar to the mass-spring equation; which has been proven earlier in this thesis to be applicable for moonpool water motions. The equation of the water plug can be written as [1]:

$$(M + A_{WP33})\ddot{\zeta} + C_s|\dot{\zeta} - \dot{\zeta}_s|(\dot{\zeta} - \dot{\zeta}_s) + C_b|\dot{\zeta} - \dot{\zeta}_b|(\dot{\zeta} - \dot{\zeta}_b) + K_w\zeta = F(t) \quad (3.48)$$

where

M	= mass of water plug [kg]
A_{WP33}	= added mass of water plug [kg]
ζ	= motion of water plug [m]
ζ_s	= heave motion of ship [m]
ζ_b	= motion of body in moonpool [m]
ζ_w	= sea surface elevation outside moonpool [m]
C_s	= damping coefficient for relative motion between water plug and vessel [kg/m]
C_b	= damping coefficient for relative motion between water plug and object [kg/m]
K_w	= $\rho g A$ water plane stiffness [kg/s ²]
$F(t)$	= wave excitation force on water plug [N]

The added mass of the water plug can according to DNV [1] be taken as:

$$A_{WP33} = \rho \kappa A(-h) \sqrt{A(-h)} \quad (3.49)$$

Konopka [13] has found that 3.49 is valid also for the reduced mass of the water plug and increased damping, which justifies using the equation also when the pump unit is present. However, the reduced area of the moonpool opening due to the pump unit is neglected. It is also believed that different fittings inside the moonpool will affect the added mass.

Assuming a moonpool with constant cross-sectional area (7,2 x 7,2 m) the added mass of water plug will be 175,3 tons, using equation 3.49. This assumes no bottom plates, which will have a reducing effect on water plug added mass. Øritsland [22] tested a circular bottom plate with opening for the diving bell; the plate reduced the opening by 48,8 %. Such a reduction of moonpool opening would have decreased the added mass in our moonpool by a factor of 3.

3.5.1. Vessel

The ship heave motion is related to the sea surface elevation by a transfer function G_s [1]:

$$\zeta_s = G_s \zeta_w \quad (3.50)$$

The vessel transfer function, commonly referred to as RAO's (Response Amplitude Operators), defines the vessel reaction to the action of waves. The vessel motion transfer function is normally derived using dedicated software, and is often verified by model tests. RAOs are exclusive to its respective vessel and load case.

The vessel RAO is a complex function which returns a complex number for each wave frequency. The real part of the function gives the response amplitude to the wave amplitude, while the argument gives the phase angle or motion delay.

To utilize a vessel RAO we need information about the sea state in which the vessel shall operate. Generation of an irregular sea state (as described in 3.4) is often based on a wave spectral density function. For North Sea waves, we may use the JONSWAP wave spectrum. Figure 3.23 shows a standard JONSWAP spectrum.

When solving non-linear problems, we may transform the wave spectrum into time series. This is often referred to as the inverse problem as the wave spectrum itself is derived by use of time series; the first transformation basically divides an arbitrary signal (though limited in time and assumed periodic) into its frequency dependent components (spectrum). Given sufficient sampling frequency, the inverse transform of a signals spectrum rebuilds the original signal [13].

When we obtain a wave spectrum from time series, we lose the phase angle. When doing the inverse transformation we need the phase angle to generate the time record, and therefore we must choose a new set of random angles, i.e. $0 - 2\pi$. Our newly obtained time series will thus be different from the original one. However, the energy density is equal and statistically they are also identical. Figure 3.19 shows the time series from the wave record analysis and the results from the inverse transformation.

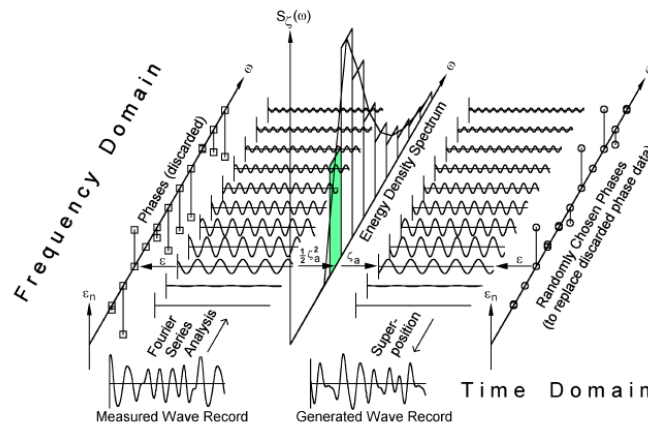


Figure 3.19: Wave record analysis and regeneration [12]

3.5.2. The Water Plug

This section briefly outlines the simplified method for calculating the water plug response presented in DNV [1].

The hydrodynamic pressure force on the water plug can be related to the sea surface elevation by a transfer function G_w :

$$F(t) = G_w \zeta_w \quad (3.51)$$

If we disregard the lifted object in equation 3.48, the motion of the water plug can be written as:

$$M\ddot{\zeta} + C_{sl}(\dot{\zeta} - \dot{\zeta}_s) + K_w\zeta = F(t) \quad (3.52)$$

where M is the total mass of the water plug, included the added mass and C_{sl} is the linearized damping coefficient between the water and the vessel, and is defined as $C_{sl} = 2\eta\sqrt{KM}$. η is the damping ratio relative to critical damping. Substituting 3.52 into 3.51 and thus rewrite it on a frequency dependent form gives:

$$-\omega^2 M\zeta + i\omega C_{sl}(\zeta - G_s \zeta_w) + K_w\zeta = G_w \zeta_w \quad (3.53)$$

From 3.53 DNV [1] defines a transfer function between the surface elevation and the motion of the water plug:

$$\frac{\zeta}{\zeta_w} = \frac{i\omega C_{sl} G_s + G_w}{-\omega^2 M + i\omega C_{sl} + K_w} = \frac{\frac{G_w}{\rho g A} + 2i G_s \eta \frac{\omega}{\omega_0}}{1 - \left(\frac{\omega}{\omega_0}\right)^2 + 2i\eta \frac{\omega}{\omega_0}} \quad (3.54)$$

To be able to find a relationship between transfer functions G_s and G_w , DNV [1] suggests some simplifying assumptions:

- Moonpool dimensions are small compared to ship breadth
- Excitation force due to incoming waves and due to ship motions can be assessed as for a ship without moonpool
- Fluid pressure expressions valid for long waves can be used
- Deep water is assumed

Based on these assumptions, the following approximate expressions for the forces on the water plug can be used:

$$F(t) = F_{wave}(t) + F_{vessel}(t) \quad (3.55)$$

$$= P_{FK}A + A_{33}\ddot{\zeta}_s \quad (3.56)$$

$$= \rho A g \zeta_w e^{-kD} + \kappa \rho \sqrt{A} A \ddot{\zeta}_s \quad (3.49)$$

$$= \rho A \zeta_w (g e^{-kD} - \omega^2 \kappa \sqrt{A} G_s) \quad (3.50)$$

where P_{FK} is taken as the Froude-Krylov dynamic fluid pressure, and A_{33} is the added mass of the water plug.

Equation 3.51 can thereby be extended to give a complete expression for the transfer function between the surface elevation and the exciting force:

$$G_w = \frac{F(t)}{\zeta_w} = \rho A (g e^{-kD} - \omega^2 \kappa \sqrt{A} G_s) \quad (3.51)$$

where k is the wave number and can be expressed as $k = \frac{\omega^2}{g}$, based on the deep water assumption.

The damping amount in the moonpool has a fairly large impact on the response calculations. For the illustrated moonpool in figure 3.6 it is recommended by DNV [1] to use a 45 % damping coefficient.

3.6. Water Entry

Water entry is an essential phase of any marine lifting operation. It is commonly assumed that the dynamic forces are largest in this phase of the lift; hence the highest loads may occur here. Slack lifting wire and resulting snap loads are critical features during water entry and should as far as possible be avoided.

Analysis and estimation of hydrodynamic loads during water entry is a complex matter. Different stages of submergence for lifted object causes large non-linearities; water impact effects will vary constantly along with drag and added mass values. As a result the lifting operation should be analyzed using a number of different load cases. Establishing load cases should identify main items on lifted object contributing to hydrodynamic forces [1].

Slamming

As mentioned under the description of installation steps of the Framo products, it is crucial to keep launched object from residing in the splash zone. Impulse loads with high pressure peaks occur during impact between an object and water [7]. This is referred to as slamming. The characteristic slamming impact force on the parts of the object that penetrate the water surface may be taken as [1]:

$$F_{slam} = 0,5\rho C_{sl}A_s v_s^2 \quad (3.52)$$

where C_{sl} is the slamming coefficient, taken to be not less than 5,0 for a structure such as the Framo pump unit [1]. A_s is the projected area on a horizontal plane that will be subject to slamming loads during crossing of water surface, and v_s is the slamming impact velocity. The slamming velocity is given as:

$$v_s = v_c + \sqrt{v_{ct}^2 + v_w^2} \quad (3.53)$$

where v_c is the hook lowering velocity, v_{ct} is the characteristic single amplitude vertical velocity of the crane tip and v_w is the characteristic vertical water particle velocity.

Varying Buoyancy

Wave surface elevation causes constant change in buoyancy force in the splash zone. Figure 3.20 illustrates the phenomenon. The left triangular object is suspended in a wave crest and will be subject to a substantial uplift due to buoyancy. The second triangular object is suspended in wave trough and will not be subject to any uplift due to buoyancy.

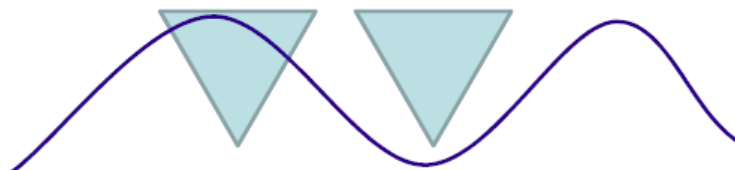


Figure 3.20: Illustration of varying buoyancy in the splash zone

The change in buoyancy force is given as [1]:

$$F_p = \rho \delta V g \quad (3.54)$$

where δV is the change in volume of displaced water from still water surface to wave crest or wave trough.

Mass force

The mass force term is here considered as a combination of the inertia force and the hydrodynamic force contributions from Froude-Krylov forces and diffraction forces. The characteristic mass forces on an object due to combined acceleration of object and water particles may be taken as [1]:

$$F_M = \sqrt{[(M + A_{33})a_{ct}]^2 + [(\rho V_i + A_{33})a_w]^2} \quad (3.55)$$

Added mass has been discussed earlier and will not be given any further attention in this section.

Drag force

The characteristic drag force on an object may be taken as [1]:

$$F_D = 0,5 \rho C_D A_b v_r^2 \quad (3.56)$$

Drag has been discussed earlier and will not be given any further attention in this section.

Resulting force

From the previous it is clear that the resulting hydrodynamic force acting on lifted object is a time dependent function of slamming impact forces, varying buoyancy hydrodynamic mass forces and drag forces, and can be estimated as [1]:

$$F_{hyd} = \sqrt{(F_D + F_{slam})^2 + (F_M - F_p)^2} \quad (3.57)$$

Note that slamming forces only act upwards. Total load on lifted object (maximum and minimum) is found by adding or subtracting the resulting hydrodynamic force to the static weight of the object.

Snap force

Snap loads occur if the upward hydrodynamic forces exceed the static weight of the lifted object. The characteristic snap load may be taken as [1]:

$$F_{snap} = v_{snap} \sqrt{K(M + A_{33})} \quad (3.56)$$

where v_{snap} is the snap velocity, and is dependent on free fall velocity of lifted object, lowering velocity, characteristic single amplitude vertical velocity of the crane tip and the

characteristic vertical water particle velocity. K is the stiffness of the hoisting system. If snap loads occur then total force on lifted object should be taken as the static weight of the object plus snap force.

3.6.1. Moonpool vs. Overside Water Entry

If properly designed, relative motions in moonpool should be smaller compared to wave motions on the ship side. As earlier mentioned a moonpool is preferably located close to centre of roll and pitch axis to reduce adverse effects of vessel angular motions. To mathematically prove this, we use a vessel with six degrees of freedom of a vessel. The motion of any point on the vessel is then given as [7]:

$$\mathbf{s} = (\eta_1 + z\eta_5 - y\eta_6)\mathbf{i} + (\eta_2 - z\eta_4 + x\eta_6)\mathbf{j} + (\eta_3 + y\eta_4 - x\eta_5)\mathbf{k} \quad (3.57)$$

where η_i denotes displacement in respective direction, 1, 2 and 3 are translatory motion in surge, sway and heave, and 4, 5 and 6 are the angular motions roll, pitch and yaw. x , y and z is the coordinates at the centre of gravity. Knowing that the moonpool is located close to this point the angular motions may be disregarded, meaning $\eta_4 = \eta_5 = \eta_6 = 0$. Consequently will vessel motion be reduced to:

$$\mathbf{s} = (\eta_1)\mathbf{i} + (\eta_2)\mathbf{j} + (\eta_3)\mathbf{k} \quad (3.58)$$

However, 3.58 is not applicable for oversee water entry, as the crane tip is positioned further away from vessel centre of gravity. Therefore we may expect greater crane tip velocities and accelerations when launching oversee compared to moonpool. Assuming the same wave conditions this implies that the water entry forces will be larger during oversee launching, as they are a function of the relative velocities and accelerations between crane tip and waves.

Water oscillations in moonpool excited by waves and heave motion of vessel may reach great magnitudes in resonance condition. If so happens, the characteristic vertical water particle velocity will increase causing the slamming impact velocity to increase.

A vital difference between lifting through moonpool and over the vessel side is the moonpool cursor system. Lifted object is fixed to cursor when launched through moonpool, which prevents horizontal and also rotary motion of object. Consequently will an object launched through the moonpool always meet the water with bottom first, while an over side launching operation may not have the ability of keeping a constant alignment of object at all times.

Pendulum motion of lifted object is also avoided by using a cursor system. During an oversee lift pendulum motion may arise when horizontal forces act on the object, both from waves and from wind.

The moonpool cofferdam will induce a milder water entry; a reduction of the surface elevation due to the cofferdam increases the difference between the surface pressure in the moonpool and the exciting fluid pressure below [13]. Equation 3.12 relates the pressure

gradient in the moonpool to the vertical fluid acceleration, and from that it follows that fluid accelerations will be smaller in the cofferdam.

Air injection in moonpool may also induce a milder water entry. When aerating the water we can decrease the impact load on the object passing through the moonpool.

The location of the moonpool may, however, not be at the exact centre of roll and pitch motions, and also, centers of roll and pitch motions do not always correspond to the same location. We must therefore take into account that roll and pitch motions of the vessel will, to some degree, affect the crane tip motion in the moonpool.

During an overside lift we expect the highest loadings to occur when going through the splash zone. Through the moonpool it is not necessarily given that the splash zone will induce the highest loadings. A critical area, mentioned in 3.2.3, is the phase where lifted object leaves the moonpool. It is very hard to obtain detailed information about forces acting below the moonpool entrance and consequently it becomes very difficult to predict forces acting on the object. A possible high momentum can arise when object is exposed to horizontal wave forces and still connected to cursor system. As a result we may experience high forces on the object-cursor interface. Combined with vessel rotational motions the forces may be enhanced. The scenario is illustrated in figure 3.21. High momentum is an issue during the total lift through the moonpool and it is important that object-cursor interface can withstand these loads.

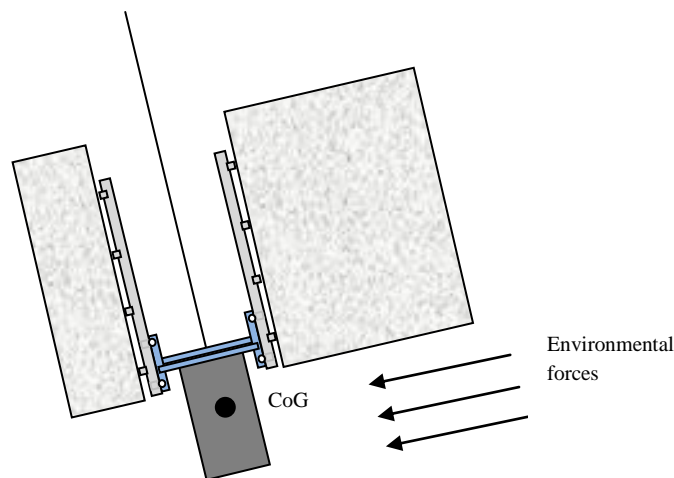


Figure 3.21: Lifted object below moonpool

3.7. Moonpool Resonance Period

The resonance period has been calculated using equation 3.29 where constant cross-sectional area of moonpool is assumed. The horizontal cofferdam will increase the surface area some distance above mean water level but this is disregarded as no information about cofferdam exists. Varying cross-sectional area due to the vertical cofferdam is also disregarded in 3.29 and a somewhat higher resonance period than what indicated in figure 5.1 could be expected. Figure 3.22 shows the resonance period as a function of the vessel draft. Vessel draft is chosen based on typical drafts of installation vessels.

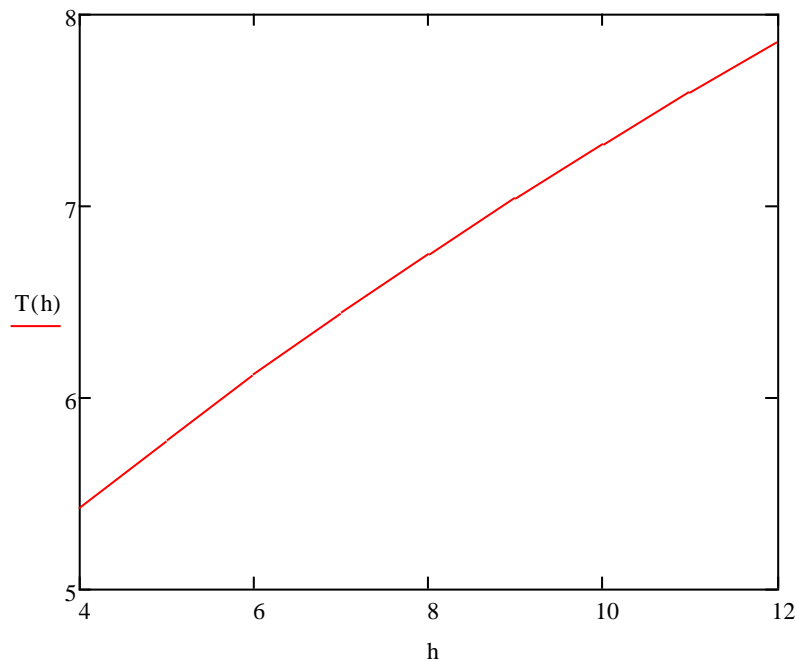


Figure 3.22: Resonance period as a function of vessel draft

We see that the moonpool resonance period has a value lying between 5,4 and 7,8 seconds. The graph shows a clear, almost linear, correlation between resonance period and draft of vessel.

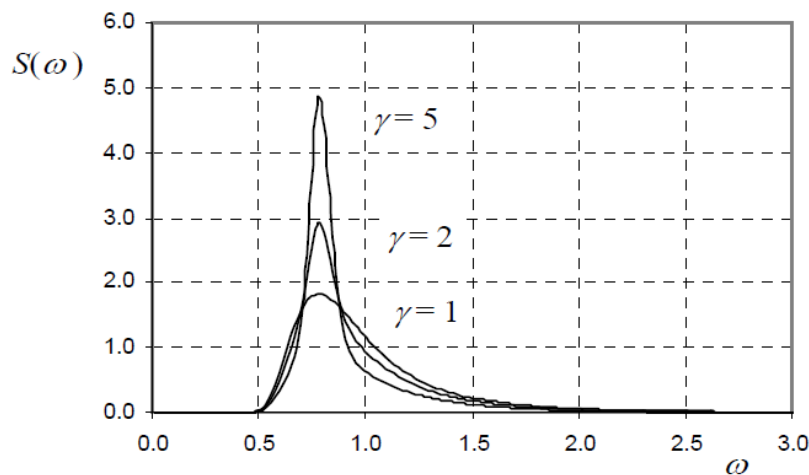
Øritsland [22] presents results for relative motion in a 3,9 x 3,9 m moonpool. He used a hull model in irregular seas, simulating a diving operation condition on station keeping at 60° heading to the waves and scaled his result using Froude scaling law. The draught of used vessel was 5,44 m. His results are reproduced in table 3.8.

We see that the agreement between test results from table 3.8 and calculated resonance period in figure 3.22 is satisfactory. Test results also shows that damping chambers installed in moonpool will increase the resonance period slightly.

Test no.	Wave $H_{1/3}$ (m)	Relative motion in moonpool				Reduction		Remarks
		$H_{R 1/3}$ (m)	T_1 (s)	RAO max.	Peak Period T_P (s)	$H_{R 1/3}$ (%)	RAO (%)	
13	2.3	1.840	5.60	1.25	5.26	-17,5	-31.3	“Comex” Cursor Rails
14	4.2	2.578	6.01	1.08	5.26	-12,1	-27.5	
19	2.3	0.889	6.15	0.50	6.76	-60.1	-72.5	“Comex” + damping chambers, 17 % light area
20	4.2	1.769	6.62	0.63	6.33	-39.7	-57.7	
21	2.3	0.822	6.11	0.45	~6,7	-63.1	-75.3	“Comex” + damping chambers, 35 % light area
22	4.2	1.462	6.64	0.49	6,33	-50.2	-67.1	

Table 3.8: Test results for moonpool relative motion [22]

Resonance has the largest influence on the amplitude of the water oscillations, and one way of avoiding large oscillations is thus to avoid the resonance condition. However, figure 3.23 shows dominant wave frequencies for the North Sea, which to a great extent coincide with the moonpool resonance period (wave period = 2π / wave frequency). In other words, it will be very hard to completely avoid resonance conditions when operating in the North Sea.


 Figure 3.23: JONSWAP spectrum for $H_s = 4,0$ m, $T_p = 8,0$ s for $\gamma=1$, $\gamma=2$ and $\gamma=5$

4. Conclusion

Framo Engineering AS delivers key equipment to the oil and gas industry. Enhanced recovery system technologies have become their speciality with innovative subsea solutions. Field operators want to keep a high operability of Framo equipment as it directly influences the production rate. The demand for replacing damaged equipment effectively has therefore become an important issue, and it is a desire that the sea state in which interventions can be done is as high as possible. Despite the development of intervention technology, the hazard of the air/sea interface still remains a troublesome hurdle. An alternative to the conventional overside crane operation is the use of a moonpool system. The main advantages of this system include avoidance of horizontal force components from waves and winds and smaller crane tip motions.

However, the moonpool has a major drawback in its water oscillations. The wave amplitude inside the moonpool may become larger than the outside wave amplitude if excited at resonance, which can create unpredictable loadings on lifted objects. To avoid that moonpool natural frequency has the same value as the wave frequency would seem like a good solution. But in practice, when operating in the North Sea, this approach will be difficult as the moonpool resonance periods are normally within the period range of the typical North Sea wave spectrums. Thus, it becomes important to reduce response amplitude in resonance conditions by implementing damping features in the moonpool. Test results show that a vertical cofferdam reduces amplitude with more than 60 percent compared to a naked moonpool. Other effective damping features are horizontal cofferdams and bottom plates.

It has been proven that moonpool water oscillations resemble a mass-spring system and its behavior can be approximated as such. In order to compute responses from such a system it is necessary to obtain information about hydrodynamic parameters. DNV-RP-H103 introduces a simplified method for computation of added mass and drag coefficient with the use of well-known geometries. Framo pump with running tool is a very complex structure and computation of hydrodynamic coefficients is hence difficult. It is possible to obtain approximated values by dividing the structure into smaller elements and apply formulas presented in DNV-RP-H103. Results should still be used with caution as they are subject to large uncertainties. When doing lifting analysis the hydrodynamic coefficients should be accurately found from free decay test, forced oscillation model tests or CFD-analysis.

Theory related to the moonpool water motions is without doubt a complex matter. Apart from the already mentioned difficulties, there is the vessel-moonpool interaction to consider. Investigating the coupled moonpool problem is a formidable task as it stands, and dedicated software is preferred to obtain realistic results. Adequate input data such as information about sea state and vessel RAO is required.

When planning a lifting operation through moonpool it is very important to have knowledge about the main characteristics of the system. Its limitations and difficulties should be carefully investigated early in the planning phase. If failing to do so, one may be taken by surprise by the moonpool features. On the other side, if able to overcome the drawbacks of a moonpool installation system, the approach would offer some distinct advantages compared to an overside crane operation. It would also offer an opportunity to increase the installation weather window and consequently we obtain a longer installation season.

5. Recommendation for Further Work

From *my* point of view it is very difficult to assess the calculated hydrodynamic parameters; they may indicate reasonable values but should not be directly applied in any lifting analysis. In such analysis it is important to obtain accurate values, especially if acceptance criteria are somewhat marginal. It is strongly recommended that models tests are carried out and that a further theoretical study is performed.

Although heave motions are commonly assumed to influence the moonpool water oscillations the most, it should be investigated that it is in fact so. If moonpool is mistakenly placed in proportion to centre of roll and pitch axis, these rotational motions may give a large effect on vertical water oscillations in the moonpool.

The effect of employed damping devices should be investigated to obtain accurate damping values for the specific moonpool. If bottom hatches are used, it is important (and obvious) that launched or retrieved objects can pass through with satisfying clearance.

In a realistic moonpool problem it is conceivable that the water oscillations will affect the motion of the vessel by altering the flow pattern near the bottom opening of the moonpool. In the same way vessel motion will affect the water motions inside the moonpool. DNV-RP-H103 suggests a conservative approach to this coupled problem by describing the wave flow using linear wave theory. However, this approach may be subject to a large error as the flow physically is strongly influenced by the moonpool water flow. The phase where lifted object passes the bottom opening needs to be analysed to predict the forces acting on the cursor-moonpool interface.

The vessel to be used during the lifting operation must be pre-defined to obtain necessary sea keeping capabilities. This is required input data to the moonpool problem. Corresponding sea states at the actual location must also be known.

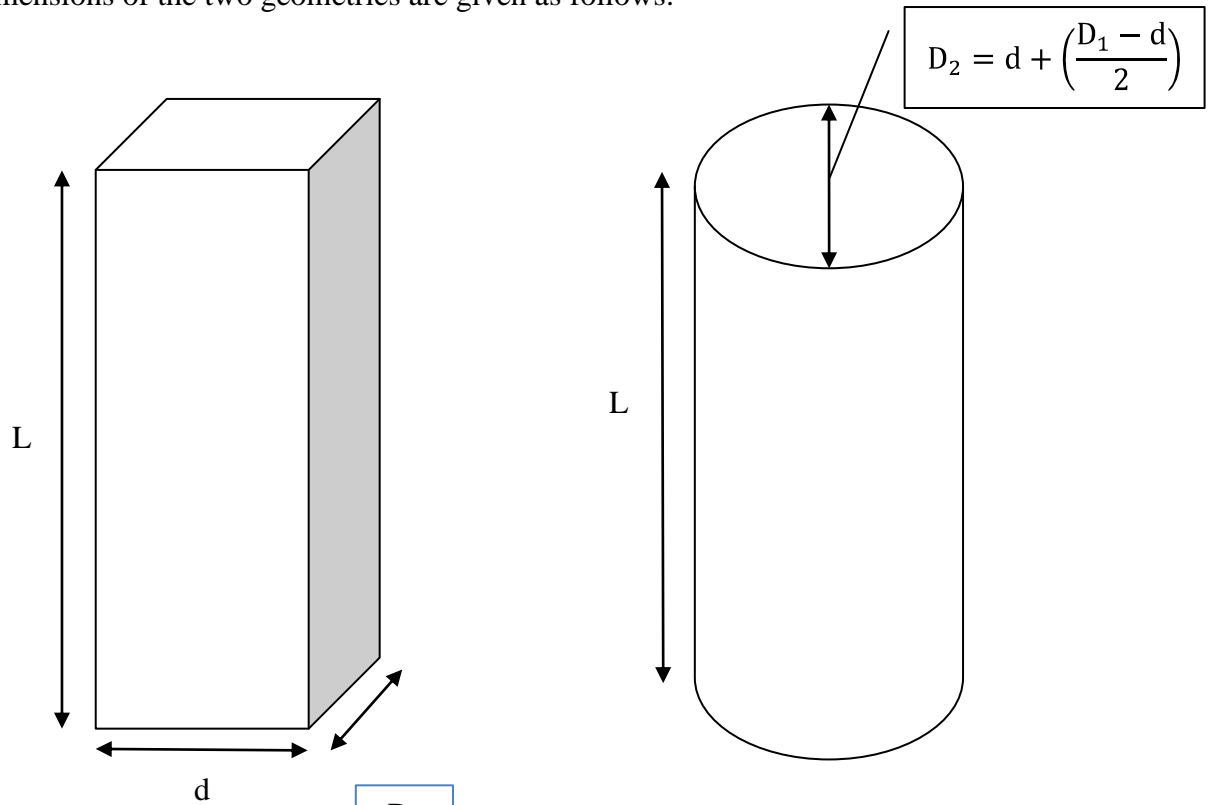
6. References

- [1] Det Norske Veritas. (2010) *DNV-RP-H103 Modelling and Analysis of Marine Operations*.
- [2] Alsgaard, J.A. (2010) *Numerical Investigation of Piston Mode Resonance in a Moonpool Using OpenFOAM*. Master Thesis, The Norwegian University of Science and Technology, Trondheim
- [3] Chakrabarti, S.K. (1987) *Hydrodynamics of Offshore Structures*. Southampton, WIT Press
- [4] Day, A.H. (1990) The Design of Moonpools for Subsea Operations. *Marine Technology*, vol. 27 (3), pp. 167-179
- [5] Det Norske Veritas. (2010) *DNV-RP-C205 Environmental Conditions and Environmental Loads*
- [6] Eidvin, T. & Øverland, J.A. (2009) *Tolket Tordis feil*. [Online]. Accessed from <http://www.npd.no/Publikasjoner/Norsk-sokkel/Nr2-20091/Tolket-Tordis-feil/> [Downloaded 21st of March 2011]
- [7] Faltinsen, O.M. (1990). *Sea Loads on Ships and Offshore Structures*. Cambridge: Cambridge University Press
- [8] Gaillarde, G. & Cotteleer A. (2004) Water motions in moonpools – Empirical and numerical approach. Proceedings of the *Association Technique Maritime et Aeronautique*, Paris, France
- [9] Gemba, K. (2007) *Shape Effects on Drag*. Academical paper, Department of Aerospace Engineering, California State University, California
- [10] Grenland Group. (2010) *Multi Intervention Tower* ® Grenland Group ASA. [Online]. Accessed from <http://www.grenlandgroup.com/getfile.php/Filer/Attachments%20Products/Multi%20Intervention%20Tower%20Brochure.pdf> [Downloaded 29th of April 2011]
- [11] Gudmestad, O.T. (2010) *Lecture notes in Marine Technology*. University of Stavanger, Stavanger
- [12] Journèe, J.M.J & Massie, W.W. (2001) *Offshore Hydrodynamics* (First Edition). Delft: Delft University of Technology.
- [13] Konopka, B. (2009) *Simulation of the Loads and Responses of a Diving Bell Launched Through a Moon Pool*. Master Thesis, The Norwegian University of Science and Technology, Trondheim
- [14] Kuo, C. (1978) A Controlled Handling Method for Effective Offshore Support Operations. Proceedings of the *10th Annual Offshore Technology Conference*, Houston, Texas
- [15] Lallier, E.B., Ross, C.L. & Davis, C.I. (2003) Protective Deployment of Subsea Equipment. Proceedings of the *2003 Offshore Technology Conference*, Houston, Texas

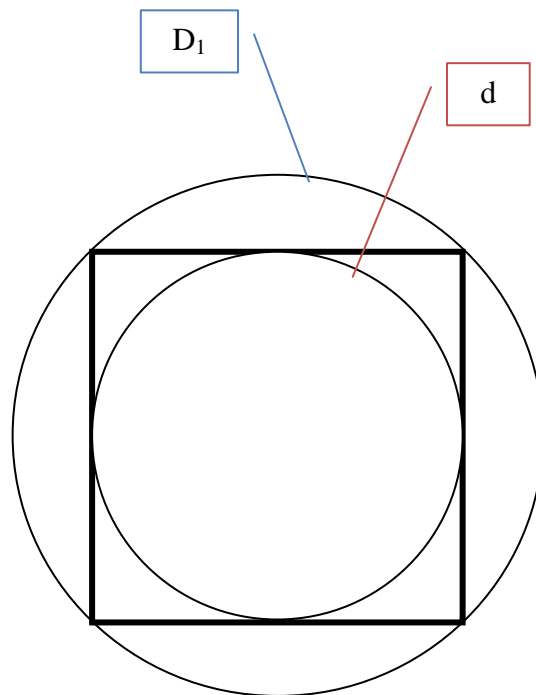
-
- [16] Lee, B.S. (1982) *On the Properties of Vertical Water Oscillation in a Moonpool*. Doctoral Thesis, University of Strathclyde, Department of Ship and Marine Technology, Glasgow
- [17] Madsen, N.F. (1980) Prediction of Water Level Motion and Forces Acting on a Diving Bell During Launching Through a Moonpool. Bulletin no. 45, Danish Ship Research Laboratory, Lyngby
- [18] Molin, B. (2000) On the Piston and Sloshing Modes in Moonpools. *The Journal of Fluid Mechanics*, vol. 430, pp. 27-50
- [19] Newman, J.N. (1977) *Marine Hydrodynamics*. Cambridge: The Massachusetts Institute of Technology Press
- [20] PennEnergy (2010) *Tordis Becomes World's First Subsea Processing Installation*. [Online] Accessed from <http://www.pennenergy.com/index/petroleum/offshore/display/315249/articles/offshore/volume-67/issue-12/top-five-projects/tordis-becomes-worlds-first-subsea-processing-installation>. [Downloaded 4th of May 2011]
- [21] Sarkar, A. & Gudmestad, O.T. (2010) Splash Zone Lifting Analysis of Offshore Structures. Proceedings of the *ASME 2010 20th International Conference on Ocean, Offshore and Arctic Engineering*, Shanghai
- [22] Øritsland, O. (1982) *Relative Motion in Moonpool: Diving Support Vessel*. Report, NHL (Sintef)
- [23] Henriksen, P.R. (2010) Subsea Technology – Norwegian and International Perspectives. Speech at the *Underwater Technology Conference*, Bergen [Online] Accessed from http://www.regjeringen.no/nb/dep/oed/aktuelt/taler_artikler/politisk_ledelse/taler-og-artikler-av-statssekretar-per-r/2010/Subsea-Technology--Norwegian-and-International-Perspectives.html?id=620417 [Downloaded 4th of May 2011]

APPENDIX A - Comparison of Drag Coefficient and Forces for Square and Cylindrical Structure

The dimensions of the two geometries are given as follows:



where



The estimation of the drag coefficients for the two geometries is based on DNV-RP-H103, ref. table 3.3 from chapter 3.3.2.2.

The comparison of the drag forces on the two geometries will have a small error due to the difference in cross-sectional area, ref. the formula for the drag force:

$$F_D = \frac{1}{2} \rho C_{DS} S u^2$$

where S is the projected area normal to flow direction. To minimize this error the diameter of the cylinder has been taken as the middle value of the distance between the outer corners and diameter of the square, as shown above, where the weighted line represents the cross-section of the square geometry.

Table A.1 and A.4 show how the drag coefficient for steady flow varies with varying cross-sectional area of the square and the cylinder, respectively. Table A.2 and A.5 show the corresponding moonpool drag coefficient, while table A.3 and A.6 show how the drag force per square velocity vary with the varying blocking coefficient. C_{DS} represents the calculated drag coefficient for steady flow, while C_D is the consequent moonpool drag coefficient.

Note! The blue column represents length of structure equal to 4 meters, pink 4,5 meters, green 5 meters, and blue 5,2 meters.

CALCULATIONS FOR SQUARE GEOMETRY

L [m]	D [m]	C _{DS} [-]	L [m]	D [m]	C _{DS} [-]	L [m]	D [m]	C _{DS} [-]	L [m]	D [m]	C _{DS} [-]
4	1	0,95	4,5	1	0,95	5	1	0,95	5,2	1	0,95
4	1,2	0,94	4,5	1,2	0,95	5	1,2	0,95	5,2	1,2	0,95
4	1,4	0,92	4,5	1,4	0,93	5	1,4	0,94	5,2	1,4	0,94
4	1,6	0,9	4,5	1,6	0,92	5	1,6	0,93	5,2	1,6	0,94
4	1,8	0,9	4,5	1,8	0,9	5	1,8	0,92	5,2	1,8	0,92
4	2	0,87	4,5	2	0,89	5	2	0,9	5,2	2	0,9
4	2,2	0,9	4,5	2,2	0,87	5	2,2	0,89	5,2	2,2	0,89
4	2,4	0,94	4,5	2,4	0,9	5	2,4	0,87	5,2	2,4	0,88
4	2,6	0,96	4,5	2,6	0,92	5	2,6	0,89	5,2	2,6	0,87
4	2,8	1	4,5	2,8	0,95	5	2,8	0,91	5,2	2,8	0,9
4	3	1,03	4,5	3	0,97	5	3	0,94	5,2	3	0,92
4	3,2	1,06	4,5	3,2	1	5	3,2	0,96	5,2	3,2	0,96
4	3,4	1,08	4,5	3,4	1,03	5	3,4	0,98	5,2	3,4	0,98
4	3,6	1,11	4,5	3,6	1,06	5	3,6	1	5,2	3,6	0,99
4	3,8	1,13	4,5	3,8	1,08	5	3,8	1,03	5,2	3,8	1,02
4	4	1,15	4,5	4	1,1	5	4	1,06	5,2	4	1,04
			4,5	4,2	1,12	5	4,2	1,08	5,2	4,2	1,06
			4,5	4,4	1,14	5	4,4	1,1	5,2	4,4	1,08
						5	4,6	1,12	5,2	4,6	1,1
						5	4,8	1,13	5,2	4,8	1,12
						5	5	1,15	5,2	5	1,14
									5,2	5,2	1,15

Appendix Table A.1: Drag coefficient for steady flow, square geometry

A _{projected} [m ²]	C _D [-]	A _{projected} [m ²]	C _D [-]	A _{projected} [m ²]	C _D [-]	A _{projected} [m ²]	C _D [-]
1	0,98	1	0,98	1	0,98	1	0,98
1,44	0,98	1,44	0,99	1,44	0,99	1,44	0,99
1,96	0,97	1,96	0,99	1,96	1,00	1,96	1,00
2,56	0,97	2,56	0,99	2,56	1,00	2,56	1,01
3,24	0,99	3,24	0,99	3,24	1,01	3,24	1,01
4	0,98	4	1,00	4	1,02	4	1,02
4,84	1,04	4,84	1,01	4,84	1,03	4,84	1,03
5,76	1,12	5,76	1,08	5,76	1,04	5,76	1,05
6,76	1,19	6,76	1,14	6,76	1,10	6,76	1,08
7,84	1,28	7,84	1,22	7,84	1,17	7,84	1,15
9	1,38	9	1,30	9	1,26	9	1,23
10,24	1,48	10,24	1,40	10,24	1,34	10,24	1,34
11,56	1,59	11,56	1,52	11,56	1,44	11,56	1,44

12,96	1,73	12,96	1,65	12,96	1,56	12,96	1,54
14,44	1,87	14,44	1,79	14,44	1,70	14,44	1,69
16	2,03	16	1,95	16	1,88	16	1,84
		17,64	2,14	17,64	2,06	17,64	2,02
		19,36	2,36	19,36	2,28	19,36	2,24
				21,16	2,55	21,16	2,50
				23,04	2,85	23,04	2,82
				25	3,26	25	3,23
						27,04	3,71

Appendix Table A.2: Moonpool drag coefficient, square geometry

F/u^2 [kg/m]	A_0/A [-]	F/u^2 [kg/m]	A_0/A [-]	F/u^2 [kg/m]	A_0/A [-]	F/u^2 [kg/m]	A_0/A [-]
501,3	0,02	501,3	0,02	501,3	0,02	501,3	0,02
723,7	0,03	731,4	0,03	731,4	0,03	731,4	0,03
979,3	0,04	990,0	0,04	1000,6	0,04	1000,6	0,04
1274,4	0,05	1302,7	0,05	1316,9	0,05	1331,0	0,05
1647,2	0,06	1647,2	0,06	1683,8	0,06	1683,8	0,06
2013,4	0,08	2059,7	0,08	2082,8	0,08	2082,8	0,08
2589,1	0,09	2502,8	0,09	2560,4	0,09	2560,4	0,09
3316,8	0,11	3175,7	0,11	3069,8	0,11	3105,1	0,11
4111,4	0,13	3940,1	0,13	3811,6	0,13	3726,0	0,13
5155,7	0,15	4897,9	0,15	4691,7	0,15	4640,1	0,15
6352,8	0,17	5982,8	0,17	5797,7	0,17	5674,4	0,17
7785,4	0,20	7344,7	0,20	7050,9	0,20	7050,9	0,20
9416,4	0,22	8980,5	0,22	8544,5	0,22	8544,5	0,22
11468,5	0,25	10951,9	0,25	10332,0	0,25	10228,7	0,25
13829,0	0,28	13217,1	0,28	12605,2	0,28	12482,8	0,28
16684,4	0,31	15959,0	0,31	15378,7	0,31	15088,5	0,31
		19306,1	0,34	18616,6	0,34	18271,8	0,34
		23433,5	0,37	22611,3	0,37	22200,2	0,37
				27600,1	0,41	27107,3	0,41
				33624,5	0,44	33326,9	0,44
				41712,5	0,48	41349,8	0,48
						51473,7	0,52

Appendix Table A.3: Drag force per square velocity, square geometry

CALCULATIONS FOR CYLINDRICAL GEOMETRY

L [m]	D [m]	C _{DS} [-]	L [m]	D [m]	C _{DS} [-]	L [m]	D [m]	C _{DS} [-]	L [m]	D [m]	C _{DS} [-]
4	1,21	0,86	4,5	1,21	0,86	5	1,21	0,88	5,2	1,21	0,88
4	1,45	0,86	4,5	1,45	0,86	5	1,45	0,86	5,2	1,45	0,87
4	1,69	0,86	4,5	1,69	0,86	5	1,69	0,86	5,2	1,69	0,86
4	1,93	0,85	4,5	1,93	0,85	5	1,93	0,86	5,2	1,93	0,86
4	2,17	0,86	4,5	2,17	0,85	5	2,17	0,85	5,2	2,17	0,85
4	2,41	0,87	4,5	2,41	0,86	5	2,41	0,85	5,2	2,41	0,85
4	2,66	0,88	4,5	2,66	0,87	5	2,66	0,86	5,2	2,66	0,85
4	2,90	0,89	4,5	2,90	0,88	5	2,9	0,87	5,2	2,9	0,86
4	3,14	0,89	4,5	3,14	0,88	5	3,14	0,87	5,2	3,14	0,87
4	3,38	0,9	4,5	3,38	0,89	5	3,38	0,88	5,2	3,38	0,88
4	3,62	0,9	4,5	3,62	0,9	5	3,62	0,89	5,2	3,62	0,89
4	3,86	0,91	4,5	3,86	0,9	5	3,86	0,89	5,2	3,86	0,89
4	4,10	0,92	4,5	4,10	0,9	5	4,1	0,9	5,2	4,1	0,89
4	4,35	0,93	4,5	4,35	0,91	5	4,35	0,9	5,2	4,35	0,9
4	4,59	0,94	4,5	4,59	0,92	5	4,59	0,9	5,2	4,59	0,9
4	4,83	0,95	4,5	4,83	0,92	5	4,83	0,91	5,2	4,83	0,91
			4,5	5,07	0,93	5	5,07	0,91	5,2	5,07	0,91
			4,5	5,31	0,94	5	5,31	0,92	5,2	5,31	0,91
						5	5,55	0,93	5,2	5,55	0,92
						5	5,79	0,94	5,2	5,79	0,93
						5	6,04	0,95	5,2	6,04	0,94
									5,2	6,28	0,95

Appendix Table A.4: Drag coefficient for steady flow, cylindrical geometry

A _{projected} [m ²]	C _D	A _{projected} [m ²]	C _D	A _{projected} [m ²]	C _D	A _{projected} [m ²]	C _D
1,14	0,89	1,14	0,89	1,14	0,91	1,14	0,91
1,65	0,90	1,65	0,90	1,65	0,90	1,65	0,91
2,24	0,92	2,24	0,92	2,24	0,92	2,24	0,92
2,93	0,93	2,93	0,93	2,93	0,94	2,93	0,94
3,71	0,96	3,71	0,95	3,71	0,95	3,71	0,95
4,58	1,00	4,58	0,99	4,58	0,98	4,58	0,98
5,54	1,04	5,54	1,03	5,54	1,02	5,54	1,01
6,59	1,09	6,59	1,08	6,59	1,07	6,59	1,06
7,74	1,14	7,74	1,13	7,74	1,11	7,74	1,11
8,97	1,20	8,97	1,19	8,97	1,18	8,97	1,18
10,30	1,26	10,30	1,26	10,30	1,25	10,30	1,25
11,72	1,35	11,72	1,33	11,72	1,32	11,72	1,32

13,23	1,45	13,23	1,42	13,23	1,42	13,23	1,40
14,83	1,56	14,83	1,53	14,83	1,51	14,83	1,51
16,53	1,70	16,53	1,67	16,53	1,63	16,53	1,63
18,31	1,87	18,31	1,81	18,31	1,79	18,31	1,79
		20,19	2,01	20,19	1,97	20,19	1,97
		22,16	2,25	22,16	2,21	22,16	2,18
				24,22	2,51	24,22	2,48
				26,37	2,90	26,37	2,87
				28,61	3,43	28,61	3,39
						30,94	4,10

Appendix Table A.5: Moonpool drag coefficient, cylindrical geometry

F/u^2 [kg/m]	A_0/A [-]	F/u^2 [kg/m]	A_0/A [-]	F/u^2 [kg/m]	A_0/A [-]	F/u^2 [kg/m]	A_0/A [-]
521,6	0,02	521,6	0,02	533,7	0,02	533,7	0,02
762,5	0,03	762,5	0,03	762,5	0,03	771,4	0,03
1056,7	0,04	1056,7	0,04	1056,7	0,04	1056,7	0,04
1393,2	0,06	1393,2	0,06	1409,6	0,06	1409,6	0,06
1827,9	0,07	1806,7	0,07	1806,7	0,07	1806,7	0,07
2347,2	0,09	2320,2	0,09	2293,2	0,09	2293,2	0,09
2964,2	0,11	2930,5	0,11	2896,8	0,11	2863,1	0,11
3695,6	0,13	3654,1	0,13	3612,6	0,13	3571,0	0,13
4511,4	0,15	4460,7	0,15	4410,0	0,15	4410,0	0,15
5528,3	0,17	5466,9	0,17	5405,4	0,17	5405,4	0,17
6663,6	0,20	6663,6	0,20	6589,6	0,20	6589,6	0,20
8093,0	0,23	8004,0	0,23	7915,1	0,23	7915,1	0,23
9809,7	0,26	9596,4	0,26	9596,4	0,26	9489,8	0,26
11886,3	0,29	11630,7	0,29	11502,9	0,29	11502,9	0,29
14420,6	0,32	14113,8	0,32	13807,0	0,32	13807,0	0,32
17547,0	0,35	16992,9	0,35	16808,2	0,35	16808,2	0,35
		20783,6	0,39	20336,6	0,39	20336,6	0,39
		25596,4	0,43	25051,8	0,43	24779,5	0,43
				31152,9	0,47	30817,9	0,47
				39230,0	0,51	38812,6	0,51
				50228,3	0,55	49699,6	0,55
						65056,8	0,60

Appendix Table A.6: Appendix Table A.3: Drag force per square velocity, cylindrical geometry

APPENDIX B - Estimation of Drag Coefficient for Tordis Pump Unit

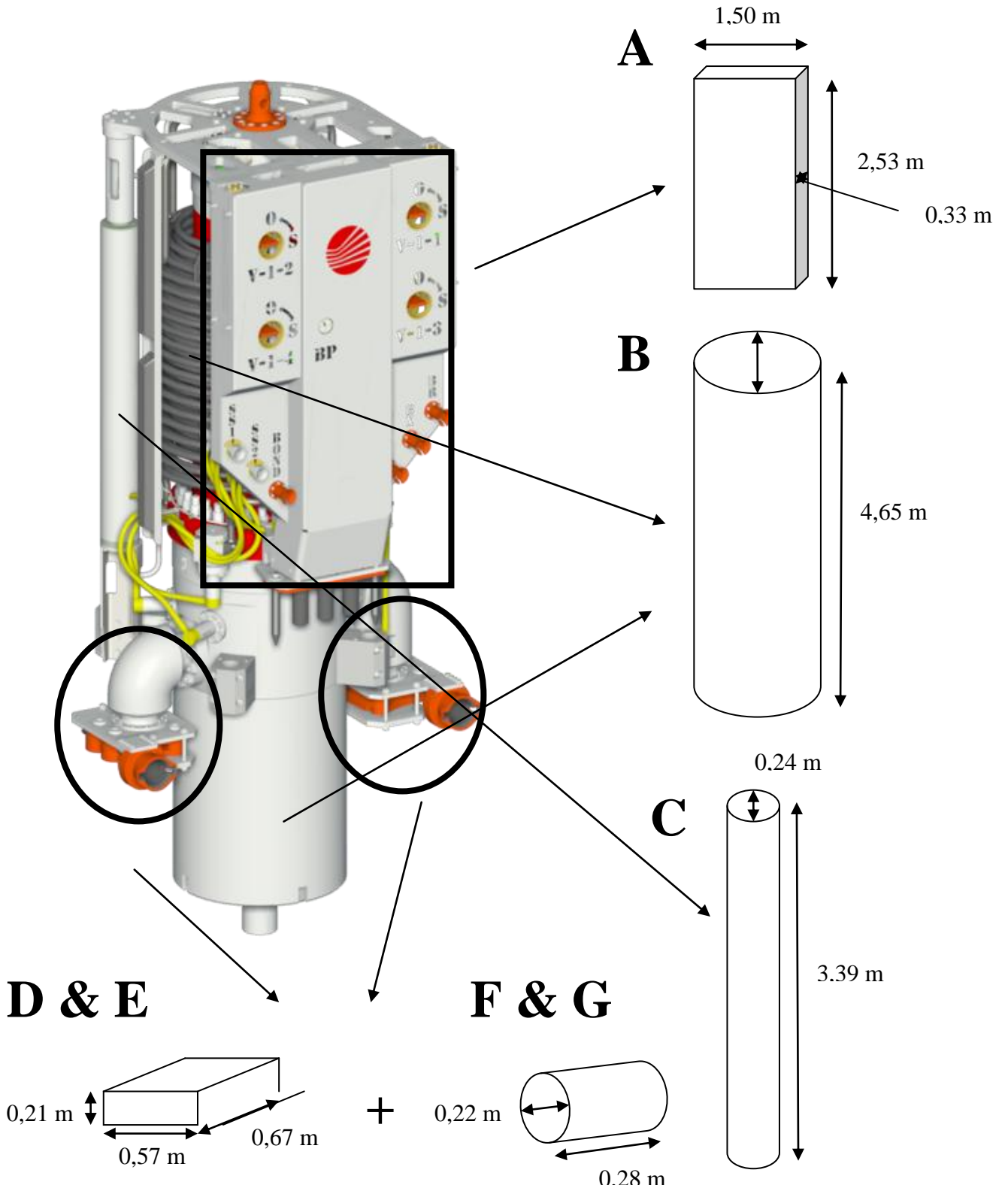
The estimation of the drag coefficient for the Tordis pump with running tool has been done by dividing them into separate elements and to calculate consequent drag coefficient according to DNV [1]. The coefficients for the different elements have been weighted by its respective projected area to find the total drag coefficient. Results are shown in table B1-B5.

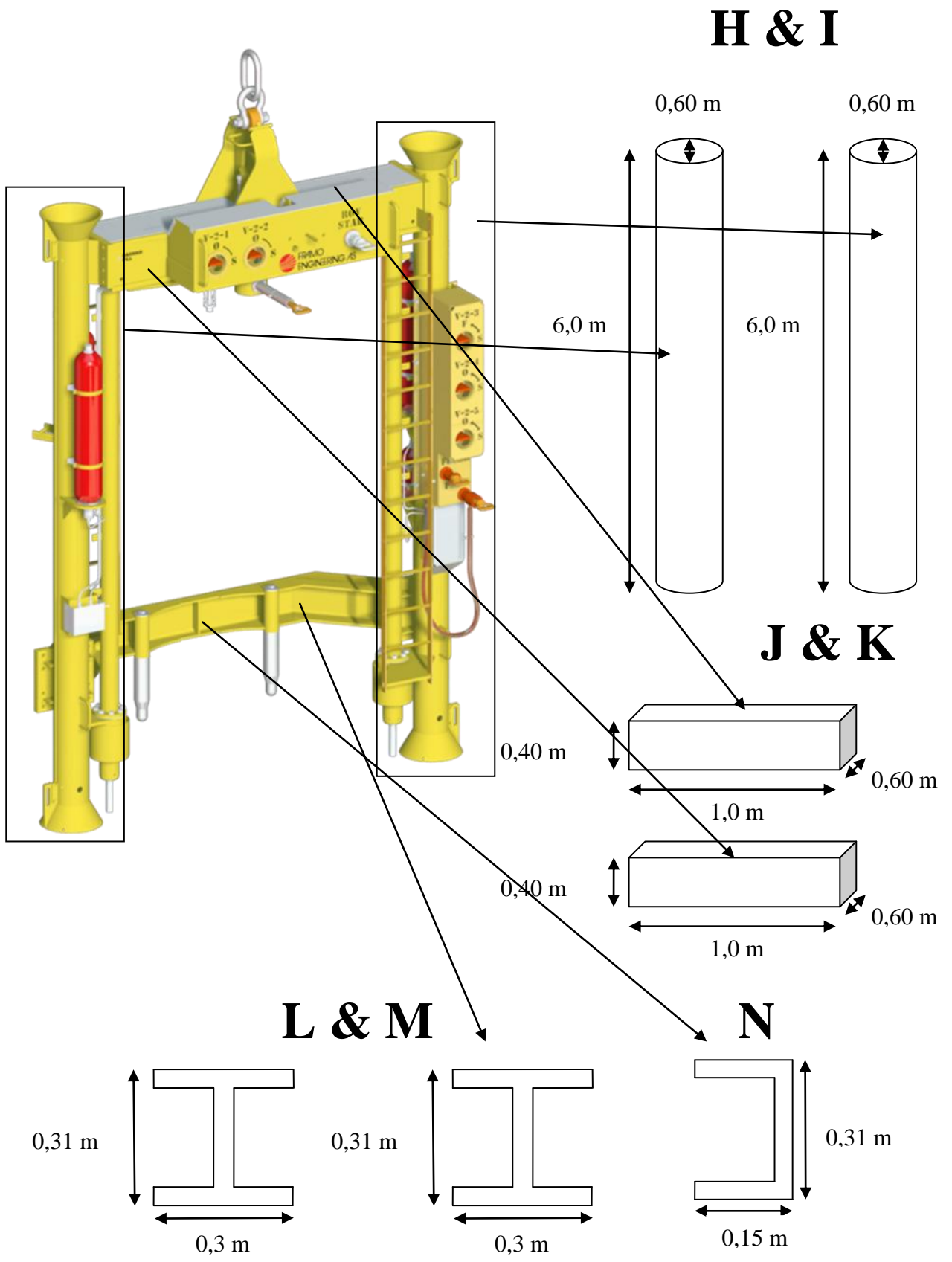
The lifting operation has been divided into four different phases. Table B2-B5 shows which elements of pump and running tool is analysed in the different phases.

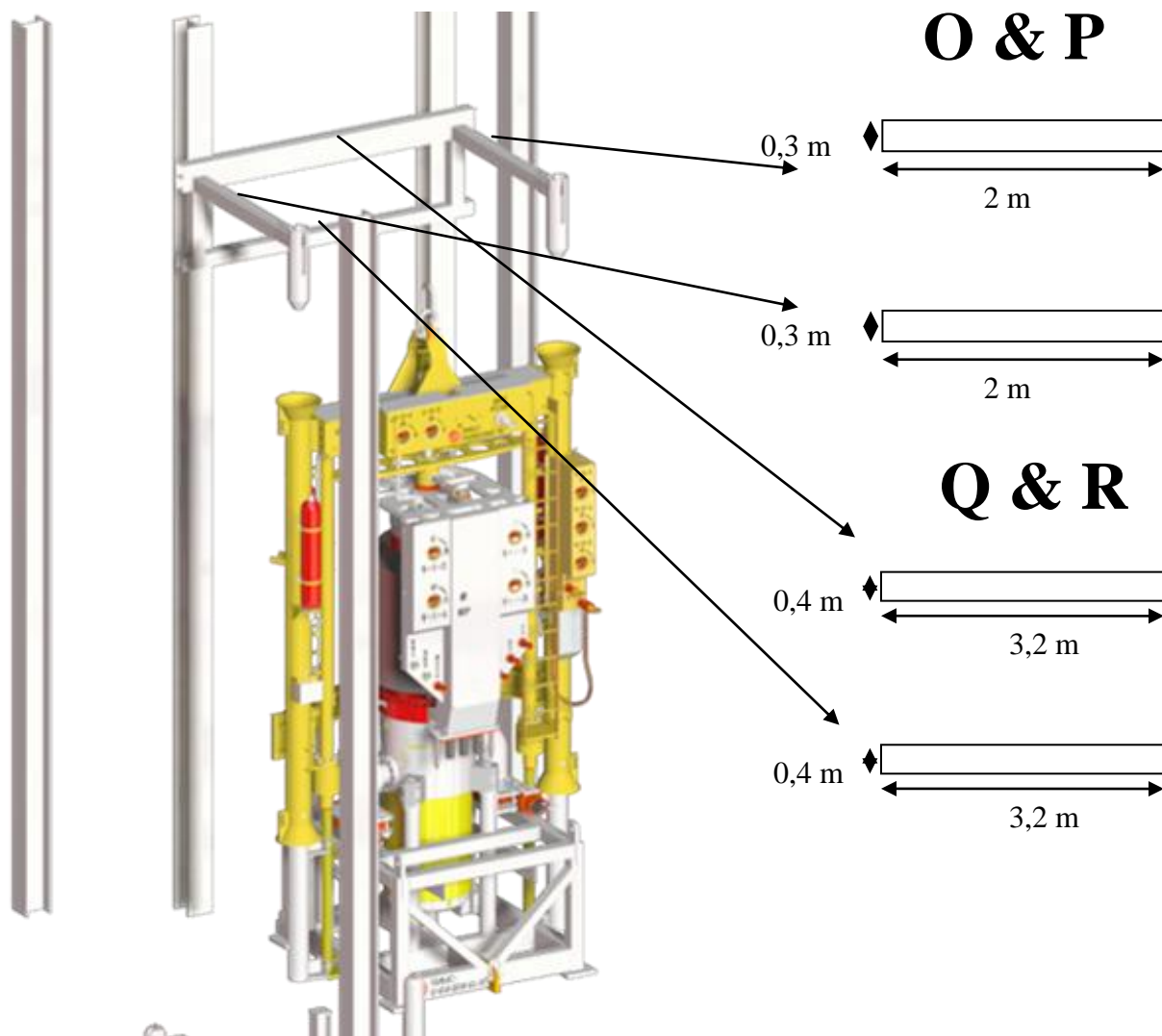
Due to the complex geometry of launched structure certain simplifications are made. Note the following:

- The back beam on running tool has been divided into three different elements to be able to predict drag coefficient, their geometry has been assumed as a C-beam and I-beam
- The top transverse beam on running tool has been divided into three different elements. The middle part, where pump is located right underneath, is disregarded.
- The ROV-panel on the pump has been simplified to square geometry. Projected area has been estimated due to actual geometry to account for sharp edges.
- Cursor will be a part of the total system when the pump is launched, and its drag coefficient and projected area must thus be accounted for. However, we hold no information about the cursor system, and for that reason we assume its geometry to be as illustrated. We use four thin beams in the calculations, two rectangular ones and two cylindrical ones. The top beam of those on the wall will to some extent be hidden in the wake of the lower beam, thus only half its projected area will be taken into account.
- Running tool guide funnels are assumed massive.

Also regarding the cursor system the following items will be launched during installation of the pump unit:







Module	C_{DS} [-] Estimated	Projected Area [m ²]	% of Total Area
A	0,90	0,70	8,25
B	0,87	1,10	12,97
C	1,20	0,05	0,59
D	1,00	0,38	4,48
E	1,00	0,38	4,48
F	2,00	0,06	0,71
G	2,00	0,06	0,71
H	1,20	0,30	3,54
I	1,20	0,30	3,54
J	1,90	0,60	7,08
K	1,90	0,60	7,08
L	1,60	0,29	3,42
M	1,60	0,29	3,42
N	2,10	0,25	2,95
O	1,00	0,60	7,08
P	1,00	0,60	7,08
Q	1,90	1,28	15,09
R	1,90	0,64	7,55
Sum	-	8,48	100

Appendix – Table B. 1: Drag coefficients and projected area for all elements

Phase 1

Parts submerged	C_{DS} [-] Estimated	C_{DS} [-] Applied	C_D [-] Applied in MP	Projected Area [m ²]
B	0,87	0,90	0,93	1,10

Appendix - Table B. 2: Drag coefficient for phase 1

Phase 2

Parts submerged	C_{DS} [-] Estimated	C_{DS} [-] Applied	C_D [-] Applied in MP	Projected Area [m ²]
B + D-I	1,04	1,05	1,13	2,58

Appendix - Table B. 3: Drag coefficient for phase 2

Phase 3

Parts submerged	C_{DS} [-] Estimated	C_{DS} [-] Applied	C_D [-] Applied in MP	Projected Area [m ²]
A-I	1,01	1,10	1,22	3,33

Appendix – Table B. 4: Drag coefficient for phase 3

Phase 4

Lifted object fully submerged

Parts submerged	C_{DS} [-] Estimated	C_{DS} [-] Applied	C_D [-] Applied in MP	Projected Area [m ²]
A - S	1,41	1,5	2,0	8,48

Appendix - Table B. 5: Drag coefficient for phase 4

APPENDIX C - Estimation of Added Mass for Tordis Pump Unit and Running Tool

The estimation of the added mass for the Tordis pump and running tool has been done by dividing them into separate elements. Two different approaches have been used in terms of finding added mass. The first one is entirely based on known geometries given in DNV-RP-H103 [1]. The second approach is based on the approximation of taking added mass of the hemisphere at top and bottom in addition to geometries given in DNV-RP-H103 [1]

The calculations assume a fully submerged pump unit. Cursors system has been disregarded.

Due to the complex geometry of launched structure certain simplifications are made. Note the following:

- Running tool guide funnels are taken as 1. Square prisms and 2. Circular cylinders. They are assumed massive. The dimensions of the square prisms have been set to a value in order to obtain a cross-sectional area equal to cross-sectional area of circular cylinders.
- The top transverse beam on running tool has been simplified to a cylinder to be able to use known geometries from the DNV [1]. Diameter of cylinder is assumed equal to the largest length in the cross-sectional area of beam.
- The lower transverse beam on running tool has been simplified to a cylinder to be able to use known geometries from DNV [1]. Diameter of cylinder is assumed equal to the largest length in the cross-sectional area of beam.
- Projected area of the transverse beam has been calculated by use of rectangular beams. This would have been an overestimation if beams were cylindrical, but the fact that they are actually rectangular makes it realistic.
- The pump body has been taken as a 1. Square prism and 2. Circular cylinder. The diameter of the pump body has been set to a value somewhat higher than what was used in Appendix B. This is due to the different fittings around the pump body that has not been accounted for here.
- The process inlet and outlet has been simplified to two square prisms. Added mass have been estimated by assuming 2D-structure and to modify it into 3D.
- The pump ROV-panel has been taken as a square prism, as in Appendix B. Added mass have been estimated by assuming 2D-structure and to modify it into 3D.
- When estimating added mass as hemispheres at top and bottom, we do not apply any added mass coefficients and therefore is formula 3.38 for the increased added mass coefficient not applicable. Increased added mass in moonpool in this method will for that reason be increased equally in percentages as for the DNV-method.

1. By use of only DNV [1] formulas

Elements	A ₃₃ [kg] Estimated	A ₃₃ [kg] in MP	A ₃₃ [kg] Applied in MP	Projected Area [m ²]
2 x RT Guide Funnel	276,4	276,4	280	0,57
RT Transverse Upper Beam	923,1	923,1	925	2,1
RT Transverse Lower Beam	253,6	253,6	255	1,05
Pump Body	2520,2	2520,2	2525	2,25
Pump ROV-panel	998,2	998,2	1000	0,50
Process Inlet and Outlet	121,8	121,8	125	0,72
Total	5093,3	5093,3	5110	7,19

Appendix - Table A. 1: Estimated added mass by use of DNV [1] formulas

2. By use of hemispherical + DNV formulas

Elements	A ₃₃ [kg] Estimated	A ₃₃ [kg] in MP	A ₃₃ [kg] Applied in MP	Projected Area [m ²]
2 x RT Guide Funnel	231,8	231,8	235	0,57
RT Transverse Upper Beam	923,1	923,1	925	2,1
RT Transverse Lower Beam	253,6	253,6	255	1,05
Pump Body	1811,3	1811,3	1815	1,77
Pump ROV-Panel	998,2	998,2	1000	0,50
Process Inlet and Outlet	121,8	121,8	125	0,72
Total	4339,8	4339,8	4355	6,71

Appendix - Table A. 2: Estimated added mass by use of hemispherical + DNV [1] formulas